THE GRAIN SIZE DISTRIBUTION OF ALUMINUM

By

BURTON ROE PATTERSON

A DISSERTATION PRESENTED TO THE GRADUATE COUNCIL OF
THE UNIVERSITY OF FLORIDA
IN PARTIAL FULFILLMENT OF THE REQUIREMENTS FOR THE
DEGREE OF DOCTOR OF PHILOSOPHY

UNIVERSITY OF FLORIDA

1978

Copyright 1978

by

Burton Roe Patterson

Dedicated to my wife, Ellen,
without whose impatience this work
might never have been finished

ACKNOWLEDGEMENTS

The author would like to sincerely thank Dr. F. N. Rhines whose guidance and suggestions have contributed much to the formulation and performance of the research. His inspiration and conviction have been the foundation of this study.

The author is also grateful to the following members of his supervisory committee for their contributions: Dr. R. T. DeHoff, for his helpful discussions and advice, especially in relation to the application and testing of the stereological models; Dr. Richard Scheaffer, Chairman of the Department of Statistics, for his numerous suggestions concerning the analysis of the data; and, Dr. R. E. Reed-Hill, Assistant Chairman of the Department of Materials Science and Metallurgical Engineering, for his helpful advice concerning mechanical deformation.

In addition, the author would like to acknowledge the numerous beneficial interactions he has had with his fellow students throughout the course of this study.

TABLE OF CONTENTS

TABLE OF CONTENTS - continued.

TABLE OF CONTENTS - continued.

Abstract of Dissertation Presented to the Graduate Council of the University of Florida in Partial Fulfillment of the Requirements for the Degree of Doctor of Philosophy

THE GRAIN SIZE DISTRIBUTION OF ALUMINUM

By

Burton Roe Patterson

June 1978

Chairman: Frederick N. Rhines
Major Department: Materials Science and Engineering

The form of the grain size distribution in polycrystalline aluminum has been investigated through the examination of individual grains, separated from the aggregate with liquid gallium. The grain volumes, represented by the grain weights, have been found to be statistically approximated by the log-normal distribution. The variability of the width of the size distribution has been investigated with respect to the amount of deformation prior to recrystallization and grain growth, and with respect to the rate of solidification of cast material. Increasing deformation, observed over a range of 3 to 80%, has been found to continuously reduce the width of the grain size distribution, measured through $\ell n\ \sigma_V$, the standard deviation of the logarithms of the grain sizes. Grain growth following recrystallization did

not affect $\ell n\ \sigma_V$ significantly. The width of the grain size distribution of cast Al-10 wt.% Zn was found to decrease with increasing rate of a solidification.

The frequency distributions of the numbers of faces per grain (F_G) and edges per face (E_F) were determined through direct observation of grains separated from the deformed and annealed high purity aluminum specimens. The widths of the distributions of E_F and F_G, $\ell n\ \sigma_E$ and $\ell n\ \sigma_F$ respectively, were found to decrease with increased deformation, and to correlate directly with $\ell n\ \sigma_V$, supporting the theoretical relation of the grain size and topological distributions. The frequencies of 3-edged faces and 4-faced grains were also found to be related directly to the widths of the topological distributions, and therefore to $\ell n\ \sigma_V$.

The effect of the frequency of 3-edged faces on the rate of grain growth was tested through the comparison of the growth rates of two series of specimens, deformed 25% and 80%, respectively, before annealing. The rate of change of the average grain volume ($\bar{V}$), with time, at equal values of $\bar{V}$, was found to be greater by a factor of 20 for the 25% series than for the 80% series, throughout growth. The difference in percentage of 3-edged faces, projected for the two series from the prior results, was

approximately of this magnitude. These results support a mechanism of grain growth, in which the rate of growth is controlled by the rate of occurrence of discrete topological events, necessary for continuous grain annihilation.

INTRODUCTION

The grains comprising polycrystalline metals traverse a large range of sizes in any given specimen. That this is so is generally known but is seldom considered in metallurgical theory or practice. The difficulty of analyzing or even visualizing the three-dimensional aggregate of grains has instead led to the historical reliance on the more convenient concept of "average grain size." Knowledge of the grain size distribution and its effect on the properties of materials has thus developed slowly.

Most of what is known about the distribution is related to its form. Stereological calculations, based on models of constant grain shape, have generally indicated a skewed array of sizes, closely approximated by the log-normal distribution (1-3). Experiments utilizing these two-dimensional measurements (3,4) and the more exact three-dimensional investigation of Okazaki and Conrad (5) have further shown that the relative spread of this distribution remains unchanged over extended periods of grain growth. Analysis of the data from the three-dimensional studies by Hull (6) and Williams and

Smith (7) have confirmed the log-normality of the distribution and have revealed that the volumes of the individual grains in a given specimen may vary by factors of several hundred to a thousand.

Other than the results from these few valuable investigations, little is known about grain size distributions and many questions remain unanswered:

What is the range of variability of the form of the distribution?

If variable, how is the form affected by the variation of common processing parameters, such as solidification rate, and the rate, degree and mode of deformation prior to recrystallization?

How is the topological state of a polycrystalline body affected by the grain size distribution?

To what extent does the distribution influence the rate of grain growth and mechanical properties of materials?

What beneficial properties are obtainable through the intentional control of the grain size distribution?

This investigation has sought to go beyond the measurement of polycrystalline size distributions as an end

in itself by employing the measured parameters as investigative tools for gathering other information. The following chapters will describe the investigation of several of the above areas. Although these topics are all related to the distribution of grain sizes in polycrystalline aggregates, the subject addressed by each is sufficiently deep to warrant individual treatment. Accordingly, each chapter will present the appropriate background of the problem to be addressed, the experimental method, and the discussion of the findings and their significance to the overall topic.

The first chapter deals with the problems of accurate representation of the size distribution and estimation of its parameters. A three-dimensional approach involving grain separation is employed for the measurement of the individual grain sizes, the frequencies of which are statistically shown to be well approximated by the log-normal distribution. This enables the use of $\ell n\ \sigma_V$, the standard deviation of this distribution to monitor the effects of various processing parameters on the variation of the resulting grain sizes. Solidification rate and the degree of deformation prior to recrystallization are explored and are found to affect $\ell n\ \sigma_V$ significantly. The results of these studies also allow observations to be

made concerning the theories of the mechanism of grain formation by these processes.

In the second chapter, the frequency distributions of topological parameters, such as the number of faces per grain and edges per face, and their relationship to the grain size distribution are investigated. Theoretically, the number of faces on the individual grains in an aggregate should be a function of their own size and that of their neighbors. The sizes of these faces and their numbers of edges should also result from the overall grain size distribution.

Interest in the topological distributions results primarily from their theoretical relation to the rate of grain growth. C. S. Smith (8), Rhines and Craig (9), and Steele (10) have explained this process as a progression of topological events involving triangular faces and tetrahedral grains. Thus, knowledge concerning the relation between grain size distribution and the topology of the grain boundary network may provide still more insight into the mechanism of grain growth. The nature of this relationship is investigated through the examination of grains separated from the size distribution specimens of Chapter I.

The grain growth process itself is examined experimentally in the third chapter. Grain growth rate,

measured as $\frac{d\bar{V}}{dt}$ at constant average grain volume, $\bar{V}$, is compared among samples deformed different amounts before recrystallization. The interrelation of deformation, grain size distribution and topological state, demonstrated in Chapters I and II, suggests that the presently found differences in $\frac{d\bar{V}}{dt}$ may be due to variation in the degree of topological restriction of the process. The nature of grain growth in the specimens discussed above is also examined in terms of the global metric properties: S_V, grain boundary surface area per unit volume; L_V, length of grain edge (triple line) per unit volume; M_V, total grain boundary curvature per unit volume; and the topological property N_V, number of grains per unit volume.

The distributional, topological, and metric properties each report a different piece of information about the polycrystalline aggregate and the grain growth process. These pieces are all related, however, and may now be examined in combination, yielding a more complete picture of this process than has been available from any one type of information alone.

CHAPTER I
THE GRAIN SIZE DISTRIBUTION

Introduction

The grain size distribution is a very subtle property of a material. Resulting from microstructural processes such as solidification, recrystallization, and grain growth, which are themselves not fully understood, its nature and effect on other properties is generally unknown. The difficulty of its measurement has also restricted knowledge in this area. This chapter will explore the form of the grain size distribution and its variability in relation to the above processes through which it evolves. This information should add to the knowledge of the nature of polycrystalline microstructures and may yield insight into the evolutionary processes themselves.

Numerous stereological techniques have been developed for the analysis of grain size distributions (1, 11). Generally, these methods require measurement of the distribution of some aspect of two-dimensional grain sections, such as chord lengths, diameters, or areas. With the assumption of some constant model grain shape,

such as a sphere or tetrakaidecahedron, for which the distribution function of the measured feature is known, the spatial grain size distribution may be calculated. These methods are only approximate, however, since grains do vary in shape and are often unequiaxed.

Unbiased determination of the grain size distribution must be performed directly, through a technique which examines a spatial property of the microstructure. Only a few such investigations have been performed previously.

In 1952, Williams and Smith (7) employed micro-radiography to measure the spatial sizes of the grains in an Al-Sn alloy. The sizes were approximated by comparison of their magnified three-dimensional images with spheres of known volume. The resulting distribution of grain volumes is illustrated in Fig. (1). In Fig. (2), these data are seen to plot linearly on a logarithmic X probability scale, indicating good approximation of the log-normal distribution (12). This is consistent with the findings of numerous stereological investigations as well (1,2).

Hull (6) separated almost 1000 grains from a β-brass casting, disintegrated with a solution of mercurous nitrate and nitric acid. He then sized the grains by sieving. His data, illustrated in Fig. (17), are also representative of the log-normal distribution.

Figure (1). Frequency histogram of the volumes of grains in a 5.2 wt.% Al-Sn alloy. From the data of Williams and Smith (7).

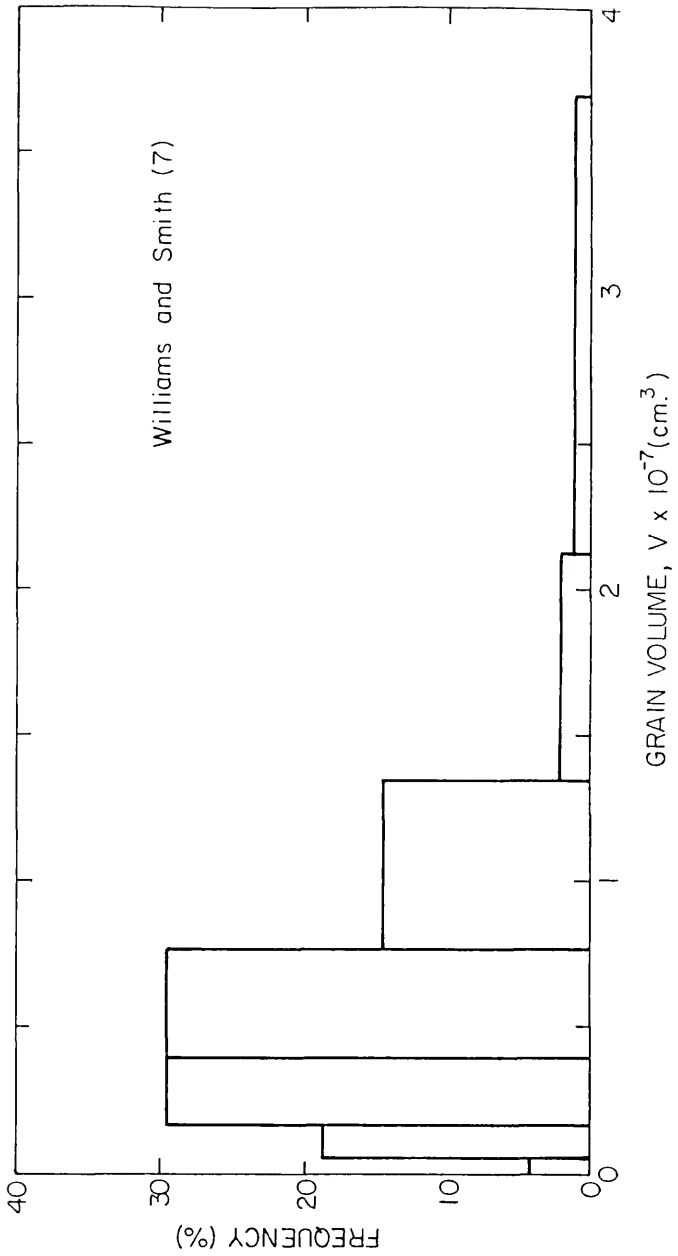
Williams and Smith (7)
FREQUENCY (%)
0
10
20
30
40
0
1
2
3
4
GRAIN VOLUME, V x 10^{-7} ($cm.^3$)

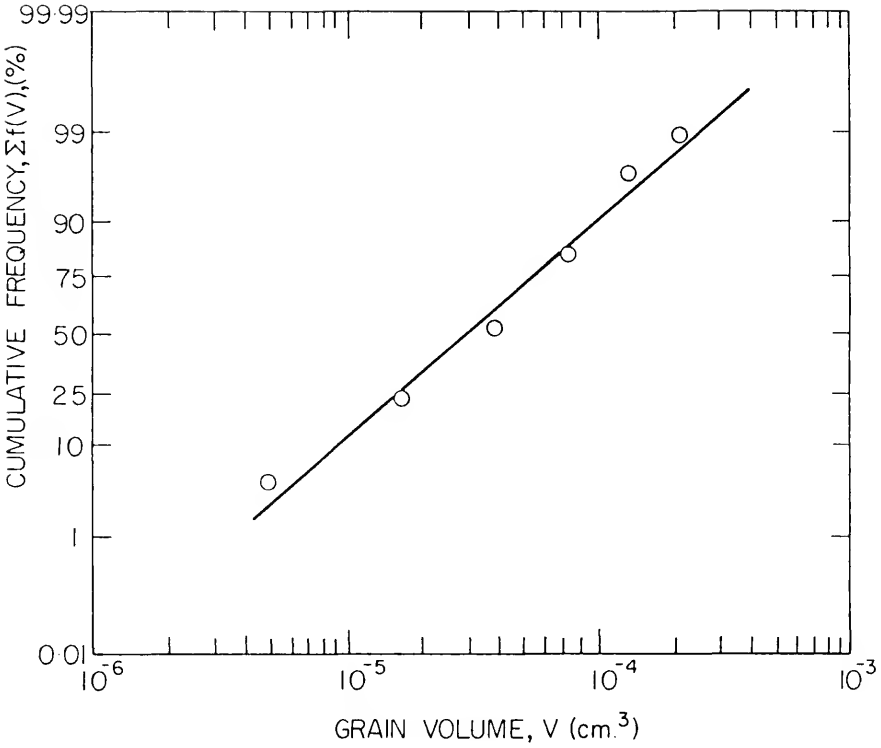

Figure (2). Log-normal probability plot of the grain volume data of Williams and Smith (7).

In 1972 Okazaki and Conrad (5) employed serial sectioning to obtain grain volume distributions for Ti. They examined samples which had been swaged identically but annealed for different times and temperatures, resulting in a wide range of final average grain sizes. The data from these samples were also consistently linear on a log-normal plot. The slopes of the lines from the various samples were identical, indicating similar relative widths of their grain size distributions, regardless of the average grain size. These findings tended to support the earlier hypothesis that the grain size distribution of a given material remains constant during grain growth. It was also of interest that the variation of the recrystallization and grain growth temperature had little influence on the resulting grain size distribution. Their investigation of directly measured grain size distributions was the first to be performed over a coherent range of experimental conditions.

In addition to the laborious methods previously mentioned, Otala (13) has recently reported a magnetic method for volume distribution analysis. This technique, applicable to ferromagnetic materials, is based on the pinning of magnetic domain walls by grain boundaries.

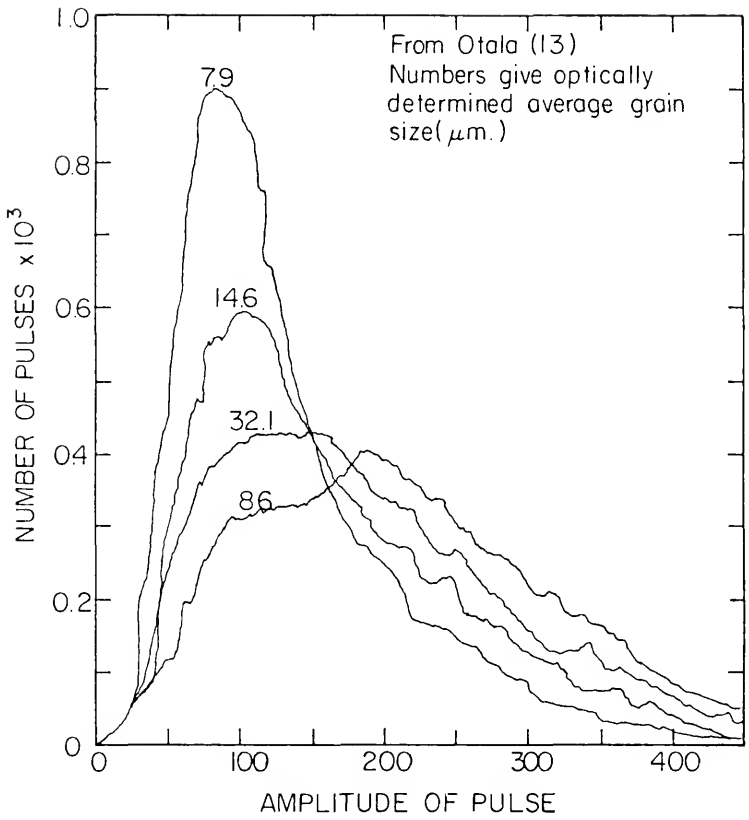

Figure (3). Frequency of pulse height—directly proportional to frequency of grain volume—for four low-carbon steel specimens, from the magnetic technique of Otala (13). The apparent distribution widths vary with the average grain size.

The volume distribution, measured as a distribution of electronic pulse heights, is obtained directly from an X-Y recorder or an oscilloscope. Figure (3) illustrates several distributions measured from low-carbon steels with different average grain sizes. Unfortunately, Otala did not further analyze the forms of these distributions. In light of the rapidity and experimental ease of the magnetic method and the large numbers of grains included in its analysis, it appears to be the most efficient means available for the direct determination of grain volume distribution. A disadvantage is that it does require the use of special electronic equipment.

The principal observations of the size distribution investigations performed to date may be listed as follows.

(1) The distributions of spatial grain sizes are consistently well approximated by the log-normal distribution.

(2) The relative width of the grain size distribution is variable with material and processing history.

(3) The distribution maintains a constant relative width during grain growth.

These observations indicate that there is an underlying commonality among the various processes by which

microstructures evolve, tending to produce similar types of grain size distributions. There also appears to be a degree of freedom within this constraint, which allows some variation of the distribution width. Further knowledge of the distributional forms resulting from controlled variation in processing would undoubtedly aid the understanding of the mechanisms of these processes.

This investigation will explore the variability of the grain size distribution with respect to the solidification rate of a casting and the amount of cold work given a material prior to recrystallization and grain growth. These variables influence their respective processes strongly, through their effects on the rates of nucleation and growth of new constituent. The great differences in the types of microstructures, theoretically produced by different nucleation and growth conditions (14-16), suggest that the above methods may well be expected to yield different size distributions experimentally.

Size distributions may be determined through the weighing of individual grains which, in the case of aluminum and its alloys, can be separated from the aggregate by liquid gallium penetration. The distribution

of weights is directly proportional to the grain volume distribution. Through systematic variation of the solidification rate or amount of deformation, the relative effects of these parameters on the resulting distributions may be assessed.

In addition to this, the validity of the log-normal approximation may be tested further. Good comparison between the theoretical and measured distributions should justify the use of $\ell n\ \sigma_V$, the standard deviation of the logarithmic distribution, as a measure of distribution width. Continual agreement with the log-normal distribution would also tend to restrict the theoretical mechanisms of these evolutionary processes, allowing only those capable of producing such distributions. Of still further interest is the comparison of the theoretical distribution parameters of the Johnson-Mehl and cell models of nucleation and growth (15) with experimental data, and the test of the Hillert model of grain growth (17).

Experimental Procedure

Material

High purity aluminum of the composition listed below* was employed in the experiments involving

*As given in reference (18).

deformation, recrystallization and grain growth, prior to analysis of the grain size distribution.

Composition (%)	
Al	99.998
Si	0.0003
Fe	0.0009
Cu	0.0001
Mg	0.0005
Ca	0.0002

This material was chosen for the following reasons.

(1) Pure aluminum has a single phase microstructure with few annealing twins or precipitates.

(2) Its grains are easily separated through boundary penetration with gallium.

(3) There is an abundance of experimental recrystallization and grain growth data, with which results may be compared.

For the experiments investigating the effect of solidification rate on the grain size distribution, an alloy of Al-10 wt.% Zn was used. X-ray diffraction indicated that the zinc ingot contained some copper impurity. The aluminum was obtained from the previously described lot.

Aluminum was chosen as a base material for the first two of the reasons given above. Castings of pure aluminum

were found to be composed of columnar grains only, however. An alloy was required in order to produce an equiaxed microstructure. The Al-Zn system was chosen because of the relative simplicity of the aluminum-rich side of the phase diagram.

Sample Preparation

Preparation of specimens for testing the effect of prior deformation

In order to determine the effect of the amount of deformation prior to recrystallization on the grain size distribution after annealing, a series of four samples was prepared identically, except for the amount of deformation in each sample. The method of production of the specimens from the high purity aluminum ingot, and their individual treatments, are described below.

A block of sound material, measuring 4.2 cm. x 7 cm. x 7.6 cm., was sawed from the commercially supplied aluminum ingot. This piece was unidirectionally rolled at room temperature from 4.2 cm. to 2 cm. in thickness, a reduction of 54%. The 13.5 cm. x 7 cm. x 2 cm. slab was stored in a freezer at -18°C until given a recrystallization anneal in a forced air furnace at 380°C for 1 hr. It was then sawed across its width to yield two strips, each 3 cm. wide.

The 3 cm. x 7 cm. x 2 cm. strips were cooled in liquid nitrogen (-196°C) and drop-hammer forged in the 3 cm. direction to a final height of 1.5 cm. (50% reduction). During forging, the pieces were recooled intermittently to prevent recrystallization. The pieces were stored in liquid nitrogen until given a recrystallization anneal in a forced air furnace at 380°C for 40 min. They were then sawed into small pieces, 1.5 cm. x 1.5 cm. x 3 cm., which were machined into cylinders approximately 1.4 cm. in diameter by 2.4 cm. high. The surfaces were polished with coarse and fine grinding papers to remove the metal disturbed by machining and to reduce friction during the later compression treatment.

Four specimens were then cooled in liquid nitrogen and individually compressed, using a hand-operated hydraulic press, to reductions in height of 3%, 7%, 16%, and 30%. The compression strain rates were approximately 1×10^{-2} (sec.^{-1}). These specimens were stored in liquid nitrogen until given recrystallization anneals in a molten salt bath at 635±2°C. The samples were kept in the bath for 1.5 hr. and quenched to room temperature. They were then annealed for 20 more hours in a forced air furnace at 635±1°C and quenched. The extra anneal was needed to increase the sizes of the grains in the

higher deformation samples, so that they could be easily handled and weighed after separation.

Only grains from the central areas of the specimens were taken for the following analyses, to avoid any effects of the specimen surfaces on deformation and grain growth. The samples will be referred to by the following designations:

Sample	% Deformation
C-3	3
C-7	7
C-16	16
C-30	30

Preparation of specimens for testing the effect of grain growth

A second experiment was performed in order to confirm Okazaki and Conrad's (5) finding that the grain size distribution remains constant throughout grain growth. Two samples, obtained from the same deformed tensile bar, were recrystallized and allowed to grain grow for different lengths of time at the same temperature. Their respective grain size distributions, determined through grain separation, were then compared. A sample from a second tensile bar, given a lesser amount of deformation, was annealed at a similar temperature for comparison. The method of preparation and the treatments of these samples are described below.

Two blocks of sound material, each measuring approximately 8 cm. x 5 cm. x 20 cm. were sawed from high purity aluminum ingots from the previously mentioned lot. These were rolled at room temperature to 50% reductions in thickness, and flattened with several light taps from a drop hammer. The large slabs, in contact with thermocouples, were annealed in an air furnace at 400°C for 1 hr., in addition to the 40 min. heat-up period, to produce complete recrystallization.

A strip approximately 2.5 cm. square by 36 cm. long was cut from each slab. These were machined into round tensile bars with gage sections measuring 0.750±0.001 in. in diameter by 12 in. long. The bars were deformed in tension at strain rates of 2.7×10^{-4} $(sec.^{-1})$, while immersed in liquid nitrogen. Their final elongations were 3% and 6%, engineering strain.

Two cross-sectional specimens were sawed from the bar deformed 6% and one specimen was sawed from the bar deformed 3%. The bars were kept cool during sectioning and the specimens were stored in liquid nitrogen. They were later annealed for varying lengths of time in a molten salt bath at 600±1°C, and quenched. The corresponding sample designations and treatments are as follows:

Sample	% Deformation	Time of anneal (600°C)
T-3	3	10 min.
T-6-1	6	1.5 min.
T-6-2	6	1 hr.

After annealing, the size distributions of the internal grains of each specimen were determined through the separation and weighing method.

Preparation of specimens for testing the effect of solidification rate

In order to study the effect of solidification rate on the resulting grain size distribution, several castings were produced by similar means, varying only their manner of freezing. These melts of Al-10 wt.% Zn were individually prepared in the following manner.

Two or three pieces of aluminum, weighing a total of 680 gm., and one 70 gm. piece of zinc were cleaned with acid. The aluminum was placed in a graphite crucible, and melted in an air furnace. When the aluminum had completely melted, the crucible was removed from the furnace and the zinc added. The melt was then stirred for several seconds with a graphite rod to assure uniform zinc distribution.

The individual melts were then given the following separate treatments, in order to achieve three different rates of solidification.

(1) Rapid solidification rate - One melt was poured into a long, narrow (3.5 cm. diameter) cavity in a thick graphite crucible at room temperature. The sample was completely solidified within five seconds.

(2) Intermediate solidification rate - Another melt was poured into the large central cavity (5.5 cm. diameter) of a relatively thin-walled graphite crucible which was at room temperature. Solidification was complete in less than one minute.

(3) Slow solidification rate - The hot crucible (7 cm. internal diameter) containing the third melt was removed from the furnace, covered with a hot top, and placed on a large steel plate at room temperature. Solidification was complete in approximately three minutes.

The three specimens will be referred to by the following designations:

Sample	Solidification Rate
S-1	fast
S-2	intermediate
S-3	slow

On sectioning, the castings were found to contain no significant porosity. All possessed a rim of columnar

grains about their circumference, surrounding a central mass of equiaxed grains. Only grains from the equiaxed region were employed in the grain size distribution analyses.

Measurement of Grain Size Distribution

The grain size distributions of the above samples were all determined in the same manner. Approximately 100 grains were separated from each specimen by gallium penetration and the weights of these grains were obtained. The properties of the grain volume distribution were then determined from the distribution of grain weights.

Separation technique

The technique of separating individual grains from an aggregate, for observation, was first used by Desch (19) in 1919. Using mercury, he separated grains from a β-brass casting in order to count the numbers of facets and edges. This penetration phenomenon is driven by the reduction of the total surface energy through the wetting of the grain boundaries by the liquid metal. Robinson (20) has since employed a saturated aqueous solution of mercurous chloride to separate 7075 Al containing grain boundary precipitate.

Liquid gallium is also known to wet the grain boundaries of aluminum at near-ambient temperatures.

The melting point of pure gallium is 29.75°C, and from the Al-Ga phase diagram [Fig. (4)], it can be seen that an eutectic is formed at almost 98.9% Ga and 26.6°C. Since it was desired to use pure aluminum in the grain growth studies of this investigation (Chapter III), gallium penetration was chosen as the means of separation. The procedure found to be the most satisfactory is described below.

The sample to be disintegrated was first cleaned with an aqueous solution of HF, rinsed and dried. It was then placed on a glass slide and heated to approximately 50°C on a hot plate. A small piece of solid gallium was placed on the sample and allowed to melt. Scraping the aluminum oxide from beneath the drop of gallium with a knife blade enabled the liquid metal to wet the sample and penetrate the grain boundaries. A slight excess of gallium was added and spread over the entire surface. The coated specimen was left on the hot plate for 3-5 min., and then removed and allowed to cool to room temperature. Slight squeezing of the sample, with pliers or in a vice, loosened the grains and facilitated their later separation.

The outer grains were removed with tweezers and several clumps of 20 to 50 grains were removed from the

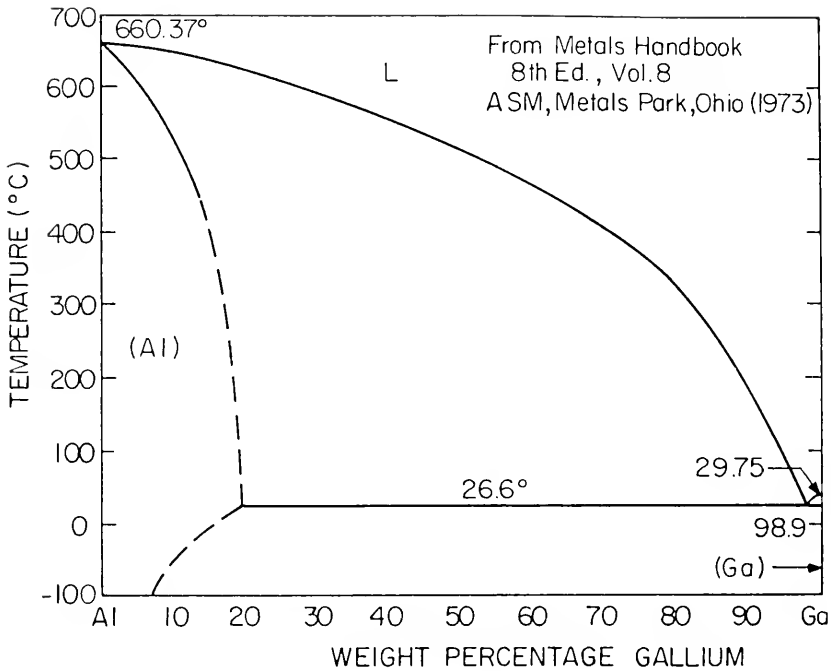

Figure (4). Aluminum-gallium phase diagram.

central area of the specimen. Removal of the grains in groups assured a representative sampling of grains of all sizes. These clumps were placed on a piece of double-sided tape on a glass slide, and the individual grains were separated with tweezers. The separation was performed beneath the binocular microscope to assure that all grains were separated. The gallium film generally remained liquid for several days. If separation of another group of grains was desired after it had solidified, the specimen was simply reheated on a glass slide.

Occasionally, two or more grains would remain stuck together. These were separated by forceably twisting them with tweezers or cutting them apart with a razor-edged knife. This had to be done with only a small portion of the grains and had no effect on the results since the grains could usually be separated at their boundary.

The separated grains were rolled about on the tape or on Silly Putty to remove any excess gallium, and were placed in rows on a clean piece of tape to prevent their loss. A sampling of 76 grains from specimen T-3 is shown in Fig. (5).

Weight determination

The majority of the grains from each sample could be weighed on a Mettler electronic balance, with a scale

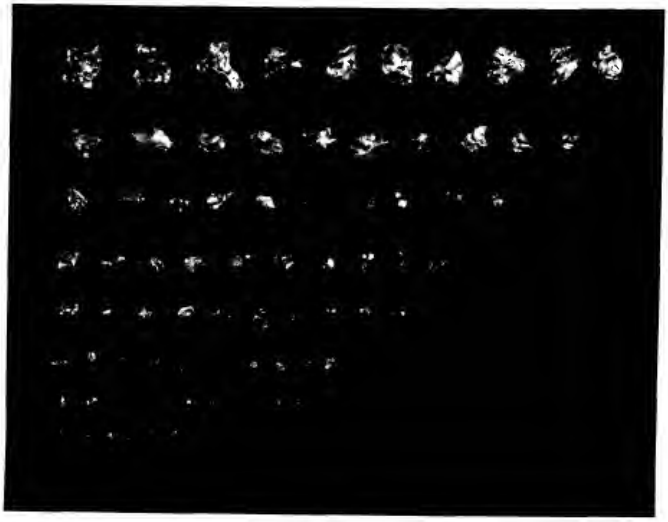

Figure (5). Representative sample of aluminum grains, separated from specimen T-3, using gallium.

readable to 10^{-4} gm. Most samples, however, contained some portion of grains smaller than this. These grains were sized under the microscope, by comparison with small glass beads of several known diameters. The grain weights were calculated from the volume of the beads which most closely approximated their size.

Coulter Counter Analysis

The grain volume distribution of specimen 80-1, described in Chapter III, was also analyzed for comparison with the present specimens. Since the grains separated from this sample were much too small to weigh, their volumes were measured using a Coulter Counter (electronic particle size analyzer). This type of device has previously been used to measure the sizes of inclusions in steel (21).

In operation, the Coulter Counter draws a fluid, in which the separated grains are suspended, past an aperture across which an electrical current flows. The change in resistance across the aperture is measured as the grain passes. The signal is transformed to a measurement of the grain volume, which is stored in the memory of the device. The volumes of thousands of grains may be measured in less than a minute.

The specimen was penetrated with gallium, as before, and several thousand grains were scraped from an internal location, using the point of a razor-edge knife. These fine grains were held together by a film of liquid gallium. The agglomerate was placed in a beaker of the Coulter Counter fluid, containing glycerol to prevent violent reaction with the gallium. On immersion in an untrasonic cleaner, the gallium separated from the grains. The contaminated fluid was poured off and the grains were observed through a binocular microscope to assure that all were separated. Any clusters of grains were broken apart with tweezers. The few grains which were too coarse to pass through the aperture were then removed by sieving. These were only a few out of several thousand grains, and their absence did not affect the analysis. The grains were then placed in the fluid reservoir of the machine and processed.

Artificial counts, resulting from electronic noise, are always present in the output from the machine. To allow for these, a run was performed using clear fluid, containing no grains. The number of counts produced in each size class during this run were subtracted from the previous output, to obtain the true distribution of grain volumes.

Experimental Results

The grain weight data from the various samples are presented in Appendix A. It can be seen that the weights within individual samples often varied by factors of several hundred to several thousand. The size distributions plotted from these data are typically unimodal and are distinctly skewed towards the larger grain sizes. This is illustrated in Fig. (6), with the data from sample C-4. Since volume and weight are directly proportional, the distribution of the volumes of these grains would appear identical to the weight distribution shown here.

The cumulative frequency of grains which are greater than or equal to some given weight may be plotted on a logarithmic probability graph, as shown in Fig. (7), again using the data from sample C-4. The linearity of the data on this type of plot indicates that the distribution of grain weights is approximately log-normal (12), the generally assumed form of the distributions of grain diameters and volumes. As with the skewed distribution, the proportionality of grain weight and volume enables the representation of the volume distribution through the plot of the corresponding weight distribution.

The log-normal distribution is convenient to use for the representation of grain sizes, since its relation

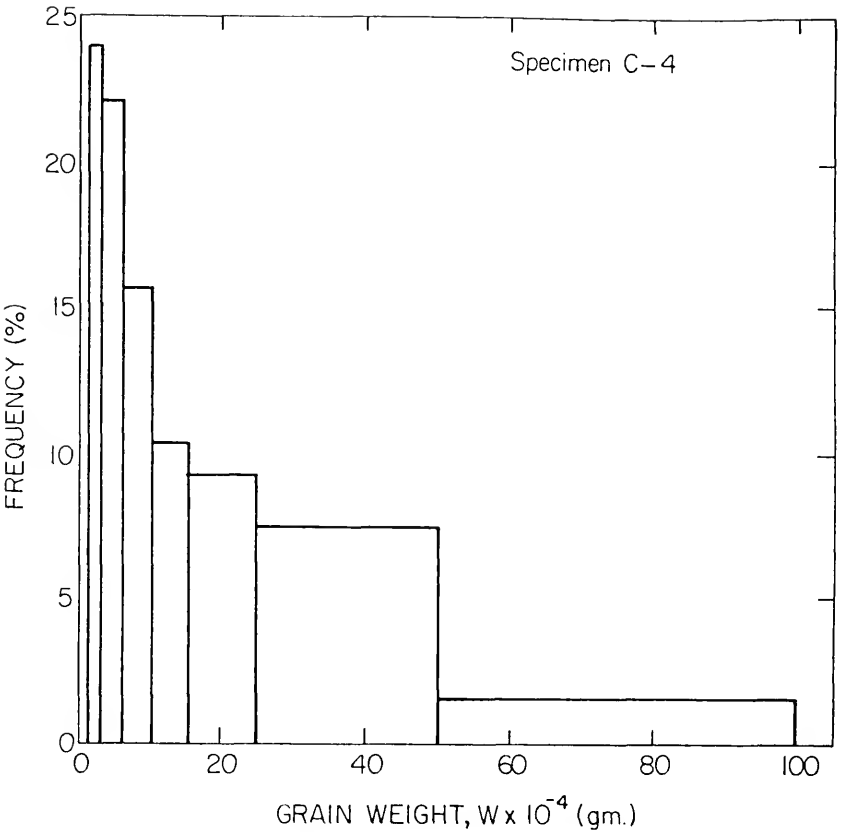

Figure (6). Frequency histogram of the weights of 372 aluminum grains, separated from specimen C-4.

Figure (7). Log-normal probability plot of grain weight data from specimen C-4.

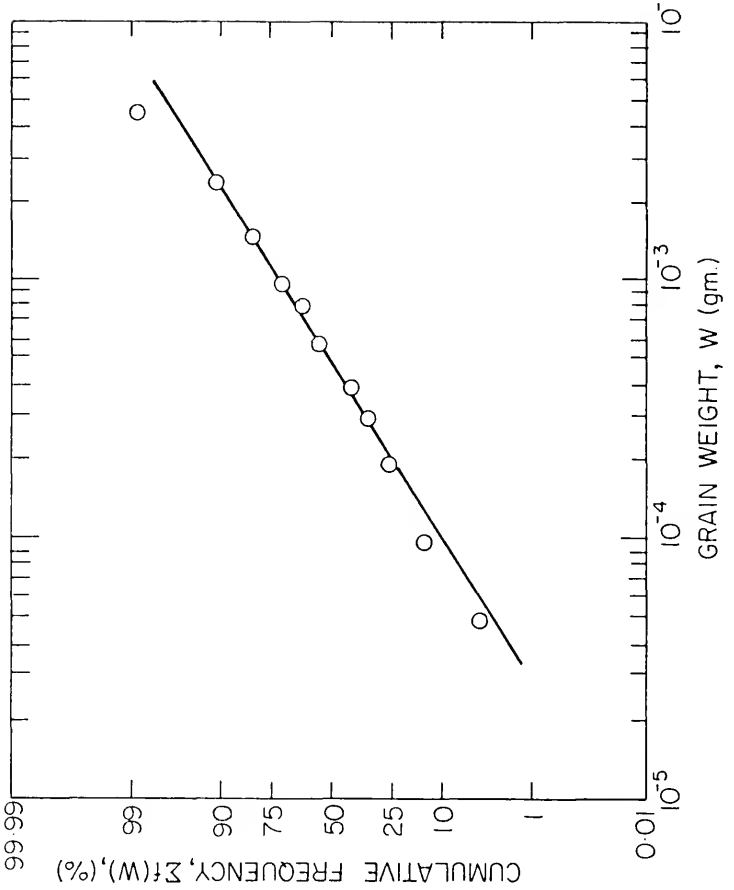
99.99
99
90
75
50
25
10
1
0.01
CUMULATIVE FREQUENCY, Σf(W), (%)
10^-5
10^-4
10^-3
10^-2
GRAIN WEIGHT, W (gm.)

to the normal distribution simplifies its mathematical treatment. The logarithms of features which are distributed log-normally are themselves normal, or Gaussian, in distribution, as illustrated in Figs. (8a) and (8b).

Test of Log-Normal Distribution

It was of interest to this investigation to test the validity of the log-normal approximation of the grain size distribution. Despite the widespread use of this model, the actual degree to which directly measured grain volume distributions compare with the theoretical one has not been measured previously. Also, in choosing a parameter for the representation of the width of the distribution, it was desired to employ one which was closely related to the actual form of the distribution.

The degree of fit of the size distributions were determined using the chi-square (χ^2) test (22). Most of the deformed and recrystallized specimens exhibited acceptable fit (significant at 2%-29%). The three cast specimens, however, were rejected at levels less than 0.5%. The causes of rejection of these specimens were generally localized at one or two size classes possessing erratic values. The majority of the other size classes deviated very little from their theoretical values. The

Figure (8). (a) Skewed, log-normal frequency distribution of the variable, X. (b) Normal frequency distribution of ln X.

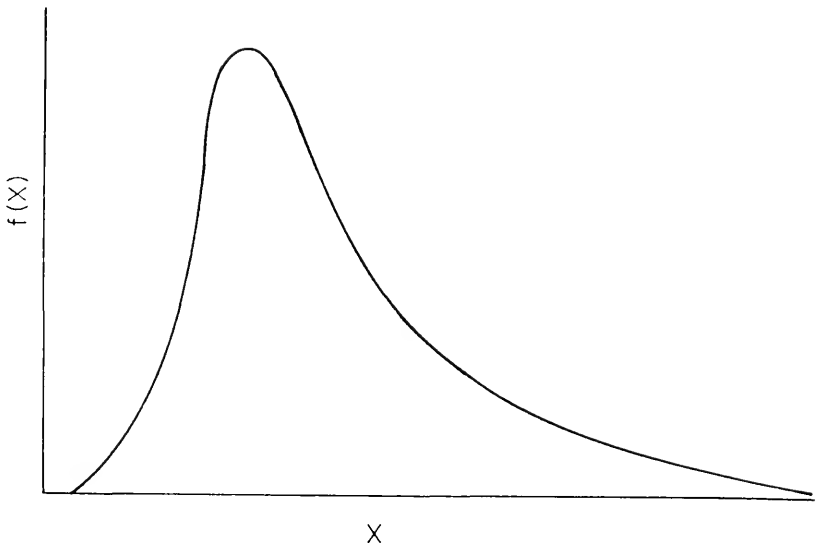

(a)

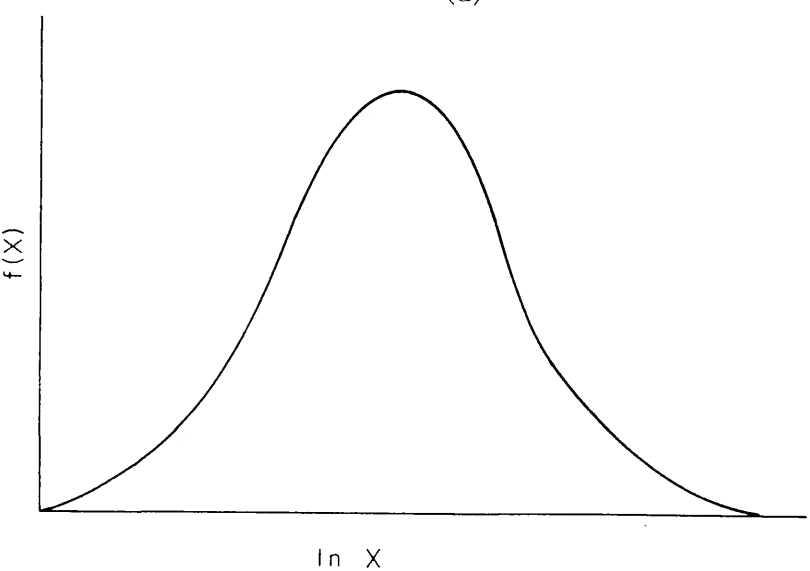

(b)

erratic cells were located at different locations among the different samples, indicating that there was no systematic difference between the mathematical and the experimentally obtained distributions. Thus, the above rejections seem to be due more to experimental deviation (inhomogeneity) than to the nature of the grain size distribution of the casting. Thus, the distribution of the recrystallized and cast specimens will be considered as representable through the log-normal distribution.

Modeling the grain size distribution as log-normal enables the use of its easily calculable parameters for representation of the experimentally determined distributions. The standard deviation of the normal distribution of the logarithms of the grain volumes, $\ell n\ \sigma_V$, is an especially useful parameter for representing the relative widths of size distributions. Distributions which are proportional in form but vary in scale, i.e. have different means, possess $\ell n\ \sigma_V$'s of equal size. This simplifies the comparison of grain size distributions among samples which differ in average grain size and, thus, possess different values of the conventional standard deviation.

In this investigation, the distributions of grain volumes have been analyzed through the distributions of

the grain weights. Since these distributions are proportional, the standard deviations of the normalized distributions of the logs of the weights and volumes are identical. Thus, the calculated widths of the weight distributions of the samples analyzed in this study have been reported, and will be discussed, as $\ell n\ \sigma_V$, since grain size distributions are most meaningfully considered in terms of grain volume.

Calculation of $\ell n\ \sigma_V$

The value of $\ell n\ \sigma_V$ may be determined either graphically or analytically. The slope of the line of data on the log-normal plot [Fig. (7)] is inversely proportional to $\ell n\ \sigma_V$; the steeper the slope, the narrower the size distribution, and vice versa. The value of $\ell n\ \sigma_V$ may be calculated from the logarithms of the grain weights at cumulative frequencies of 16% and 84%, on the ordinate, by convention (12).

$$\ell n\ \sigma_V = \frac{\ell n(\text{weight})_{84\%} - \ell n(\text{weight})_{16\%}}{2} \qquad (1)$$

This is a convenient method, but is limited by the accuracy with which the best-fit line is drawn on the graph. It is preferable to calculate $\ell n\ \sigma_V$ through the basic equation for the standard deviation, using the logs of the

grain weights:

$$\ell n\ \sigma_V = \left[\frac{\sum^{n} (\ell n\ W_i - \overline{\ell n\ W})^2}{n-1}\right]^{1/2} \qquad (2)$$

where $\ell n\ W_i$ is the logarithm of the weight of the i^{th} grain, $\overline{\ell n\ W}$ is the average of the logs of the weights of all grains, and n is the number of grains in the analysis. This method has been employed in the calculation of $\ell n\ \sigma_V$ for each specimen in this investigation.

The 95% confidence intervals for these values, calculated by the chi-square procedure, are listed in Table 1. Also supplied is the following weight and volume distribution information for each specimen:

N	- the number of grains analyzed
μ_W	- the mean grain weight
σ_W	- the standard deviation of the grain weights
$\ell n\ \sigma_W$	- the mean of the natural logs of the grain weights

Grain Growth, Deformation and Solidification Studies

Effect of grain growth

In Table 1, the 95% confidence intervals for $\ell n\ \sigma_V$ of samples T-6-1 and T-6-2 are seen to be $1.94^{+0.20}_{-0.16}$ and $1.89^{+0.15}_{-0.13}$, respectively. These samples were both deformed 6% in tension but were annealed for different lengths of

Table 1
Grain Weight and Volume Distribution Parameters

Specimen	N (grains)	$\mu_W \times 10^{-4}$ (gm.)	$\sigma_W \times 10^{-4}$ (gm.)	$\ell n\ \mu_W$	$\ell n\ \sigma_V$
C-1	177	55.6 ±12.3	$81.5\ ^{+\ 9.5}_{-\ 7.7}$	3.04±0.25	$1.66^{+0.19}_{-0.16}$
C-2	160	25.6 ± 5.6	$35.2\ ^{+\ 4.4}_{-\ 3.5}$	2.55±0.20	$1.32^{+0.17}_{-0.13}$
C-3	84	10.4 ± 1.5	$11.3\ ^{+\ 1.9}_{-\ 1.5}$	1.70±0.28	$1.29^{+0.22}_{-0.17}$
C-4	372	9.87± 1.40	$13.5\ ^{+\ 1.1}_{-\ 0.9}$	1.64±0.13	$1.22^{+0.09}_{-0.08}$
80-1	4930	–	–	–	$0.99^{+0.03}_{-0.01}$
T-3	92	326. ±93.	$445.\ ^{+72.}_{-58.}$	4.40±0.47	$2.29^{+0.37}_{-0.30}$
T-6-1	234	12.8 ± 3.6	$27.2\ ^{+\ 2.7}_{-\ 2.3}$	1.01±0.25	$1.94^{+0.20}_{-0.16}$
T-6-2	349	27.4 ± 4.9	$45.7\ ^{+\ 3.7}_{-\ 3.2}$	1.99±0.20	$1.89^{+0.15}_{-0.13}$
S-1	97	5.28±1.27	$6.26^{+\ 1.02}_{-\ 0.78}$	1.22±0.18	$0.91^{+0.15}_{-0.11}$
S-2	526	27.7 ±3.8	$44.0\ ^{+\ 2.8}_{-\ 2.5}$	2.23±0.14	$1.62^{+0.10}_{-0.09}$
S-3	252	355. ±9.6	$760.\ ^{+73.}_{-61.}$	3.50±0.32	$2.58^{+0.25}_{-0.21}$

time, producing a relatively large difference in grain size. The average grain weights are seen to vary by a factor of 2. Although $\ell n\ \sigma_V$ for the sample annealed the longest was slightly smaller than the other, there is no significant difference between them, each being well within the ranges of the other's confidence interval. This is consistent with Okazaki and Conrad's (5) finding of a constant size distribution width throughout grain growth. Despite the similarity of these findings, the values of $\ell n\ \sigma_V$ for T-6-1 and T-6-2 are over twice as great as those found by Okazaki and Conrad ($\ell n\ \sigma_V \simeq 0.84$).

Effect of prior deformation

The confirmation of the absence of an effect of grain growth on the size distribution simplified the following study. As described in the experimental procedure, specimens of high purity aluminum were deformed by different amounts before annealing, to test the effect of deformation on the grain size distribution after recrystallization. Figure (9) illustrates the comparison of $\ell n\ \sigma_V$ among the deformed specimens. The value of $\ell n\ \sigma_V$ is seen to decrease rapidly as the amount of deformation increases from 3% to 7%. Further deformation reduces $\ell n\ \sigma_V$ gradually. Although the samples represented in this figure came from several different groups, each

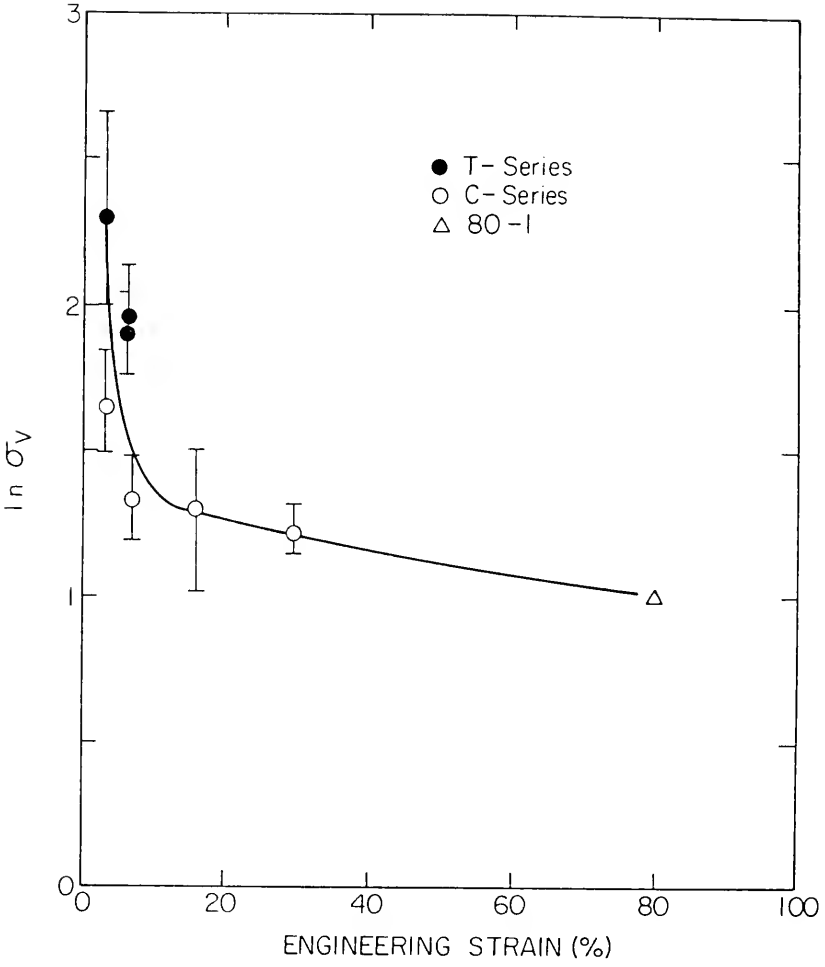

Figure (9). Width of the grain volume distributions of the C and T series specimens and specimen 80-1 versus engineering strain prior to recrystallization and grain growth.

group exhibits the same decrease of $\ell n\ \sigma_V$ with increased deformation.

The samples from the tension (T) series can be seen to have wider size distributions than those of the compression (C) series, at comparable deformations. This may be related to the fact that the starting material for the T specimens had received less initial breakdown processing then the C series, and possessed a more irregular microstructure than the C material.

Sample 80-1, described in Chapter III, was also analyzed and included in this figure. It received 80% compressive deformation in liquid nitrogen and was annealed for 20 sec. at 635°C. Except for the length of anneal and the starting material from which it came, specimen 80-1 was prepared in a manner similar to the specimens of the C series. Sample 80-1 has a lower value of $\ell n\ \sigma_V$ than any of the other specimens, in keeping with the trend of decreasing distribution width with increased prior deformation.

Figure (10) illustrates the same $\ell n\ \sigma_V$ data as shown in Fig. (9), plotted against true strain. Okazaki and Conrad's data for Ti are included here also. The decrease in $\ell n\ \sigma_V$ appears to be linear with increase in true strain, after the rapid initial drop at low strains.

Figure (10). Width of the grain volume distributions of the C and T series specimens, and those of Okazaki and Conrad (5) versus true strain prior to recrystallization and grain growth.

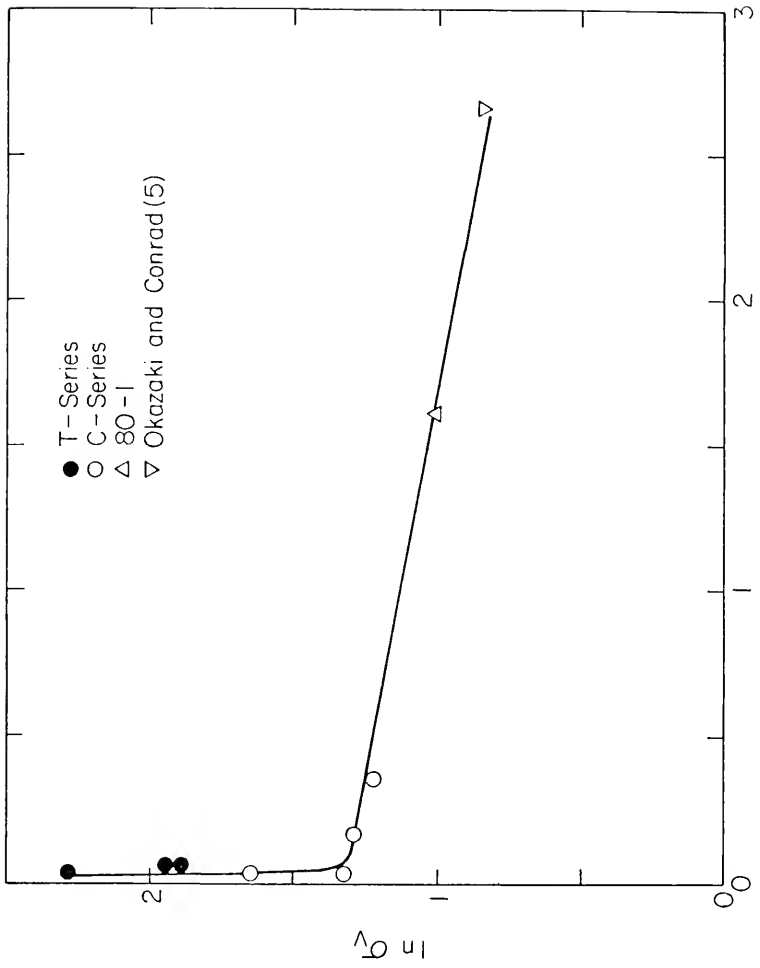
T-Series
C-Series
80-1
Okazaki and Conrad(5)
TRUE STRAIN
ln σv
0
1
2
3

Effect of solidification rate

Figure (11) illustrates the effect of solidification rate on the width of the resulting grain size distribution. The values of $\ell n\ \sigma_V$ have been plotted versus the time for complete solidification of the respective Al-10% Zn ingots, described in the experimental procedure. Since the ingot sizes varied, the time of solidification does not accurately represent the solidification rate. The time does provide some measure of rate, however, and the wide variation of the average grain weights given in Table 1, for these specimens, indicates that there was a noticeable variation in freezing rate.

In this figure, $\ell n\ \sigma_V$ is seen to increase steeply and continuously as the solidification rate decreases. The values of $\ell n\ \sigma_V$ are similar to those of the grain growth experiments, ranging from 0.91 to 2.58. From the form of the curve in this figure, it appears that $\ell n\ \sigma_V$ could be decreased still farther by an increased rate of solidification.

Discussion

Evolution of the Log-Normal Distribution

The results of this study raise the question of why grain size distributions which have evolved through such

Figure (11). Width of the grain volume distributions of the S series specimens versus time for solidification.

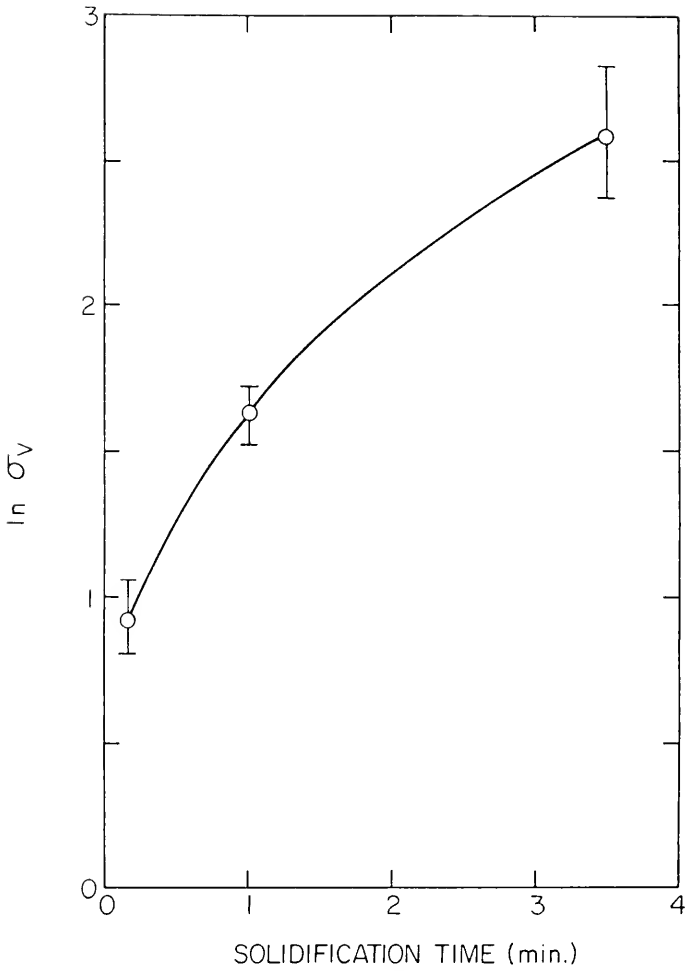
3
2
1
0
0
1
2
3
4
ln σ_v
SOLIDIFICATION TIME (min.)

a variety of processes should all be representable through the log-normal distribution. Several mechanisms by which this distribution may physically evolve have been described previously (23-25). Whereas the normal distribution may be thought of as the result of the additive effects of random events, the log-normal distribution results from effects which are multiplicative. These types of effects are common in nature and in fields such as economics (24), where the potential of an object for growth or decrease, through some stimulus, is often proportional to the immediate size of the object. Given an initial random distribution of sizes, repetitious stimulation eventually produces a skewed, log-normal distribution.

More explicitly, Kottler (25) has shown that particles which grow by an exponential law, possess a log-normal distribution of sizes if their nucleation times are distributed normally. If volume, V, is related to the time of growth, t, by Eq. (3),

$$V = A\, e^{kt} \tag{3}$$

where A and k are constants, then $\ell n\ V$ is proportional to t, i.e.

$$\ell n\ V = \ell n\ A + kt \tag{4}$$

As described in the experimental results, a normal distribution of $\ell n\ V$ infers a log-normal distribution of V.

Constant increase in grain diameter with time, which has been observed during the recrystallization of aluminum (26-27), may also lead to a log-normal distribution of grain sizes if the nucleation times are log-normal. Bell-shaped distributions of nucleation times during recrystallization have been observed by Anderson and Mehl (26). This behavior should not be uncommon among processes such as solidification and recrystallization, in which the volume fraction of untransformed material, in which nuclei may form, decreases continuously with time.

Variation of the Distribution Width

From the above arguments, the observed variability of the width of the size distribution may be explained by variation in the proportional width of the distribution of nucleation times. In this study, the experimental conditions which increased the rates of solidification and of recrystallization also tended to decrease the width of the resulting size distribution. If the combined result of increased rates of nucleation and growth produced distributions of nucleation times with narrower standard deviations, relative to their means, then the widths of the resulting grain size distributions would also be narrower.

Another reasonable explanation for the variation in $\ln \sigma_V$ is the variation of the degree of randomness in

position of the recrystallization or solidification nuclei. Recrystallization has been observed to occur by several different modes, which are typically heterogeneous at low deformations. These include strain-induced boundary migration (28), site-saturated grain edge nucleation (27), and subgrain growth (29). The degree of activity of the different modes are generally related to the degree of deformation and the recrystallization temperature (30). It is not uncommon for these mechanisms to result in clustered rather than random nucleation. The impingement resulting from the growth of clustered nuclei restricts the size of some grains while allowing others to grow unhindered to larger sizes. It is quite probable that such behavior could produce a broader final size distribution than would occur after random nucleation. Solidification also often involves heterogeneous nucleation, which could produce clustering similar to that in recrystallization.

The dislocation structure of deformed aluminum has been observed to change from random tangles, at ∿5% deformation, to a cellular subgrain structure, at deformations of 10% and greater (31). As the deformation increases, the misorientation between neighboring subgrains, and their potential for becoming nuclei increases.

Greater numbers of other sites also become more capable of being active. As the number of nuclei within a given volume increases, they necessarily become closer together. The distance separating any two active nuclei, however, is limited by the scale of the substructure of the material. A depletion of the local driving force for nucleation may also inhibit the formation of nuclei in the immediate vicinity of those which are already present.

Similarly, in solidification, the number of nuclei which form within a given volume of liquid increases with the degree of undercooling. Here again, there is a critical size below which a solidifying grain will not form without remelting. This effectively produces a limit at the small-size end of the resulting distributions. Rhines (32) has hypothesized that such ordering of the nuclei, the opposite extreme from clustering, should tend to decrease the width of the final grain size distribution.

Model of Ordering of Nuclei

To enable a study of the effect of ordering, a simple model of nucleation and growth, in which the positions of the nuclei could be progressively randomized or ordered, has been employed in the present research. The

two-dimensional Meijering cell model (14) is based upon instantaneous nucleation on a plane, followed by the growth of all cell boundaries at equal, constant rates, until impingement. The resulting microstructure contains only straight cell boundaries.

Completely ordered nucleation was modeled by placing nuclei on all of the points of line intersection on a piece of square-grid graph paper. The resulting cells were constructed by drawing the perpendicular bisectors of the imaginary lines connecting each pair of nearest-neighbor nuclei. The resulting structure, shown in Fig. (12a), consisted totally of equisized, square cells, with central nuclei.

Other structures [Figs. (12b)-(12d)] with progressively greater degrees of randomness were constructed by decreasing the probability of any given grid intersection containing a nucleus. Using dice and tables of random numbers, arrays of nuclei were generated on the square-grid paper with probabilities, P, of 1, 0.975, 0.95, 0.888, 0.75, 0.5, 0.333, 0.2, 0.05 and 0.01. The cell boundaries were constructed and the area of each cell, remote from any effects of the boundary of the array, was determined from the number of squares on the graph paper which were included within it.

Figure (12). Effect of ordered nucleation on the resulting cell structure of the two-dimensional Meijering cell model. (a) Complete ordering—the nuclei are as close together as possible and the cells are unisized. (b) Lower probability of nucleation allows the nuclei to be farther apart, allowing greater variation in cell size. (c) Nuclei are still farther apart, the presence of the limiting nuclei distance is still apparent in the cell size distribution. (d) Low probability of nucleation—the average distance between nuclei is great enough to allow them to be positioned at random.

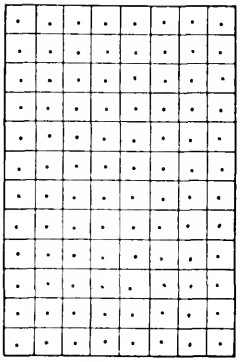

P = 1

(a)

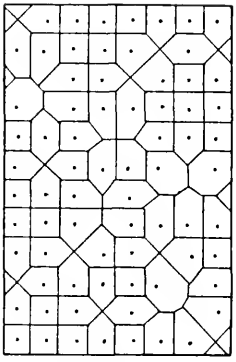

P = 0.75

(b)

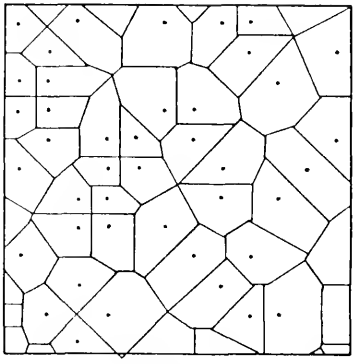

P = 0.333

(c)

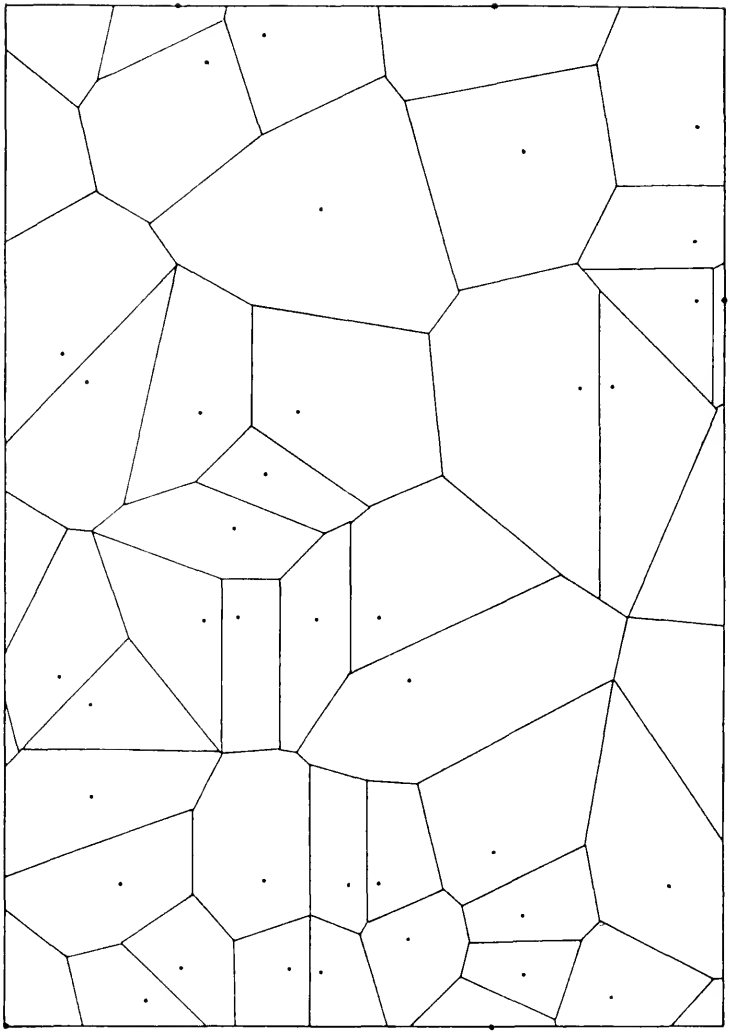

(d)

The mean (μ) and standard deviation (σ) of the individual size distributions were then calculated. As in real nucleation and growth processes, μ and σ became smaller as the density of nuclei increased. To facilitate comparison among the distributions, they were normalized with respect to average cell size through the calculation of their coefficient of variation (C.V. = σ/μ). The values of C.V. for the distributions of various values of P are listed below.

Number of cells analyzed	P (probability)	C.V.
-	1	0
192	0.972	0.070
187	0.950	0.095
173	0.888	0.145
201	0.750	0.213
126	0.500	0.332
147	0.333	0.426
166	0.200	0.466
64	0.050	0.529
129	0.010	0.502

Figure (13) illustrates the monotonic increase in C.V. as P decreases. When P = 1, C.V. = 0. As the nuclei become farther apart, the impingement of the cells becomes more random, increasing the variation of cell sizes present, and increasing C.V. At P = 0.05, the theoretical (15) value of C.V. = 0.529, for random

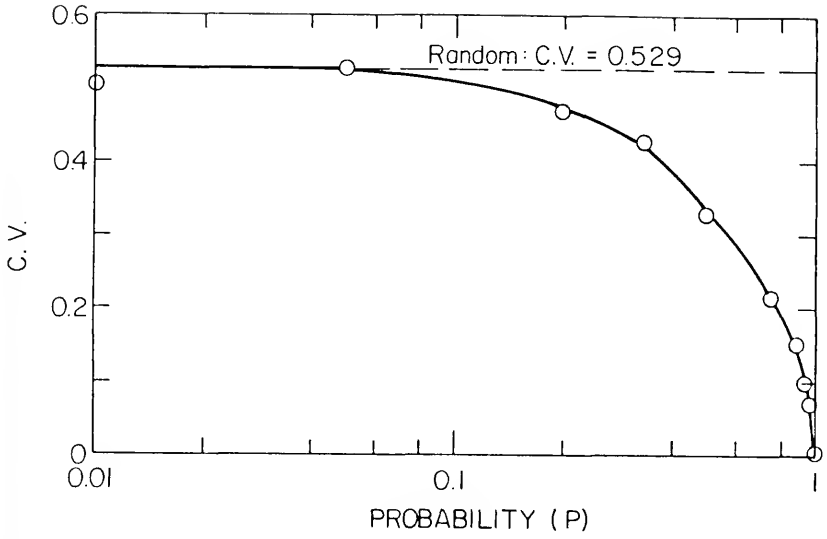

Figure (13). Probability of nucleation at a given point versus the coefficient of variation of the two-dimensional cell size distribution.

nucleation, is attained. In this structure, only 5% of the grid points possess a nucleus, and the distribution of nuclei is as random as if the grid did not exist. It is of interest that such a high degree of separation of the nuclei, in relation to the scale of the ordering features, is required to remove all effects of ordering from the final size distribution. A similar model of ordering, constructed in three dimensions, would undoubtedly indicate a similar decrease in C.V. with ordering. These results lend support to the hypothesis that ordering of the nuclei within a solidifying or recrystallizing metal decreases the width of the resulting size distribution.

Gilbert (15) has also calculated the theoretical means and variances of the three-dimensional Johnson-Mehl (J-M) and cell models. From these, the following values of C.V have been obtained.

	Model	
	J-M	Cell
C.V.	1.07	0.42

For comparison, the values of C.V. have been calculated for several of the present samples which exhibited extremely wide or narrow size distributions.

	Specimen		
	S-1	S-3	C-4
C.V.	1.19	2.14	1.37

Comparison of the theoretical and experimentally obtained values of C.V. indicates that the size distributions generated by the random cell model are excessively narrow. In Fig. (11), however, it appears that the cast distribution may become still narrower with increased solidification rate. The value (15) of C.V. = 1.07 for the J-M model (15,33) (constant rates of nucelation and growth) is more realistic, although it is also lower than the experimental values. These models may be too simple to describe complex nucleation behavior.

It appears that the effects of ordering and clustering of nuclei, controlled here through the amount of deformation prior to solidification and recrystallization, may be the cause of the variation in distribution width, observed in this study.

Distribution Behavior During Grain Growth

The invariant behavior of $\ell n\ \sigma_V$ during grain growth is illustrated in Fig. (14), through the data of Okazaki and Conrad (5) and samples T-6-1 and T-6-2. The constancy of the slopes of the lines within each set of samples reflects the similarity in the values of $\ell n\ \sigma_V$, shown in Table 1. This type of behavior implies that the normal distributions of the logs of the grain weights retain

Figure (14). Log-normal plots of the grain volume data of Okazaki and Conrad (5) and of specimens T-6-1 and T-6-2. The slopes remain constant within each group as the average grain volume increases with grain growth.

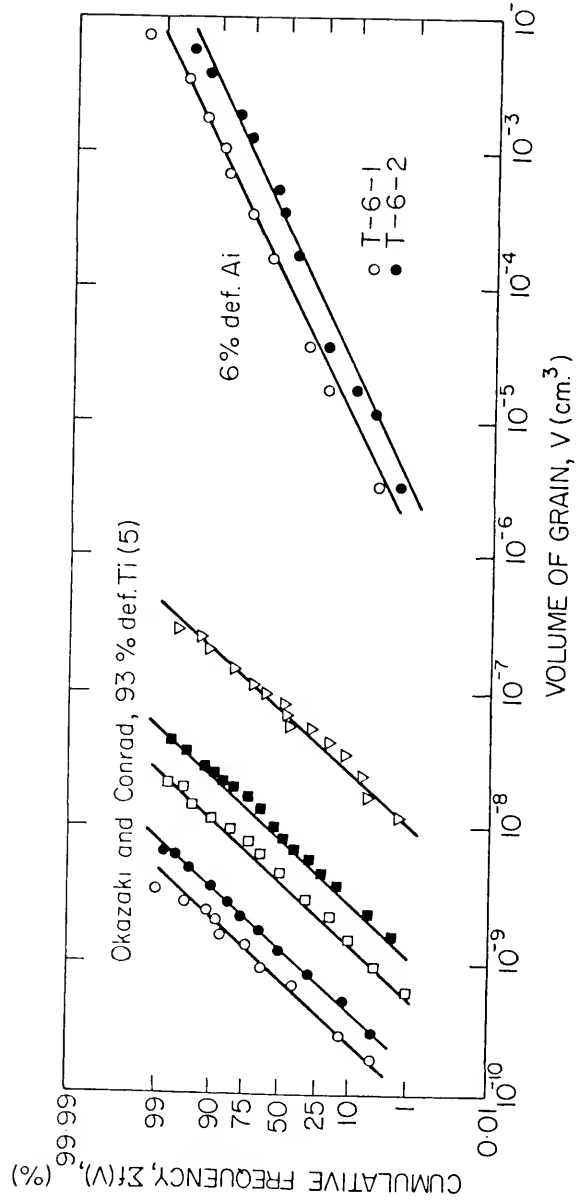
CUMULATIVE FREQUENCY, Σf(V), (%)
99.99
99
90
75
50
25
10
1
0.01
10^-10
10^-9
10^-8
10^-7
10^-6
10^-5
10^-4
10^-3
10^-2
VOLUME OF GRAIN, V (cm.^3)
Okazaki and Conrad, 93 % def. Ti (5)
6% def. Ai
T-6-1
T-6-2

their form during grain growth, with only their mean value being displaced to larger values. The skew distributions of the actual grain weights do become more spread as growth progresses. These two representations of the process are shown schematically in Figs. (15a) and (15b).

The variability in $\ell n\ \sigma_V$, observed within this study is in conflict with the prediction of Hillert (17), whose model of grain growth as a coarsening process predicts the asymptotic approach of the grain size distribution towards a constant final form. Figure (16) illustrates the comparison of the data of sample C-4 to Hillert's theoretical distribution of volumes. Even though this specimen has been annealed extensively, and also possesses a relatively narrow grain size distribution, its form is wider and more skewed than that predicted by Hillert.

One further implication of the log-normal distribution of grain volumes is that the distribution of volume fractions occupied by the various size classes is also log-normal, with the same logarithmic standard deviation as the size distribution (34). This is illustrated in Fig. (17), using the data of Hull (6). The line on the left represents the volumes of the separated

Figure (15). (a) The form of the normalized distribution of the logarithms of the grain volumes remains constant throughout grain growth. (b) The skewed distribution of grain volumes becomes more spread as grain growth progresses.

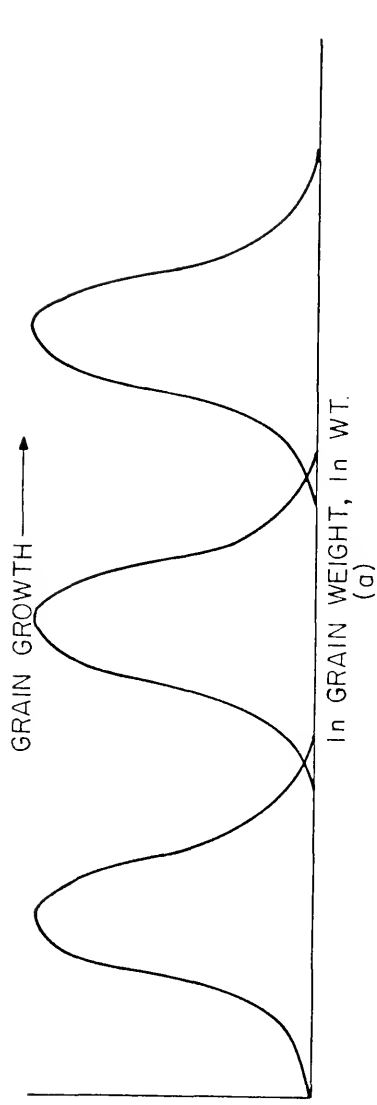
FREQUENCY, f(ln WT)
GRAIN GROWTH
ln GRAIN WEIGHT, ln WT.
(a)

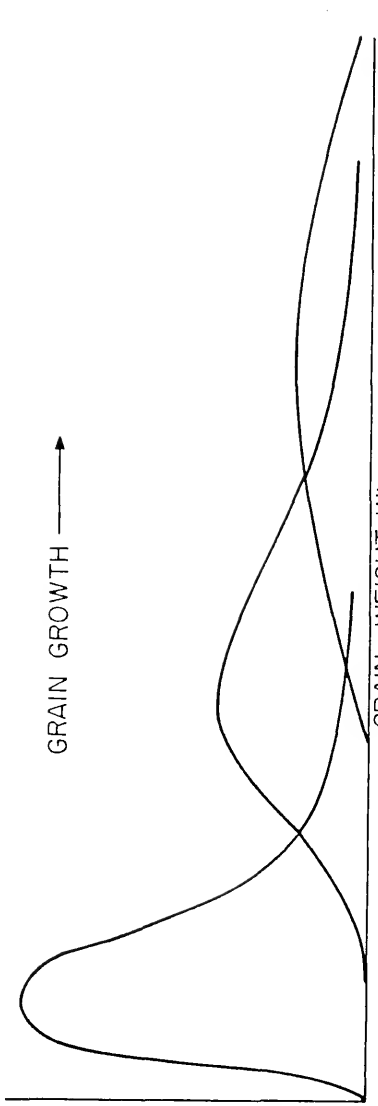
FREQUENCY, f(WT)
GRAIN GROWTH
GRAIN WEIGHT, Wt.
(b)

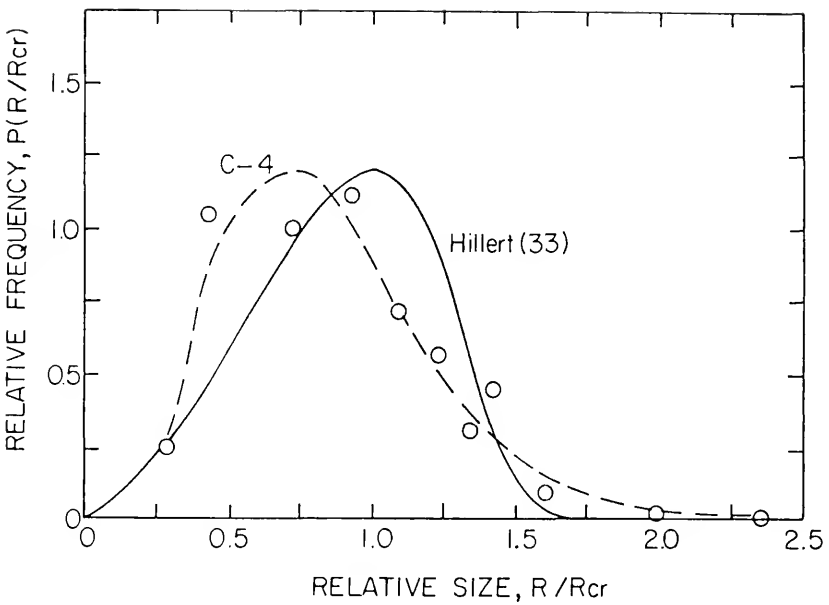

Figure (16). Comparison of the grain size distribution determined experimentally after 20.5 hours of grain growth and the theoretical distribution predicted by Hillert's (17) model. The grain radii, R, have been calculated from the weight data. $R_{cr} = 9/8\ \bar{R}$, where $\bar{R}$ is the average grain radius.

Figure (17). Log-normal plot of the grain volume data calculated for β-brass grains separated by Hull (6). The volume fractions of the various sized grains also plot log-normally.

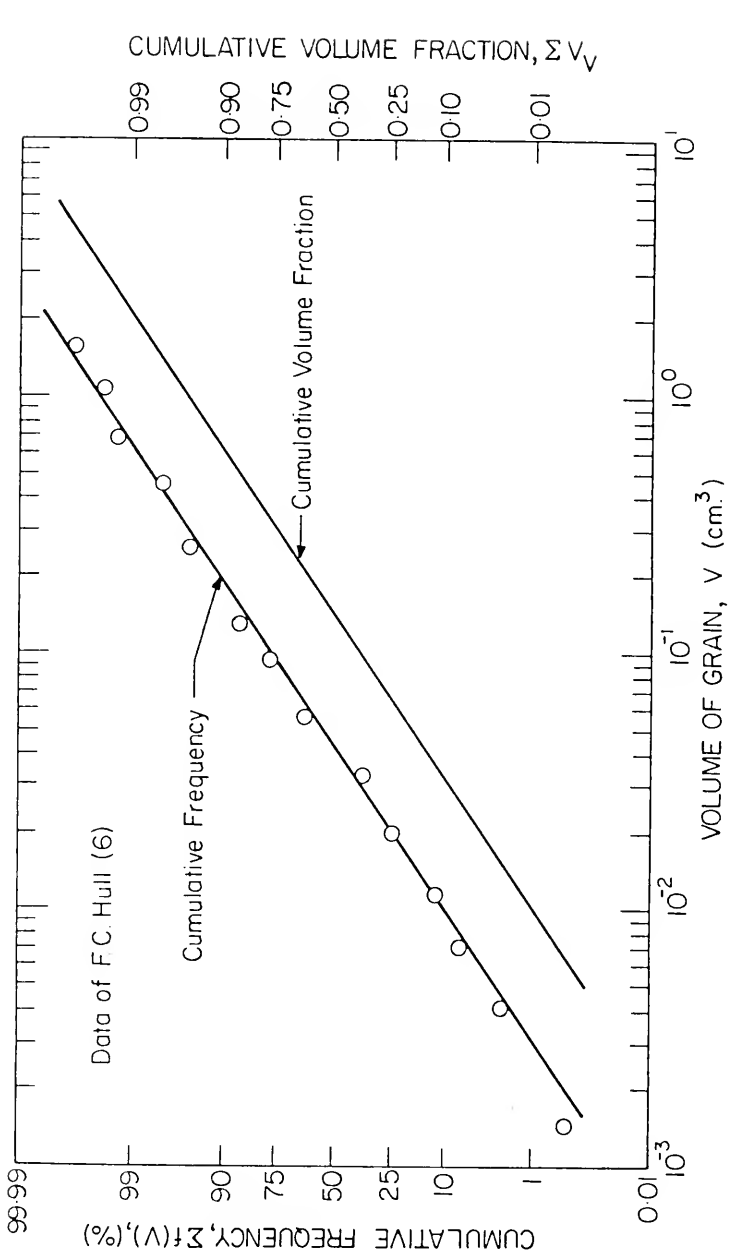
CUMULATIVE VOLUME FRACTION, Σ V_V
0·99
0·90
0·75
0·50
0·25
0·10
0·01
Cumulative Volume Fraction
Cumulative Frequency
Data of F.C. Hull (6)
CUMULATIVE FREQUENCY, Σ f(V), (%)
99·99
99
90
75
50
25
10
1
0·01
10^-3
10^-2
10^-1
10^0
10^1
VOLUME OF GRAIN, V (cm.^3)

grains, calculated from their sieve dimensions. The value of $\ell n\ \sigma_V$, calculated graphically from this line, is 1.12. The data to the right represent the calculated cumulative volume fraction of the specimen occupied by grains smaller than or equal to the various grain sizes given on the abscissa. The value of $\ell n\ \sigma_V$ for these data is also $\sim$1.12.

Comparison of the two lines indicate that 50% of the specimen was occupied by the largest 15% of the grains, while the smaller 50% of the grains occupy only 15% of the total volume. Given a broader size distribution, an even smaller percentage of grains would occupy the major part of the specimen volume. Thus, properties which are related to grain volume will be strongly influenced by only the few largest grains in a material. In this case, the behavior of the material may be unpredictable from the value of the mean grain intercept since it is only slightly influenced by the overall size distribution.

CHAPTER II
DISTRIBUTION OF TOPOLOGICAL FEATURES

Introduction

The distributions of the topological features of a polycrystalline aggregate are of fundamental microstructural interest. This chapter will investigate the frequency distributions of the number of faces per grain (F_G) and edges per grain face (E_F), which theoretically are related to the grain size distribution. If this relationship does exist, the results of Chapter I would further imply variability of the topological state with processing. The distributions of F_G and E_F are also fundamentally related to the grain growth process. Since grain annihilation requires the presence of tetrahedral grains and triangular faces, their relative frequencies resulting from the overall forms of the distributions, should affect the rate of grain growth.

The topological rules obeyed by soap films, grain boundaries and other surface tension controlled networks were first put forth in 1866 by Plateau (35). Twenty-one years later, Thomson (36) determined that the one body capable of filling space through its own repetition, while

meeting these requirements, was a 14-sided figure which he called the "minimal tetrakaidecahedron." This figure, averaging $5\frac{1}{7}$ edges per face, has ever since been considered an average or model grain shape. All topological studies of space-filling cells performed to date have, in fact, yielded average values of F_G and E_F very close to 14 and $5\frac{1}{7}$, although they include individual grains and faces which deviate widely from these values.

In 1919, Desch (19) was the first to study the topological nature of metal grains. Using mercury to separate the grains of a β-brass casting, he determined the average value of F_G for 30 grains to be 14.5 and counted the numbers of edges of their faces. Finding 5-edged faces to be the most frequent, he suggested that the shapes of grains were generally more similar to pentagonal dodecahedra than to Thomson's (36) figure. On analyzing soap and gelatin foam structures, he found close similarities and concluded that the shapes of metal grains were the result of surface tension.

In 1923, Lewis (37) began an extensive series of studies of topological shapes, primarily of plant and animal tissue cells. Joined by others (38-40), these investigations continued for 30 years. Of these studies, only those few involving aggregates of soap bubbles were

strictly comparable to surface tension controlled grain boundaries, although the results from the other studies were generally similar.

A principal interest of these and many later studies was the determination of a cell form possessing the average topological properties of the aggregate. Distributions of E_F were typically found to be normal in shape with the maximum at 5. Tetrakaidecahedral cells, possessing 6 quadrilateral and 8 hexagonal faces, were found only rarely. These results again tended to support the pentagonal dodecahedron as the archetype cell. Williams (41) later developed a variation of Thomson's cell which possessed a predominance of pentagonal faces, the β-tetrakaidecahedron, which he proposed as the ideal space-filling cell.

The studies by the biological group continued to the time of C. S. Smith's (8) reintroduction of topology to microstructural consideration. He realized that the grain boundary network was governed by the rules of Euler (42) and Plateau (35), and that as a result, grain growth was restricted to a certain sequence of events. He also pointed out the relation of the relative size of neighboring grains to their topological complexity, face curvature, and potential for growth or shrinkage, and

suggested that a fixed distribution of sizes and topological shapes might evolve during grain growth.

Williams and Smith (7) employed stereoscopic microradiography to visualize the grains of an Al-Sn alloy in situ. They observed 92 grains possessing from 6 to 23 faces, averaging 12.48. The grain faces ranged in complexity from 2 to 9 edges, averaging 5.02. Their distribution of E_F was very similar to those previously found, with a mode of 5. Their distributional results may not have been truly representative of the topological state of a network experiencing grain growth, since no tetrahedral grains were found. This may have been due to the loss of small grains in the formation of a second phase along the grain edges.

In 1953, Meijering (14) calculated the average numbers of faces, edges and corners of cells formed by two different theoretical models of nucleation and growth. His "cell model"—which assumed instantaneous nucleation and a constant growth rate—predicted an average F_G of 15.54, more complex than that usually found experimentally. The more realistic Johnson-Mehl model was calculated to have an average F_G of >13.28. Through another statistical approach, Coxeter (43) calculated a theoretical average F_G of 13.56 for compressed equisized spheres.

Hull (6) observed over 900 grains from a disintegrated β-brass casting. His observation that the average number of faces per grain and edges per face on individual grains increased with the size of the grain was similar to that found by other investigators.

The topological data presented by Okazaki and Conrad (5) in their previously mentioned serial section investigation contain a predominance of complex shapes, indicating that in sectioning they may have overlooked some smaller, more simple grains.

The frequencies of the numbers of edges on two-dimensional grain sections have been measured in numerous studies (4). This information is, however, more related to the distribution of grain sizes than the three-dimensional topological properties affecting grain growth.

Steele (10,44) derived equations relating the rates of occurrence of various events, required for grain growth, to the average topological properties. He showed that under certain conditions it is possible for the average topological grain shape to remain constant throughout grain growth. Steele and Summers (45) later obtained a distribution of E_F for recrystallized aluminum from observation of grains exposed after gallium penetration and fracture.

Craig (18), Rousse (46), and Steele (47) developed serial section techniques for the experimental measurement of the average values of F_G, E_F, and corners per grain (C_G). In 1974, Rhines and Craig (9) demonstrated for the first time, the behavior of these properties throughout grain growth. The values of these properties were seen to increase rapidly with initial growth to very near 14, 36 and 24, respectively, per separate grain. They then remained essentially constant. This implied that the average topological shape remained constant throughout a major part of the growth process, and gave significance to Steele's (10,44) equations. They also presented histograms of the distribution of F_G indicating that it also remained constant throughout growth.

Rhines and Craig (9) described the grain growth process in terms of the fundamental event of the disappearance of triangular faces. This loss removes edges from other faces, reducing their complexity until they become triangular and disappear, advancing the grain by one step in its progression towards annihilation. Joint loss of faces from large and small grains maintains the steady state distribution of F_G and, presumably, E_F.

Although there are sound theoretical relationships between the topological state, grain growth, and the grain

size distribution, there is very little related experimental data by which they may be tested. This chapter will further explore these relationships through the measurement of the topological distributions of the specimens analyzed in Chapter I. Using the same grain separation technique as outlined there, the numbers of faces and edges have been obtained by direct microscopic observation. The resulting distributions have then been compared with the corresponding grain size distributions and histories of deformation and grain growth.

Experimental Procedure

Material

The C series (compressed) and T series (tensile) specimens from the size distribution studies of Chapter I were employed in this investigation of the distribution of topological features. This enabled the investigation of the topological nature of metals over a range of conditions of deformation, recrystallization, and grain growth. The cast specimens (S series) were not examined in this study since the facets on their grains could not be easily distinguished.

Observation of Topological Features

Whole grains, separated with gallium as described in Chapter I, were examined individually to determine their

numbers of faces and the numbers of edges of their faces. As before, the grains were initially removed from the samples in clusters, which were then further separated and cleaned.

Observing the grains through a low power binocular microscope, the entire surface of each was mapped through the drawing of its Schlegel diagram (48). As illustrated in Fig. (18), for grains of different complexities, this is a simple sketch which enables one to visualize the three-dimensional arrangement of faces and edges, on a two-dimensional graph. The outer, surrounding line on the diagram represents the face on the backside of the grain. The total number of faces on each grain, and the numbers of edges on each face, were then recorded. Analysis of these data yielded information about the distributions of E_F and F_G.

Approximately 100 grains were separated from each of the T series specimens, allowing the investigation of both their E_F and F_G distributions. Only 10 to 20 grains were analyzed from each of the C series specimens. This provided adequate numbers of faces for the study of the E_F distribution, but the F_G distribution was not determined for these samples.

Figure (18). Schlegel diagrams for two grains of different topological complexities.

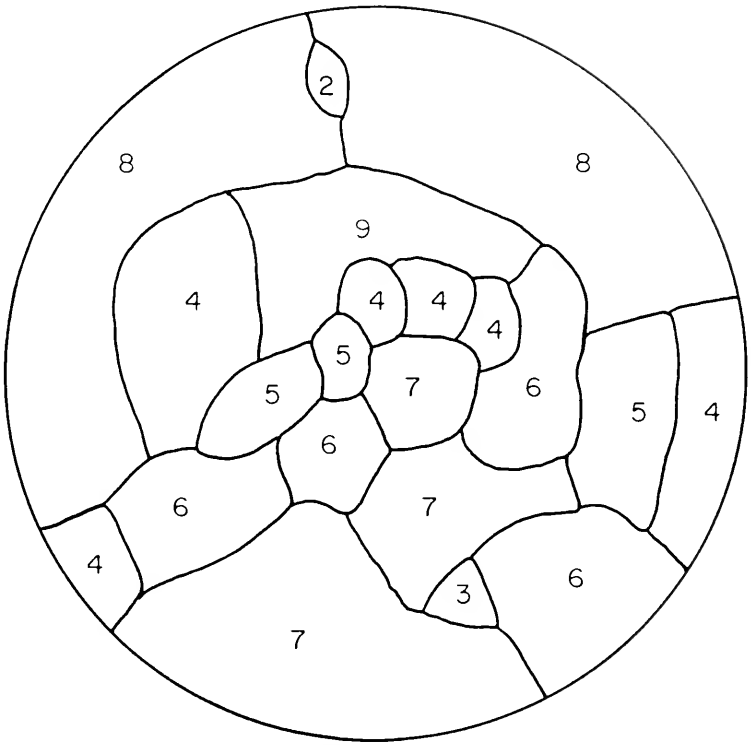

BACK = 6
22 FACES

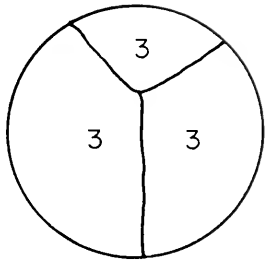

BACK = 3
4 FACES

Experimental Results

The E_F and F_G data from the samples of the C and T series, analyzed in this investigation, are given in Appendices B and C, respectively. Faces were observed with numbers of edges ranging from 2 to 26. The portion of faces with more than 8 edges was generally less than 5% of the total for any sample. The number of faces per grain was found to vary from 3 to 59, with only 5% of the grains having more than 30 faces.

The forms of the frequency distributions of E_F and F_G were typified by the histograms of Figs. (19) and (20), representing the data for specimen T-6-1. These, like the size distributions, are simple unimodal distributions, skewed towards the larger values. As can be seen from the data in Appendix B, the modes of the E_F distributions for the various samples were almost always at 4, rather than the normally observed (8) value of 5. The difference in the percentage of 4- and 5-edged faces was, however, usually small.

Figures (21) and (22) illustrate log-normal plots of the E_F and F_G data from sample T-6-1. The strong linearity of these plots indicate that they, like the size distributions, tend to approximate the log-normal distribution. The "χ^2 test of the degree of fit" has

Figure (19). Frequency histogram of the numbers of edges per grain face, specimen T-6-1.

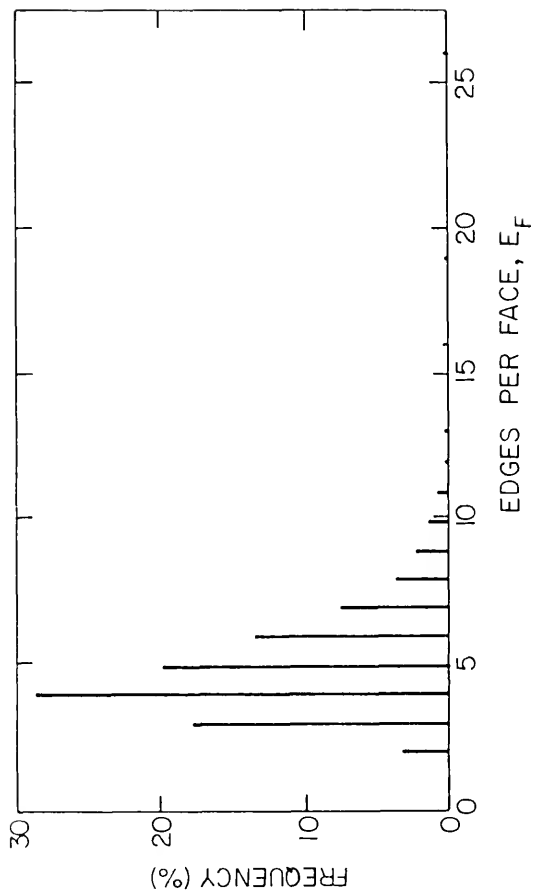
FREQUENCY (%)
30
20
10
0
0
5
10
15
20
25
EDGES PER FACE, E_F

Figure (20). Frequency histogram of the number of faces per grain, specimen T-6-1.

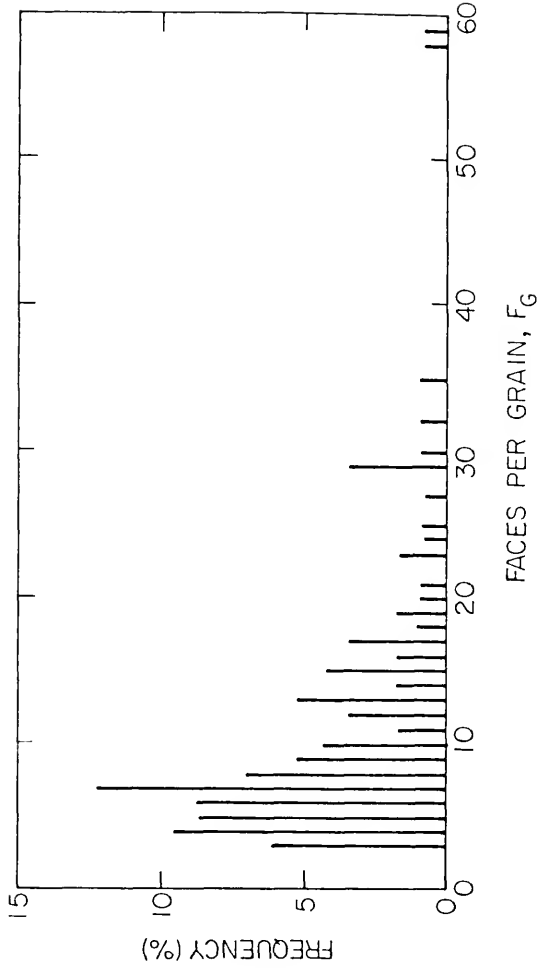
FREQUENCY (%)
0
5
10
15
0
10
20
30
40
50
60
FACES PER GRAIN, F_G

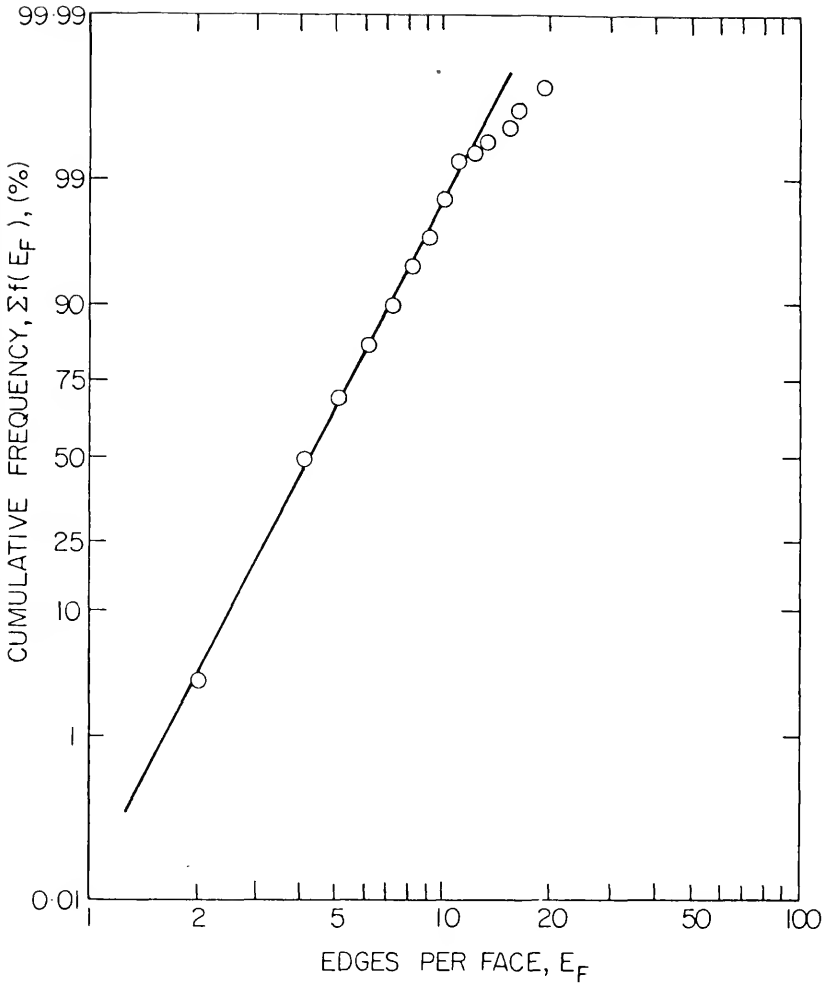

Figure (21). Log-normal plot of the numbers of edges per grain face, specimen T-6-1.

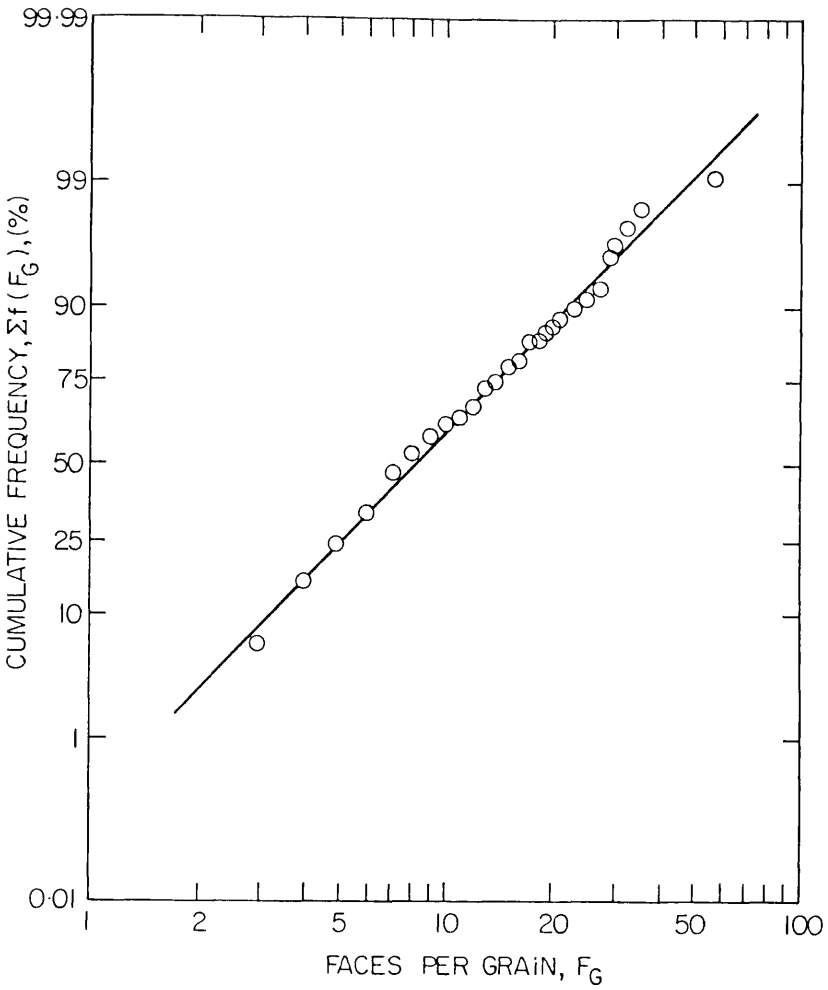

Figure (22). Log-normal plot of the numbers of faces per grain, specimen T-6-1.

confirmed this comparison at significance levels as high as 60% for the F_G distributions and >90% for the E_F distributions. This representation of the topological distributions through the log-normal distribution has not been done previously.

One benefit of this consideration is the representation of the widths of these distributions through the standard deviation of the normalized distribution of the logarithms of the values of E_F and F_G. These parameters will be referred to as $\ell n\ \sigma_E$ and $\ell n\ \sigma_F$, respectively. The usefulness of $\ell n\ \sigma$ for the comparison of distributions has been demonstrated in Chapter I. The values of $\ell n\ \sigma_E$ and $\ell n\ \sigma_F$ may be obtained through Eqs. (1) or (2), using values of E_F and F_G, rather than grain weights. Tables 2 and 3 list the calculated values of these and other parameters of the E_F and F_G distributions.

The values of $\ell n\ \sigma_E$ and $\ell n\ \sigma_F$, for the various samples, were calculated from Eq. (2), and their 95% confidence intervals were obtained using the χ^2 method, as was done in Chapter I. Other parameters included in the tables are:

N	- The numbers of grains or faces observed for each specimen
$\mu_{E,F}$	- the mean value of E_F or F_G

Table 2
Edges Per Face-Distribution Parameters

Sample	N (faces)	μ_E (edges)	σ_E (edges)	$\ell n\ \mu_E$	$\ell n\ \sigma_E$
C-1	143	4.96±0.25	$1.48^{+0.20}_{-0.15}$	1.56±0.05	$0.29^{+0.04}_{-0.03}$
C-2	172	4.85±0.17	$1.17^{+0.14}_{-0.11}$	1.55±0.04	$0.24^{+0.03}_{-0.02}$
C-3	272	5.10±0.15	$1.26^{+0.12}_{-0.09}$	1.60±0.03	0.25±0.02
C-4	171	5.01±0.16	$1.05^{+0.13}_{-0.10}$	1.59±0.03	$0.20^{+0.03}_{-0.02}$
T-3	1304	5.12±0.11	2.00±0.08	1.56±0.02	$0.37^{+0.02}_{-0.01}$
T-6-1	1303	4.96±0.11	2.02±0.08	1.53±0.02	0.36±0.01
T-6-2	1903	5.10±0.08	$1.70^{+0.06}_{-0.05}$	1.58±0.01	0.32±0.01

Table 3
Faces Per Grain-Distribution Parameters

Sample	N (grains)	μ_F (faces)	σ_F (faces)	$\ell n\ \mu_F$	$\ell n\ \sigma_F$
T-3	94	13.9±2.0	$9.50^{+1.52}_{-1.23}$	2.42±0.14	$1.66^{+0.11}_{-0.08}$
T-6-1	115	11.7±1.8	$9.66^{+1.44}_{-1.10}$	2.21±0.13	$0.68^{+0.10}_{-0.08}$
T-6-2	144	13.4±1.3	$7.96^{+1.05}_{-0.82}$	2.45±0.09	$0.54^{+0.08}_{-0.05}$

$\sigma_{E,F}$	- the standard deviation of the skewed distribution of E_F or F_G
$\ell n\ \mu_{E,F}$	- the mean of the natural logarithms of the individual values of E_F and F_G

The 95% confidence intervals for these parameters are also provided.

Figure (23) illustrates the relationship of $\ell n\ \sigma_E$ to the amount of deformation received before recrystallization and grain growth. The relative width of the E_F distribution decreases rapidly as the tensile or compressive deformation increases from 3% to ∿6%. The rate of decrease of $\ell n\ \sigma_E$ becomes less with increasing deformation. This is the same behavior that was seen to be exhibited by the grain size distribution in the investigations of Chapter I. As with the size distributions, the width of the E_F distribution is greater for the T series specimens than for those of the C series, at comparable deformations.

The values of $\ell n\ \sigma_F$, the width of the F_G distribution, given in Table 3, also exhibit a general decrease in value with increased prior deformation. The analysis of the behavior of $\ell n\ \sigma_F$ is restricted due to the lack of extensive data pertaining to large deformations.

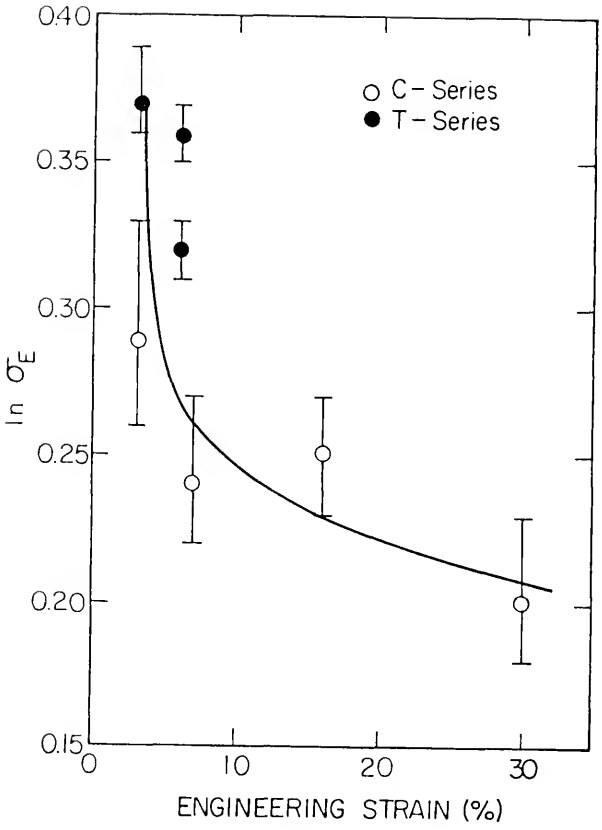

Figure (23). Width of the distribution of edges per grain face versus engineering strain prior to recrystallization and grain growth.

An apparent relationship among $\ell n\ \sigma_V$, $\ell n\ \sigma_E$, and $\ell n\ \sigma_F$ is illustrated in Fig. (24). The values of $\ell n\ \sigma_E$ and $\ell n\ \sigma_F$ are both seen to increase linearly with $\ell n\ \sigma_V$. Matzke's (39) data, for an array of equisized soap bubbles, and the datum of Williams and Smith (7), for metal grains, have been included to extend the range of observation. Their findings support the trends exhibited by the present data very well. There is thus strong evidence supporting the hypothesis that the widths of the topological distributions are proportionally related to the width of the grain size distribution.

An interesting, though slight, deviation is exhibited by samples T-6-1 and T-6-2. Although $\ell n\ \sigma_V$ remained constant over a period of grain growth in these specimens, $\ell n\ \sigma_E$ and $\ell n\ \sigma_F$ decreased noticeably [see also Fig. (23)]. This may be due to adjustment of the topological state of the material during early grain growth, with an increase in μ_F and μ_E (see Tables 2 and 3) as observed by Rhines and Craig (9).

The average values (μ) of E_F and F_G, given in Tables 2 and 3, are slightly less than the theoretical ones of $5\frac{1}{7}$ and 14, for the tetrakaidecahedron. They are similar to those which have been calculated theoretically and measured experimentally for space-filling cells by

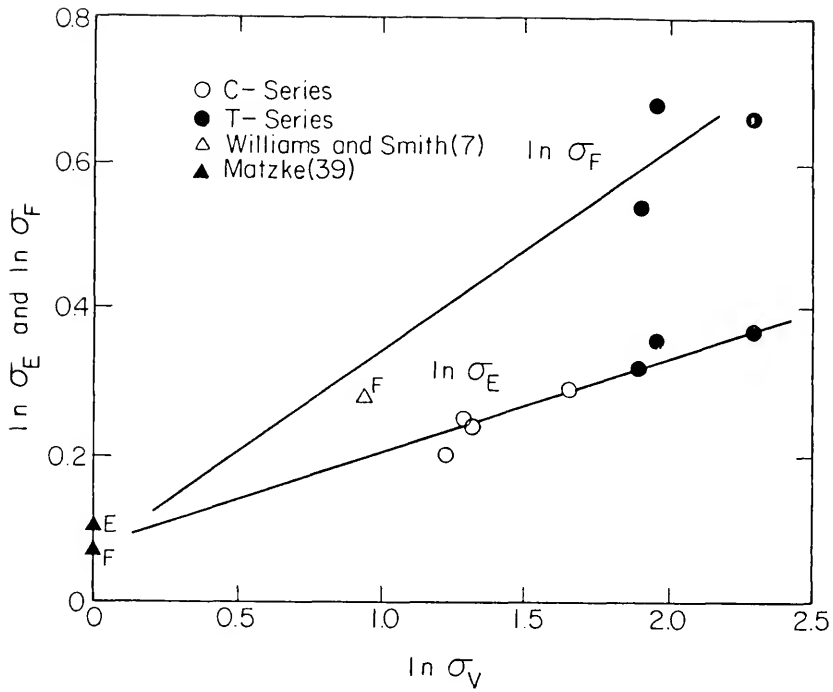

Figure (24). The widths of the distributions of faces per grain and edges per face versus the width of the grain volume distribution.

other investigators (7,9,19,45,46). The degree of experimental uncertainty in their values, however, presents the observation of their relation to $\ell n\ \sigma_V$, which exists theoretically. The values of σ_E and σ_F do decrease with increasing deformation, similar to $\ell n\ \sigma_E$ and $\ell n\ \sigma_F$.

Also of interest, in relation to the topological model of grain growth (8-10), were the proportions of 3-edged faces among the various samples. These features are required for grain growth to occur, and their frequency should thus be related to the potential rate of grain growth of a material. Figure (25) illustrates a 10-fold decrease in the presence of these faces, from 21% to 2%, as the amount of deformation prior to recrystallization increased from 3% to 30%. These data are listed in Table 4. The proportions of 4-faced grains, also required for grain growth, are seen in this table to vary noticeably among the specimens.

Figures (26) and (27) illustrate the relationships between the frequencies of these features and the widths of their respective distributions. The data from the present samples and that of other investigators (7,19,38, 39,45) exhibit a strong correlation between the fractions of 3-edged faces and $\ell n\ \sigma_E$, and also between the fractions of 4-faced grains and $\ell n\ \sigma_F$. Marvin's (38) E_F datum, for

Table 4
Relative Frequencies of 3-Edged Faces and 4-Faced Grains

Sample	Percentage of faces with 3 or fewer edges	Percentage of grains with 4 or fewer faces
C-1	15.4 (14.7-0.7)*	–
C-2	8.7	–
C-3	6.6	–
C-4	2.3	–
T-3	20.1 (17.3-2.8)	8.5 (5.3-3.2)**
T-6-1	21.1 (17.9-3.2)	15.7 (9.6-6.1)
T-6-2	14.7 (14.0-0.6)	4.2

*The percentages of faces with 3 edges and 2 edges, respectively, are given within the parentheses; i.e. (3E-2E).

**The percentages of grains with 4 faces and 3 faces, respectively, are given within the parentheses, i.e. (4F-3F).

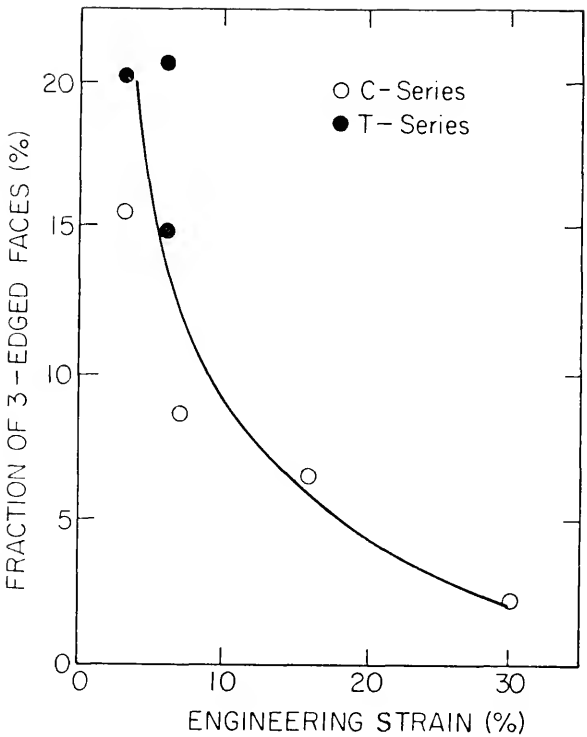

Figure (25). Percentage of grain faces with 3 or fewer edges versus engineering strain prior to recrystallization and grain growth.

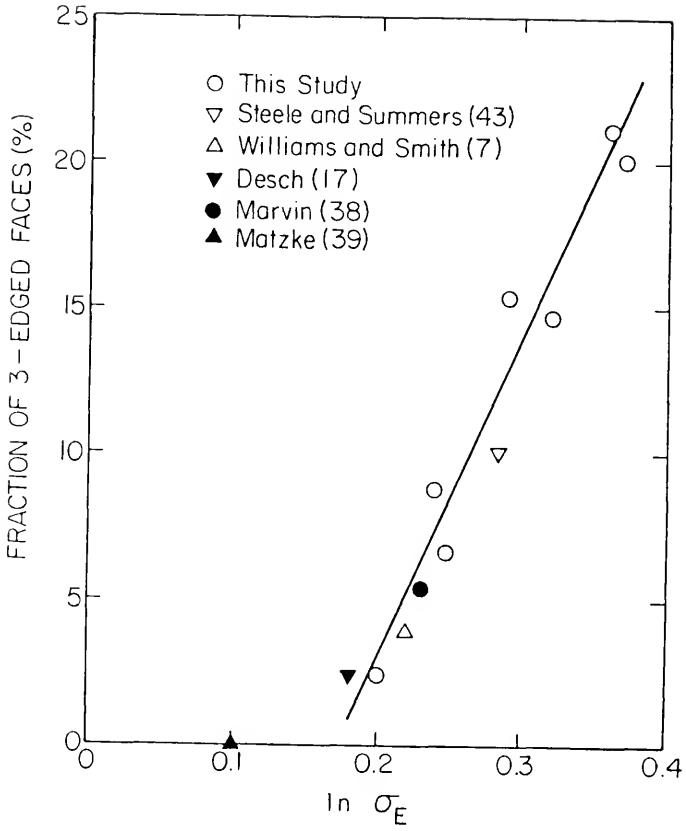

Figure (26). Percentage of grain faces with 3 or fewer edges versus the width of the distribution of edges per face.

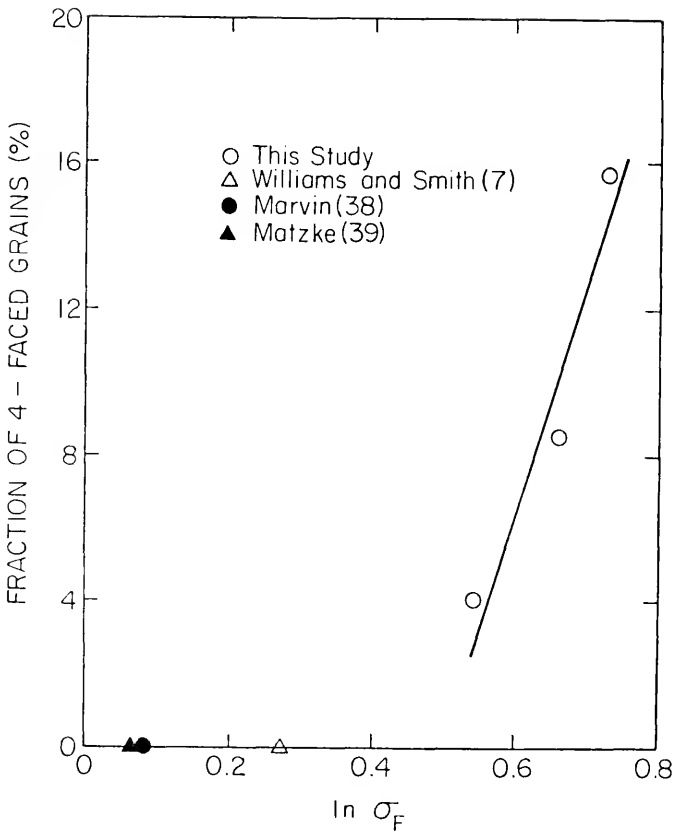

Figure (27). Percentage of grains with 4 or fewer faces versus the width of the distribution of faces per grain.

compressed, equisized lead shot, is seen to correlate well with the grain data in Fig. (26). Matzke's (39) results from observations of equisized soap bubbles are also included in these figures.

Discussion

Intuitively, the grain size distribution and the distributions of E_F and F_G should be related. The very presence of facets of various sizes (and numbers of edges) on a single grain is the result of its contact with neighboring grains of various sizes. The fact that some grains have more facets than other grains from the same aggregate is simply due to the difference in their sizes and surface areas. It follows logically that narrow or broad distributions of E_F and F_G should result from similar types of grain size distributions. As a corrollary, the distribution of the radii of curvature of individual grain faces should also be proportional to the above distributions, since small faces are generally more sharply curved than larger ones. The data shown in Fig. (24) confirms the intuitive relation between the topological and size distributions of cells in space-filling, surface tension controlled networks. Although the topological properties of the cast specimens were

not investigated, there is no reason to believe that they should not be related to the properties of their size distributions as well.

The relation between the F_G and grain size distributions may be seen from still another viewpoint, through which the log-normality of the F_G distribution may also be explained. Figure (28) illustrates a simple power law relation between the volume (shown as weight) of a grain and the number of faces which it possesses. As illustrated in Fig. (29), these data plot as a straight line on log-log graph paper. The rapid decrease in volume at 3 to 7 faces is probably due to local microstructural inhomogeneities affecting the numbers of faces on the smaller grains. Grains with 4 or fewer faces are also capable of shrinking to zero volume with no further loss of faces. Thus the relationship between the volume, V, and the number of faces, F_G, on individual grains in an aggregate is given by

$$\ell n\ V = A + b\ \ell n\ F_G \qquad (5)$$

where A is a constant related to the average grain size, and b is the slope of the line relating $\ell n\ V$ to $\ell n\ F_G$ in Fig. (29).

If $\ell n\ V$ is distributed normally with mean $\ell n\ \mu_V$ and standard deviation $\ell n\ \sigma_V$, and $\ell n\ V$ is related to $\ell n\ F_G$

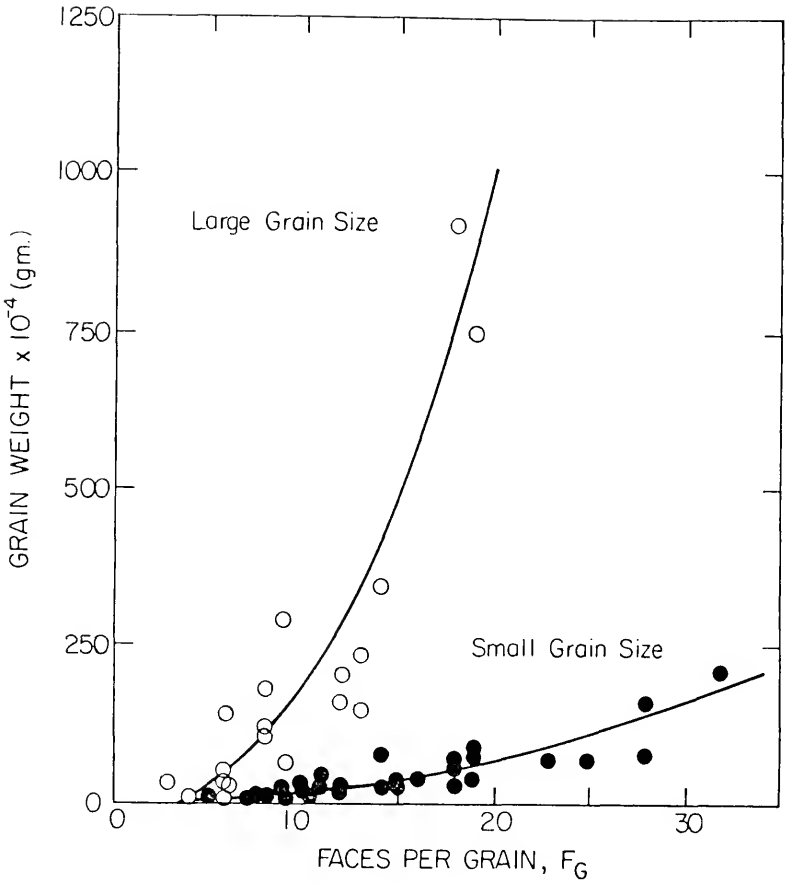

Figure (28). Grain weight versus the number of faces per grain.

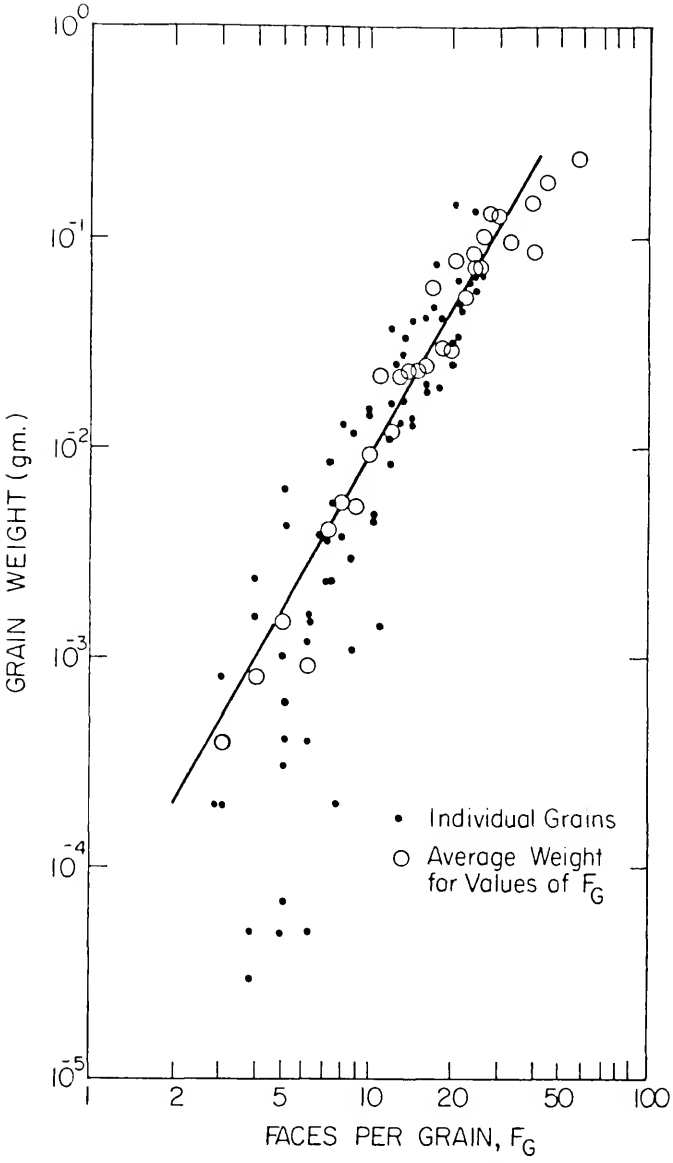

Figure (29). Grain weight versus the number of faces per grain (logarithmic axes).

by Eq. (5), it follows that $\ell n\ F_G$ will be distributed normally with mean:

$$\ell n\ \mu_F = \frac{1}{b}(\ell n\ \mu_V - A) \tag{6}$$

and standard deviation:

$$\ell n\ \sigma_F = \frac{1}{b}(\ell n\ \sigma_V) \tag{7}$$

Thus, the log-normal distribution of grain sizes and the power law relation of V to F_G requires the log-normal distribution of F_G which was observed experimentally. Equation (7) indicates that the widths of the F_G and grain size distributions should be directly proportional.

As shown in Fig. (24), this relation was found experimentally. The proportionality of $\ell n\ \sigma_V$ and $\ell n\ \sigma_E$, also shown in Fig. (24), implies that the E_F distribution should also be log-normal, as it was found to be.

The topological models of grain growth put forth by C. S. Smith (8), Rhines and Craig (9), and Steele (10) are all based on the fundamental event of the loss of triangular (3-edged) faces. These are the only types of faces which may spontaneously disappear. During grain growth, the more complex faces lose edges progressively through interaction with disappearing triangular faces. When these faces become 3-edged, they too can disappear, reducing the number of faces on their

respective grains. Successive faces degenerate and are lost from the grain until it is 4-sided and can disappear from the system, resulting in the loss of still more triangular faces. Grains which are 4-sided must be continuously regenerated in the system to allow grain growth to continue. It is apparent that the fundamental event enabling the production of this class of grain is the loss of triangular faces. In fact, only by their own action may triangular faces be regenerated. Rhines (32) has analogized the role of 3-edged faces in grain growth to that of vacancies in the diffusion process, suggesting that the rate of growth should increase and decrease proportionately with their concentration.

One of the principal reasons for interest in the topological distributions is their relation to the relative frequencies of 3-edged faces. As the width of a frequency distribution increases, the proportions of the smaller and larger valued features increase, and those of the centrally valued features decrease. The marked increase in the percentages of triangular faces and 4-sided grains as $\ell n\ \sigma_E$ and $\ell n\ \sigma_F$ increase [Figs. (26) and (27)] demonstrates this well. The significant variation in the proportions of these features, which play such an integral part in the growth process, strongly suggests an accompanying influence of the grain growth behavior.

By Rhines' (32) suggestion, an increased percentage of triangular faces should directly increase the rate of decay of complex faces and grains and also increase the rate of regeneration of still more triangular faces and 4-sided grains. The increased presence of 4-sided grains, shown in Fig. (27), as $\ell n\ \sigma_F$ increases, is actually a result of increased action by the triangular faces.

The observed relation between frequency of triangular faces and deformation provides a convenient method for testing the hypothetical effect of the topological state on the rate of grain growth. The simple comparison of the grain growth rates among specimens deformed by different amounts, producing different frequencies of triangular faces, should indicate the degree of effect of the proposed topological mechanism. Such a comparison of growth rate must be made at constant grain size, since this has an extreme effect on growth rate. Although specimens T-6-1 and T-6-2 have shown a 25% decrease in the frequency of triangular faces over a period of extensive grain growth, it is believed that this was an adjustment occurring early in the process, and not a continual decrease. The wide variation in frequency of triangular faces among specimens deformed different amounts,

even after more than 20 hours of annealing [Fig. (25)], indicates that the above effect should not interfere with the intercomparison of rates of grain growth. The test of the topological mechanism of grain growth, suggested above, is dealt with in Chapter III.

CHAPTER III
EFFECTS OF THE GRAIN SIZE AND TOPOLOGICAL DISTRIBUTIONS ON THE RATE OF GRAIN GROWTH

Introduction

The first two chapters have shown that the distributions of the sizes and topological properties of grains in polycrystalline materials possess certain degrees of variability. The potential for control of these distributions through the variation of common processing parameters, such as solidification rate and severity of deformation prior to annealing, has also been demonstrated. These results raise the question of what influence these distributions might confer on those properties of materials, which are sensitive to grain size and connectivity. Properties found to be significantly influenced in this way might then be controlled through the intentional adjustment of the appropriate parameters. One such property which has been theoretically related to both topological and size distributions is the rate of grain growth.

Jeffries and Archer (49) first suggested the dependence of grain growth on the presence of a grain size distribution in 1924. They further stated that

the rate of growth should increase with the variation in grain size. These notions have occasionally been considered theoretically in the years since, but perhaps due to the difficulty of measurement of the distribution and the lack of awareness of its relation to deformation, little has been learned experimentally. Surprisingly, even the effect of deformation prior to recrystallization on the rate of grain growth has seldom been investigated.

In the late 1940's, Burke (50,51) and Beck and his colleagues (52,53) thoroughly explored the effects of many variables such as material composition, specimen thickness, and time and temperature of anneal on the rate of grain growth. The results of these experiments, usually performed on samples receiving equal prior deformation, generally indicated that for any fixed temperature and material composition, the rate of growth was dependent only on the grain size, which was measured as the mean grain intercept. Their data were generally well represented by an equation of the form

$$\bar{\lambda} = K\, t^{n} \tag{8}$$

in which $\bar{\lambda}$ is the mean grain intercept, K is a constant, t is the time of grain growth, and n is constant for a given composition and temperature of anneal.

In one work however, Beck et al.(53) observed a slightly larger value of n for pure aluminum which had been rolled to an 80% reduction in thickness, than for that rolled 33% after annealing both at the same temperature. They also found that after a given length of anneal at 600°C, the more severely deformed material had the larger grain size, while after the same length of time at 350°C, the opposite was true. This was explained as being a result of the different times required for recrystallization. In a later review, Beck (4) presented brief data which indicated that after some adjustment of the annealing times, there was no variation in growth rate among 70-30 brass samples rolled 17% to 84%. The effect of deformation was never again seriously considered as a factor in grain growth other than through its effect on the recrystallized grain size.

In the same work, Beck presented the previously unpublished findings of Hu and Beck which suggested for the first time that the grain size distribution remained constant throughout grain growth. Apparently not realizing its possible variation otherwise, he considered distribution effects no further.

In the mean time, Burke (50) had suggested for the first time since Jeffries and Archer, that the growth rate

should be a function of the degree of grain size variation within a body. At about the same time, C. S. Smith (8) first described the topological nature of the polycrystalline aggregate, and the interrelationship of the relative sizes of grains, their topological states, and the resulting boundary curvatures propelling their growth or shrinkage. His viewpoint that grain growth was actually the result of the loss of grains from the system was that first put forth by Jeffries and Archer, although it had not received intermediate consideration.

Feltham (3) later demonstrated that Beck's distribution of grain sections was log-normal in form. He incorporated this finding and topological observations of two-dimensional grain sections in his model of grain growth which, however, neglected the possible effect of the width of the distribution.

In 1965, Nielsen (54) employed two-dimensional soap froth models to demonstrate several of the previously proposed relationships. When arrays of equisized small and large cells were placed in contact and allowed to grow, the greatest growth was found to occur at the boundary between the arrays, where the cell size gradient and curvature were the greatest.

As mentioned previously, Steele (10), determined the relative frequencies with which the events involving

triangular faces and tetrahedral grains must occur to maintain a constant topological state througout grain growth.

The first mathematical model of three-dimensional grain growth, incorporating both the topological and metric requirements of the process, was developed by Rhines and Craig (9) in 1974. They defined grain growth as the increase in $\overline{V}$, average grain volume, resulting from loss of grains from the system. Their growth law, the first to include a parameter expressing the degree of grain size variation, predicted a linear relationship between $\overline{V}$ and time, which they also found experimentally. They did not, however, test the variability of grain growth ($d\overline{V}/dt$) with this parameter.

The hypothesis put forth in many of the above works, that the rate of grain growth is an increasing function of the width of the grain size and topological distributions, has yet to be verified experimentally. This chapter will report a test of this relationship, through the comparison of the rates of grain growth of two groups of high purity aluminum specimens, deformed by widely differing amounts prior to recrystallization. The results of the previous chapters have shown that such variation in deformation does produce differences in

post recrystallization grain size and topological distributions, which are maintained throughout grain growth.

The grain growth rates, measured as $d\bar{V}/dt$ at constant $\bar{V}$, have been compared between the two groups of specimens to determine whether the differences in treatment do lead to unequal growth rates or whether, as Beck believed, the rate is a simple function of the average grain size. Further information about the process has been obtained through the measurement of the global metric parameters; S_V, L_V and M_V of the two groups of specimens. The measurement of several of these parameters has required the development and use of relatively uncommon techniques, which will be described in the experimental procedure.

The grain growth process may now be examined through a variety of types of information--topological and metric, distributional and average--all of which are different in nature. In a given polycrystalline aggregate, however, all are interrelated, and the overall process of growth is now found to be best understood through their combined examination.

Experimental Procedure

Material

High purity aluminum from the same lot as that used in the experiments of the first two chapters was

employed in this study. This facilitated the comparison of results from the related studies, and provided the previously stated experimental benefits.

Sample Preparation

Grain growth studies such as these typically require a starting material with a fine grained microstructure, to allow a large degree of growth. It was thus necessary to break down the coarse cast microstructure of the original high purity ingot through a series of cold working and recrystallization treatments. This procedure and the experimental treatments later given the individual samples will now be described.

A 2 in. cube of sound material was sawed from the original ingot. After cooling in liquid nitrogen, it was unidirectionally rolled to a final height of 1 in. (50% reduction in thickness). The slab (1 in. x 2 in. x 4 in.) was stored in liquid nitrogen until given a recrystallization anneal for 3 min. in a molten salt bath at 635°C.

It was then sawed across its width to produce two 1 in. x 1 in. x 2 in. pieces. These were cooled as before and forged in the 2 in. direction to a height of 1 in. (50% reduction). The pieces, now measuring 1 in. x 1.4 in. x 1.4 in., were kept cool and reforged in one of

the 1.4 in. directions to 1 in. in height (1 in. x $\sim 1\frac{1}{4}$ in. x $\sim 1\frac{3}{4}$ in.). This was followed by a recrystallization anneal for $2\frac{1}{2}$ min. in molten salt at 635°C. By alternating the direction of forging, and annealing for short periods of time, thick sections of relatively fine grained material were obtained. Samples measuring 1 in. in height and approximately $\frac{1}{2}$ in. square were sawed from the annealed pieces and separated into two groups which received the following separate treatments.

25% deformation group

Four samples were cooled in liquid nitrogen and, while immersed, individually compressed from 1 in. to $\frac{3}{4}$ in. (approximately 25% reduction in height). These were stored in liquid nitrogen until given their final recrystallization and grain growth anneal in molten salt at 635±2°C for periods of 0.5, 2, 30, and 60 min. The samples were then sectioned and their microstructural properties stereologically analyzed as described in the following sections.

80% deformation group

Seven samples were cooled in liquid nitrogen and, while immersed, compressed from 1 in. to 0.2 in. (approximately 80% reduction in height). These were stored in liquid nitrogen until given their final

recrystallization and grain growth anneal in molten salt at 635±2°C for 20 sec., 40 sec., 1, 3, 30, 60, and 90 min. They were then sectioned and analyzed in a manner similar to the samples in the other group.

Throughout this chapter, the samples in the above groups will be referred to by the designations given in Table 5.

Microstructural Analysis

Global properties

The microstructural changes which constitute grain growth may be examined through the stereological measurement of the following properties:

S_V - average grain boundary surface area per unit volume

L_V - average length of grain edge (triple line) per unit volume

M_V - average total grain boundary curvature per unit volume

and N_V - average number of grains per unit volume

These parameters, all of which decrease during grain growth, report the total quantity of microstructural feature per unit volume of material. Observation of their rate of change with time provides a measure of the rate of grain growth.

Table 5
Sample Treatments

Sample Designation	Deformation (%)	Time of Anneal (635°C)
25-1	25	30 sec.
25-2	25	2 min.
25-3	25	30 min.
25-4	25	60 min.
80-1	80	20 sec.
80-2	80	40 sec.
80-3	80	1 min.
80-4	80	3 min.
80-5	80	30 min.
80-6	80	60 min.
80-7	80	90 min.

Other arrangements of these property densities yield information about the average properties of the individual grains themselves:

average grain volume	$\overline{V} = 1/N_V$	(9)
average surface area per grain	$\overline{S} = 2S_V/N_V$	(10)
average length of edge per grain	$\overline{L} = 3L_V/N_V$	(11)
average total curvature per grain	$\overline{M} = 2M_V/N_V$	(12)
average mean curvature of grain boundary	$\overline{H} = M_V/S_V$	(13)
mean grain intercept	$\overline{\lambda} = 2/S_V$	(14)

These parameters permit the description of rate of grain growth in terms of the rate of change of the average grain size or other property of individual grains. The most fundamental and unbiased measure of grain growth rate, $d\overline{V}/dt$, was employed by Rhines and Craig (9) in their investigation.

Also, certain unitless ratios of the basic properties yield what have been called "metric shape factors:"

$$S_V/N_V^{1/3} = F_1 \quad (15)$$

$$L_V/N_V^{2/3} = F_2 \quad (16)$$

$$M_V/N_V^{2/3} = F_3 \quad (17)$$

$$M_V S_V/N_V = F_4 \quad (18)$$

$$L_V/S_V^2 = F_5 \quad (19)$$

$$M_V/L_V = F_6 \quad (20)$$

$$M_V/S_V^2 = F_7 \quad (21)$$

Still other combinations may be made from those listed above. Being unitless, they may remain constant valued throughout a process such as grain growth, provided that the metric state of the system, i.e. the grain size distribution and the degree of microstructural equiaxedness, remain stable. Smith and Guttman (55), DeHoff (56), and Okazaki and Conrad (57) have previously described and used such factors which were proportional to L_V/S_V^2. Rhines and Craig (9) have found $M_V S_V/N_V$ to be an integral part of their grain growth equation.

Thus, through the measurement of the four global properties, N_V, S_V, L_V, and M_V, a detailed view may be had of the polycrystalline microstructure as it changes through grain growth. This study will include the measurement of these properties for each sample of the above two series and the calculation of the related parameters. Through the analysis of this information, the corresponding rates of grain growth of the two groups of samples may be compared, enabling the acceptance or

rejection of the hypothesis that the grain size distribution, controlled through the amount of deformation prior to recrystallization, influences the rate of subsequent grain growth in a material.

Measurement

Several special stereological techniques were employed in the microstructural analysis of the specimens. These will be described in detail since the interpretation of experimental results is dependent on the validity of these methods. Some of the techniques require explanation, having been refined or developed during the course of this investigation.

S_V. The quantitative analysis of surface in space, such as grain boundary, is straightforward provided the features are either completely isotropic or completely oriented. The specimens in this study, however, possessed intermediate degrees of anisotropy even after extensive grain growth. This complicated the application of the basic stereological equations relating S_V to N_L, the number of intersections with grain boundary trace on a plane per unit length of test line. Performing measurements in numerous directions enables a better approximation of the true value of S_V, but is time consuming and destructive to the sample, which must be

further analyzed. An alternative approach is the use of N_L measurements performed in two or three principle directions and averaged by prescribed methods to obtain an N_L from which S_V may be computed.

The Saltykov model of anisotropy (11,58) provides a rational technique for doing this and in addition to total S_V, enables the estimation of the amounts of oriented and isotropic surface, and thus a relative degree of anisotropy. At present, this is the most detailed model available for the estimation of S_V of such microstructure, and has thus been employed in this study.

The type of anisotropy present in these samples is that which Saltykov has classified as "planar"—flattened in the direction in which the sample was compressed, yet symmetric in the plane perpendicular to that axis. Although more pronounced in the samples deformed 80%, directed N_L measurements have indicated the presence of such anisotropy in both series after annealing.

In the analysis of planar type microstructures, N_L measurements must be made both parallel and perpendicular to the previously mentioned orientation axis. Only one section parallel to the axis is required, as illustrated below.

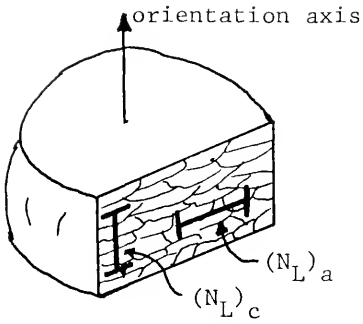

Although the annealed samples exhibited a uniform microstructure in their interior, the grains near the outer surfaces were generally much larger, probably having received less deformation. For consistency, all measurements have been restricted to the interior area of the sample. The measured values of $(N_L)_a$ and $(N_L)_c$ are then employed in the following equations to calculate the amounts of surface with various types of orientation:

$$(S_V)_{total} = (N_L)_a\ (1+q_2) \tag{22}$$

$$(S_V)_{is} = 2\ (N_L)_a \tag{23}$$

$$(S_V)_{pl} = (N_L)_a\ (q_2-1) \tag{24}$$

$$(\Omega)_{pl}^{S_V} = \frac{(S_V)_{pl}}{(S_V)_{total}} = \frac{(q_2-1)}{(1+q_1)} \tag{25}$$

where $q_2 = \frac{(N_L)_c}{(N_L)_a}$, $(S_V)_{total}$ is the total surface area of grain boundary per unit volume, $(S_V)_{is}$ is the amount of

isotropically oriented surface per unit volume, $(S_V)_{pl}$ is the area of surface per unit volume which is oriented perpendicular to the orientation axis (planar surface), and $\Omega_{pl}^{S_V}$ is the fraction of all surface which is planar in orientation. The above parameters, calculated for each sample, are listed in Tables 6 and 7.

L_V. The stereological analysis of lines in space, such as grain edges (triple lines), is also complicated if they are not arrayed isotropically. Thus, it was again appropriate to employ a model such as Saltykov's (58) for the estimation of L_V for the present samples. Although Saltykov has derived the equations for calculating L_V for the linear class of anisotropy (elongated structure, as in drawn wire), he has not considered lines in any other system. Thus it was necessary to derive the following equations, using the general Saltykov approach, to enable the measurement of L_V of these samples with planar anisotropy. In addition, the L_V equations were derived for Saltykov's third class of anisotropy, planar-linear. These derivations are presented in Appendix D.

Calculation of L_V for planar structures requires the measurement of P_A, the average number of grain edge intersections per unit area of test plane, on two section planes. One section must be parallel and the other

Table 6
Experimental Values of Grain Boundary Anisotropy Parameters

Sample	$(N_L)_a$ $X10^1$ $(cm.^{-1})$	$(N_L)_c$ $X10^1$ $(cm.^{-1})$	$(S_V)_{is}$ $X10^1$ $(cm.^{-1})$	$(S_V)_{pl}$ $X10^1$ $(cm.^{-1})$	S_V $(\Omega)_{pl}$
25-1	5.3±0.4	6.1±0.4	11. ±1.	0.8±0.8	0.07
25-2	4.0±0.3	4.4±0.3	8.0±0.6	0.4±0.6	0.05
25-3	3.1±0.2	3.4±0.3	6.2±0.4	0.3±0.5	0.05
25-4	2.9±0.2	3.3±0.3	5.8±0.4	0.4±0.5	0.06
80-1	10. ±1.	13. ±1.	20. ±2.	3. ±2.	0.13
80-2	6.8±0.7	9.4±0.7	14. ±1.	2.6±1.4	0.16
80-3	8.5±0.9	8.9±0.6	17. ±2.	0.4±1.5	0.02
80-4	6.2±0.3	7.6±0.2	12. ±1.0	1.4±0.5	0.10
80-5	4.9±0.4	5.9±0.4	9.8±0.8	1.0±0.8	0.09
80-6	4.1±0.4	5.2±0.4	8.2±0.8	1.1±0.8	0.12
80-7	3.5±0.3	4.4±0.3	7.0±0.6	0.9±0.6	0.11

Table 7
Experimental Values of Global Metric Properties

Sample	N_V X10^4 (cm.$^{-3}$)	S_V X10^1 (cm.$^{-1}$)	L_V X10^3 (cm.$^{-2}$)	M_V X10^3 (cm.$^{-2}$)
25-1	8.0± 1.9	11. ±1.	8.9±0.9	2.2
25-2	5.1± 0.9	8.4±0.1	5.4±0.6	1.4
25-3	1.4± 0.4	6.5±0.5	3.1±0.4	0.58
25-4	1.6± 0.4	6.2±0.5	3.2±0.4	0.17
80-1	52. ±13.	23.2±2.	36. ±4.	8.0
80-2	27. ± 7.	16. ±1.	25. ±2.	5.1
80-3	33. ± 9.	17. ±2.	25. ±4.	4.3
80-4	16. ± 3.	14. ±1.	12. ±1.	2.8
80-5	9.1± 2.1	11. ±1.	9.2±1.1	1.9
80-6	5.0± 0.8	9.3±1.	6.9±0.8	1.4
80-7	3.5± 0.9	7.9±1.	5.2±0.7	0.95

perpendicular to the orientation axis as illustrated. As

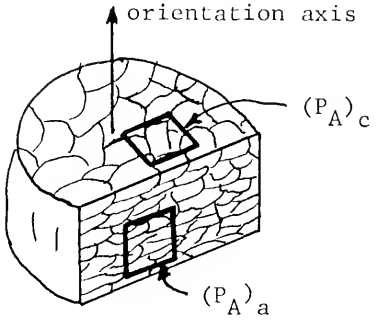

before, all counts on the 80% deformed specimens were made well away from the large exterior grains. This required grinding to a depth of $\frac{1}{4}$ to $\frac{1}{2}$ of the specimen thickness before measuring $(P_A)_c$.

Once $(P_A)_a$ and $(P_A)_c$ have been obtained, they may be employed in the following equations:

$$(L_V)_{total} = (P_A)_a\ (2-\tfrac{\pi}{2})q_2 + \tfrac{\pi}{2} \tag{26}$$

$$(L_V)_{is} = 2q_2(P_A)_a \tag{27}$$

$$(L_V)_{pl} = \tfrac{\pi}{2}(P_A)_a(1-q_2) \tag{28}$$

$$(\Omega)^{L_V}_{pl} = \frac{(L_V)_{pl}}{(L_V)_{total}} = \frac{\frac{\pi}{2}(1-q_2)}{(2-\frac{\pi}{2})q_2 + \frac{\pi}{2}} \tag{29}$$

where $q_2 = \frac{(P_A)_c}{(P_A)_a}$, $(L_V)_{total}$ is the total length of grain edge per unit volume, $(L_V)_{is}$ the length of isotropically

oriented grain edge per unit volume, $(L_V)_{pl}$ is the length of grain edge lying in the plane perpendicular to the orientation axis per unit volume, and $(\Omega)_{pl}^{L_V}$ is the fraction of all edge which is of planar orientation. The experimentally measured values of these properties for the two series of samples are given in Tables 7 and 8.

In the course of this study of the Saltykov model of anisotropy, an entirely separate microstructural model was also considered. This model, proposed by DeHoff (59), is based on the properties of an unequiaxed Kelvin tetrakaidecahedron (36) (truncated octahedron). The deviation of the equations for the calculation of L_V by this model and a test and comparison of it and the Saltykov model are also presented in Appendix D.

M_V. The tangent count method, devised by Rhines et al. (60) has been employed to measure the total grain boundary curvature per unit volume. In this procedure, a straight line is swept over the test surface and T_A, the average number of tangencies between it and curved grain boundary traces, per unit area of test surface, is determined. Total curvature of surface per unit volume, as derived by DeHoff (60), is then given by

$$M_V = \pi T_A \tag{30}$$

The result of this equation has been shown (59) to be more

Table 8
Experimental Values of Grain Edge Anisotropy Parameters

Sample	$(P_A)_a$ $X10^3$ $(cm.^{-2})$	$(P_A)_c$ $X10^3$ $(cm.^{-2})$	$(L_V)_{is}$ $X10^3$ $(cm.^{-2})$	$(L_V)_{pl}$ $X10^3$ $(cm.^{-2})$	L_V $(\Omega)_{pl}$
25-1	3.6±0.3	4.7±0.5	7.2±0.6	1.7±1.3	0.19
25-2	3.0±0.3	2.4±0.3	6.0±0.6	-	-
25-3	1.3±0.2	1.6±0.2	2.6±0.4	0.5±0.6	0.16
25-4	1.5±0.1	1.6±0.2	3.0±0.3	0.1±0.5	0.03
80-1	14. ±2.	19. ±2.	28. ±4.	7.9±6.3	0.21
80-2	6.6±0.9	14. ±1.	13. ±2.	13. ±3.0	0.52
80-3	9.8±1.0	13. ±2.	20. ±2.	3.5±4.7	0.14
80-4	5.2±0.6	6.1±0.7	10. ±1.	1.4±2.0	0.12
80-5	3.6±0.4	4.9±0.6	7.2±0.8	2.0±1.6	0.22
80-6	3.2±0.3	3.5±0.4	6.4±0.6	0.5±1.1	0.07
80-7	2.3±0.2	2.7±0.4	4.6±0.4	0.6±0.9	0.12

complex than simply the total curvature per unit volume, when T_A is measured for a grain boundary network. It does, however, provide a measure of the degree of grain boundary curvature per volume and it will be interpreted as such in this study.

The value of T_A is measured with test lines swept in two different directions on the plane parallel to the orientation axis. These measurements were designated $(T_A)_{trans}$ and $(T_A)_{long}$, as shown below.

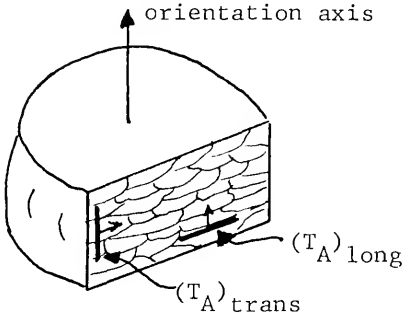

The value of M_V was then calculated using the average of the two measurements:

$$M_V = \pi\left(\frac{(T_A)_{long} + (T_A)_{trans}}{2}\right) \qquad (31)$$

A rough measure of the degree of anisotropy of total curvature was obtained from the ratio $(T_A)_{trans}/(T_A)_{long}$. The experimentally measured values of the above parameters are listed in Tables 7 and 9.

Table 9
Experimental Values of Directionally Measured Curvature Parameters

Sample	$(T_A)_{long}$ $X10^3$ $(cm.^{-2})$	$(T_A)_{trans}$ $X10^3$ $(cm.^{-2})$	$(T_A)_{average}$ $X10^3$ $(cm.^{-2})$	$\left[\frac{(T_A)_{trans}}{(T_A)_{long}}\right]$
25-1	-	-	2.2	-
25-2	-	-	1.4	-
25-3	-	-	0.58	-
25-4	-	-	0.17	-
80-1	2.8	2.2	2.5	0.79
80-2	1.9	1.3	1.6	0.68
80-3	1.5	1.2	1.4	0.80
80-4	1.9	1.6	1.8	0.84
80-5	1.3	1.1	1.2	0.85
80-6	0.46	0.43	0.45	0.93
80-7	0.27	0.16	0.21	0.59

$\underline{N_V}$. The number of grains per unit volume, N_V, is measured most unambiguously through serial sectioning. This measurement, although time consuming, is statistically exact even in the presence of anisotropy and may be performed to a degree of precision limited only by the number of counts.

First performed by Craig (61), who sectioned aluminum with a microtome, the technique has been refined with each successive use (18,46,62). For instance, it has now been found that a reasonably narrow confidence interval (coefficient of variation $\sim$0.1) may be obtained for N_V after only six to ten sections, whereas it was previously thought that as many as 250 sections might be required for satisfactory accuracy (62). The following is a description of the serial section technique employed in this study.

The specimens were first sectioned so that an interior area, away from large external grains, could be viewed. The samples deformed 25% were sectioned perpendicular to the deformation axis at mid-specimen height. Due to the possibility of a grain size gradient extending through the thickness of the samples in the 80% group, they were sectioned parallel to the deformation axis. Performing the analysis over the cross-section of the gradient yielded the <u>average</u> N_V for the specimen.

After polishing the initial section, small marker holes (0.013 in. diameter) were drilled into it, surrounding an area large enough to contain 200-300 grain sections. The holes were outlined on tracing paper placed over a photomicrograph of this region. With the overlay in place, a pin hole was made through it and the photo, in the center of the region surrounded by markers. Using a compass centered in the pin hole, a circular working area was outlined on the photomicrograph. The true area of this surface could be calculated from the photographic magnification. For ease of identification, each grain in the working area was then outlined with ink and numbered.

After measuring its thickness, each sample was ground and/or polished to remove a small layer of material and produce a new surface for examination, parallel to the original one. A photomicrograph, of the same magnification as before, was then made of this surface. After alignment of the stencil with the markers in the new photograph, the central point of the new working area was marked through the stencil pin hole, and the new working area of the same diameter as before was circumscribed from this point. The grains within this area were outlined and numbered in correspondence with the previous photograph.

Any grains appearing for the first time within the working area of this section were given numerical designations, beginning with 1000, and the number of these new grains were recorded. Remeasurement of the sample thickness with a micrometer enables calculation of the cylindrical volume within which the grains had originated. Successive sections were performed until the calculated values of N_V were of the desired accuracy.

It should be emphasized that in this technique, only those grains appearing for the first time within the working area are recorded. The number of grains which first appear outside and later enter the area, is probabilistically equal to the number first appearing within the area and later extending beyond it. Thus the boundary does not contribute any systematic error to the calculation of N_V.

It should also be mentioned that the marker holes merely provide a convenient means for relocating the same general area of the sample, and misalignment from section to section does not introduce error, as long as each area of examination can be compared to that same area in the preceding photograph. For convenience, it is best to minimize such misalignments through use of the markers.

The serial section data for each specimen have been provided in Appendix E.

The results of such serial section procedures have previously been analyzed in several ways to estimate N_V statistically, in order to obtain the true average number of grains per unit volume. One such method has been to plot graphically the cumulative number of newly appearing grains versus the cumulative volume sectioned [Fig. (30)], and consider N_V to be approximated by the slope of the straight line best fitting the data. This is actually not a meaningful approach since each successive datum point contains more information than the previous one.

The best estimator of the true N_V is obtained simply by dividing the final cumulative number of grains by the final cumulative volume, the last point on the graph, i.e.

$$\hat{N}_V = \frac{\frac{\Sigma N_i}{K}}{\frac{\Sigma V_i}{K}} \tag{32}$$

where $\hat{N}_V$ estimates the mean value of N_V, N_i is the number of grains first appearing in the i^{th} section, V_i is the volume of the i^{th} section, and K is the total number of sections analyzed.

Since the section volumes generally vary throughout a sample, the amount of information contained in them does also. In this situation, it is preferable to

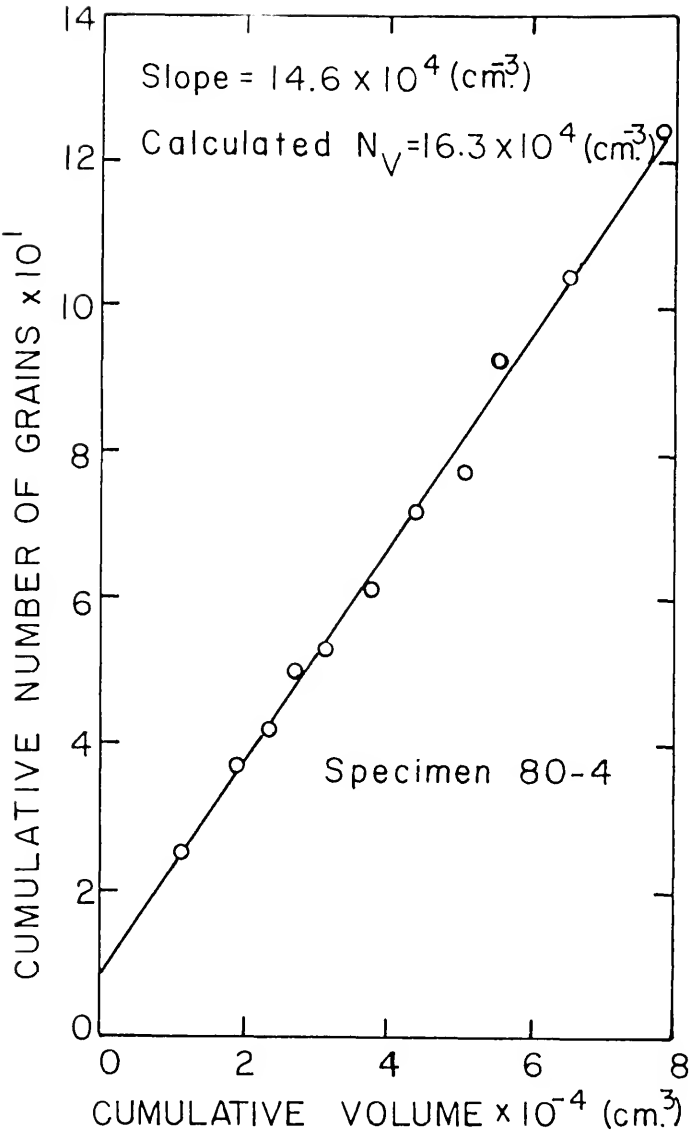

Figure (30). Cumulative number of newly appearing grains versus cumulative volume sectioned.

estimate the population variance, $(Var)_{N_V}$, by

$$(Var)_{N_V} = \frac{1}{K} \frac{1}{\overline{\gamma}} \frac{\sum_{K}(N_i - V_i \hat{N}_V)^2}{K-1} \tag{33}$$

where $\overline{\gamma}$ is the average section volume, rather than by the standard method. The 95% confidence interval for N_V is given by Eq. (34):

$$N_V = \hat{N}_V \pm 2\sqrt{(Var)_{N_V}} \tag{34}$$

The confidence intervals of N_V, obtained for each specimen are listed in Table 7.

$\underline{\overline{V}}$. The measurement of $\overline{V}$, the average grain volume, is directly related to that of N_V. Since $\overline{V} = 1/N_V$, it follows that $\hat{\overline{V}}$, the estimator of $\overline{V}$, is given by

$$\hat{\overline{V}} = \frac{1}{\hat{N}_V} = \frac{\sum_{K} V_i}{\sum_{K} N_i} \tag{35}$$

The value of $(Var)_{\overline{V}}$, the estimated population variance of $\overline{V}$, is given by

$$(Var)_{\overline{V}} = \frac{1}{K} \frac{1}{\overline{\eta}} \frac{\sum_{K}(V_i - N_i \hat{\overline{V}})^2}{K-1} \tag{36}$$

where $\overline{\eta}$ is the average number of newly appearing grains per section. The 95% confidence interval for $\overline{V}$ is then

$$\overline{V} = \hat{\overline{V}} \pm 2\sqrt{(Var)_{\overline{V}}} \tag{37}$$

The confidence intervals calculated for each specimen are given in Table 10.

Table 10
Experimental Values of Average Metric Properties of Grains

Sample	$\bar{V}X10^{-6}$ (cm.$^{-3}$)	$\bar{S}X10^{-3}$ (cm.^{2})	$\bar{L}X10^{-1}$ (cm.)	$\bar{M}X10^{-2}$ (cm.)	$\bar{H}X10^{1}$ (cm.$^{-1}$)
25-1	13. ± 3.	2.7	3.3	5.4	2.0
25-2	20. ± 4.	3.3	3.2	5.6	1.7
25-3	71. ±18.	9.2	6.6	8.2	0.89
25-4	61. ±16.	7.6	5.9	6.6	0.88
80-1	1.9± 0.5	0.88	2.1	3.1	3.5
80-2	3.7± 0.9	1.2	2.8	3.7	3.2
80-3	3.0± 0.8	1.0	2.3	2.6	2.5
80-4	6.3± 1.	1.8	2.3	3.6	2.0
80-5	11. ± 3.	2.4	3.1	4.2	1.7
80-6	20. ± 3.	3.7	4.1	5.6	1.5
80-7	29. ± 8.	4.6	4.5	5.5	1.2

Equations (33) and (36) for the variances of N_V and $\bar{V}$ do not distinguish between experimental error and variation within the sample itself. Experimental error may be minimized by taking sections thin enough that the change in microstructural appearance between sections is not so great as to produce confusion in distinguishing newly appearing grains from those formerly present. Taking thin sections also prevents the complete passing of small grains between sections. Excessively thin sections, however, are not warranted, owing to the small amount of information which they contain.

Figures (31) and (32) illustrate the average section depths which were found to be most desirable for the samples of various average grain sizes examined here. It can be seen that the optimum section depth decreases exponentially as S_V increases. The calculated best-fit line through the data of Fig. (32) has a slope very close to -1, indicating that this depth is proportional to S_V^{-1}. This is the same relationship as between S_V and $\bar{\lambda}$, the mean grain intercept. Thus, it follows that the optimum section depth—that at which the appearance of a microstructure in a photograph changes some, but not excessively—is directly proportional to the mean grain intercept, which measures the one-dimesional scale of a microstructure.

Figure (31). Optimum section thickness versus surface area per unit volume.

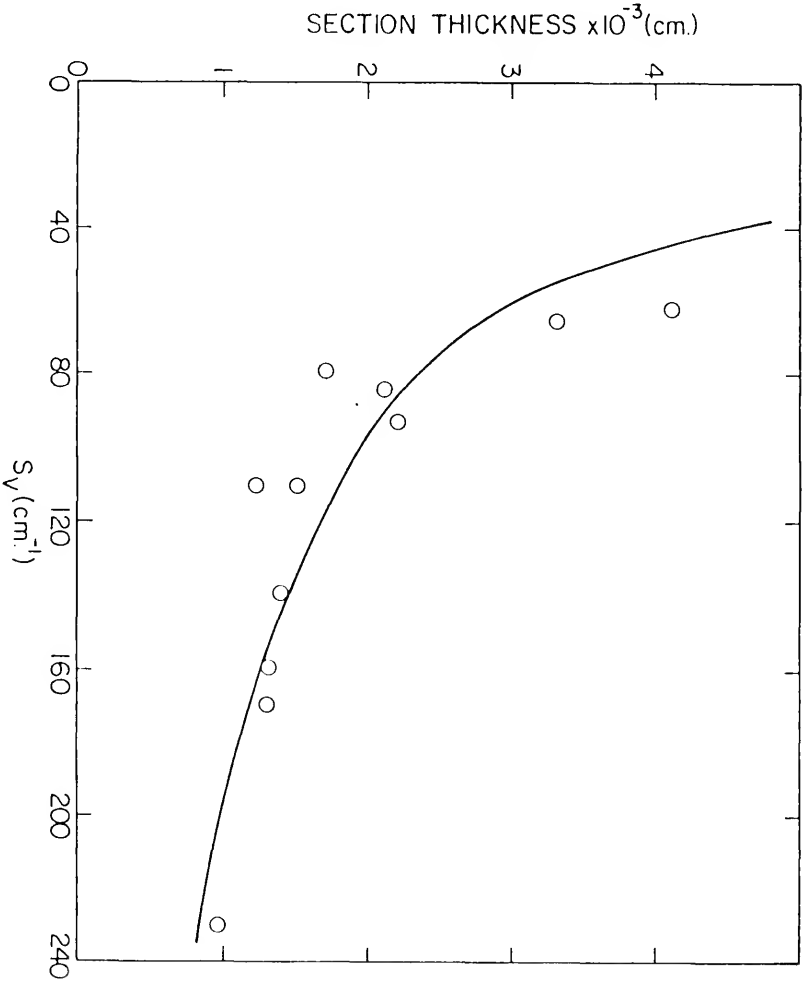
SECTION THICKNESS x10^{-3}(cm.)
0
1
2
3
4
0
40
80
120
160
200
240
S_V(cm^{-1})

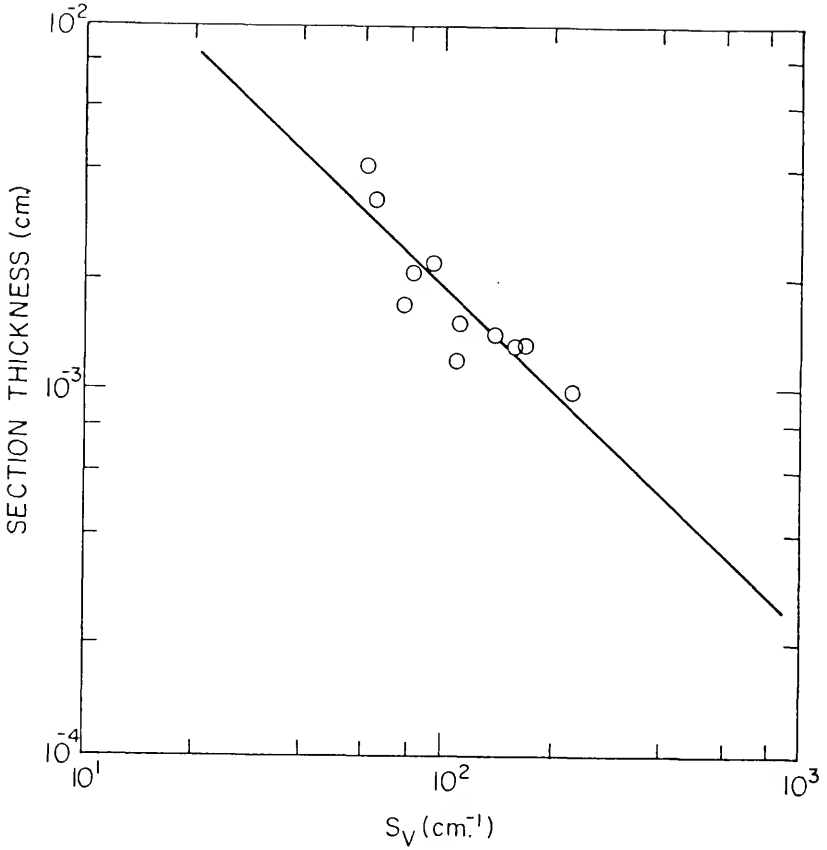

Figure (32). Optimum section thickness versus surface area per unit volume (logarithmic axes).

Also of interest is the relationship between the microstructural scale of a sample, measured by S_V, and the total volume which must be analyzed in order to attain a given degree of accuracy in the measurement of N_V or $\overline{V}$. Figures (33) and (34) illustrate this relationship for the two series of samples, all of which were analyzed to approximately the same relative accuracy (coefficient of variation $\sim$0.1). The slope of the calculated best-fit line in Fig. (34) is approximately -3, as may be deduced independently as follows.

If the sources of experimental error and the relative inhomogeneity of a sample are independent of the grain size, then the degree of accuracy attained in the analysis of equal numbers of grains from several samples should be approximately equal. The number of grains analyzed in a given sample is directly proportional to the volume sectioned. It therefore follows from the relationship of S_V and $N_V^{1/3}$ [Eq. (15)], that S_V^3 is proportional to the volume which must be sectioned in order to observe the given number of grains required to attain a certain degree of accuracy. Figures (31)-(34) should be of practical value in the performance of future serial sectioning experiments.

Figure (33). Total volume sectioned to reduce coefficient of variation of N_V to ≈ 0.1 versus surface area per unit volume.

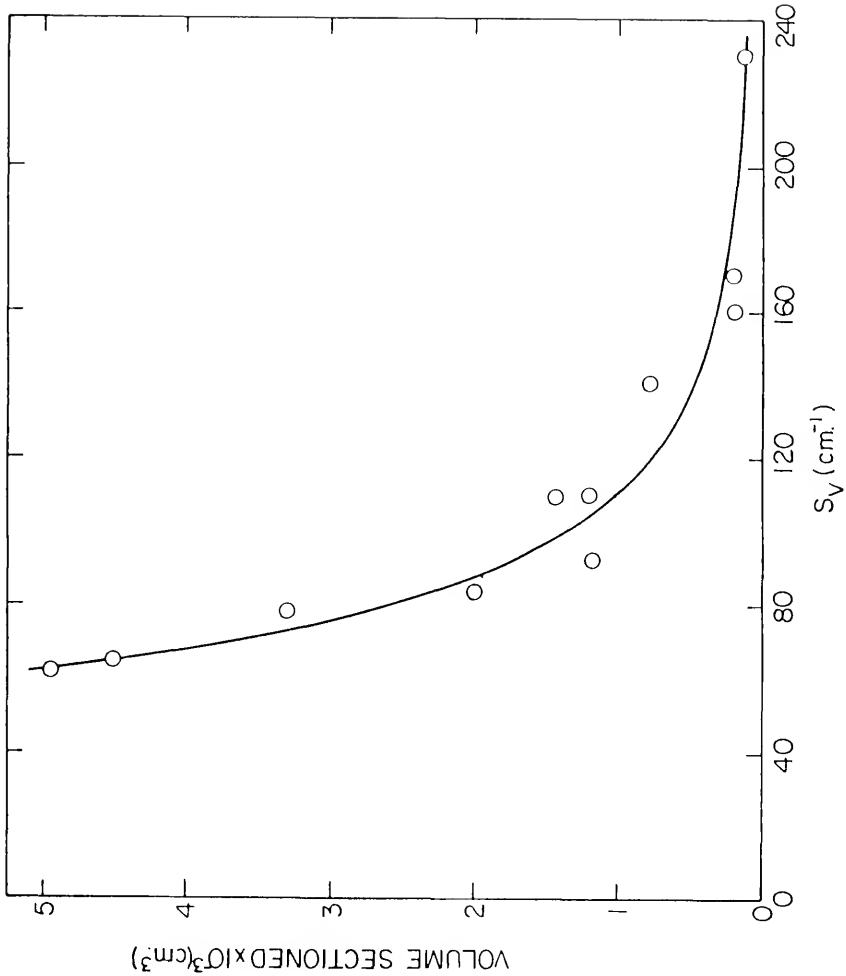
VOLUME SECTIONED x10³(cm.³)
0
1
2
3
4
5
0
40
80
120
160
200
240
S_V (cm.$^{-1}$)

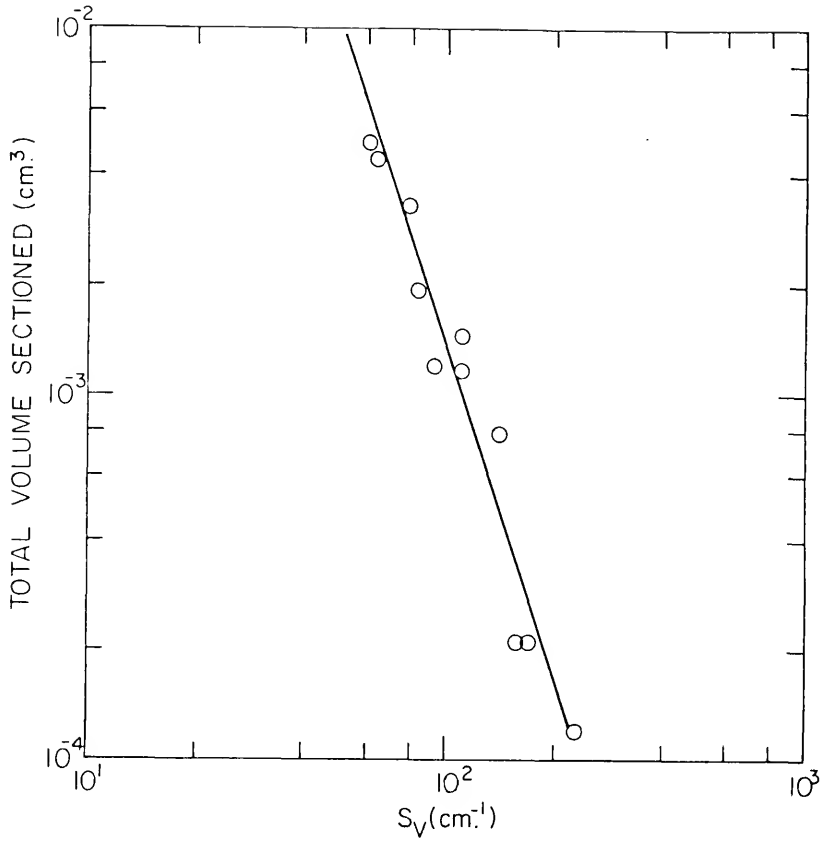

Figure (34). Total volume sectioned to reduce coefficient of variation of N_V to ≈0.1 versus surface area per unit volume (logarithmic axes).

Experimental Results

Grain Growth Rate

The global properties—S_V, L_V, M_V and N_V—have been measured by the previously described techniques for each of the grain growth specimens. The 95% confidence intervals of the measurements for each sample are given in Table 7.

In Figs. (35)-(38), the above data are plotted versus time of anneal, to illustrate the effect of grain growth on the global properties. Samples 80-1 and 25-1, which received the shortest anneal of each series, were found to be completely recrystallized after 20 and 30 seconds, respectively, in the salt bath. Both samples were also undoubtedly near or at their final annealing temperature of 635°C by these times, since the salt crust (melting point $\sim$560°C) which formed immediately on the samples had remelted within approximately 10 seconds. Displacement of each datum point along the time axis, in order to subtract the heat up and recrystallization period, would have virtually no influence on the form of these curves. They may thus be interpreted as representing the behavior of the properties as a function of the time of grain growth.

At this temperature, the quantities of each property decrease rapidly within the first several minutes of

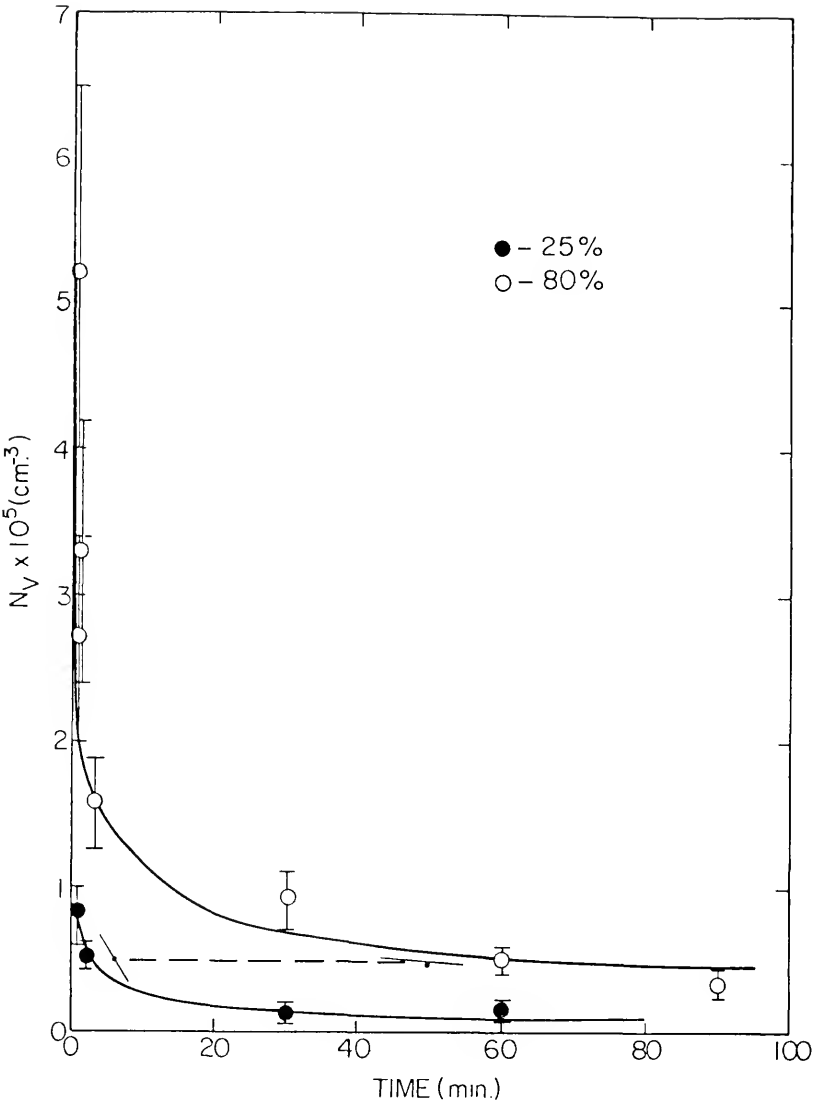

Figure (35). Number of grains per unit volume versus annealing time.

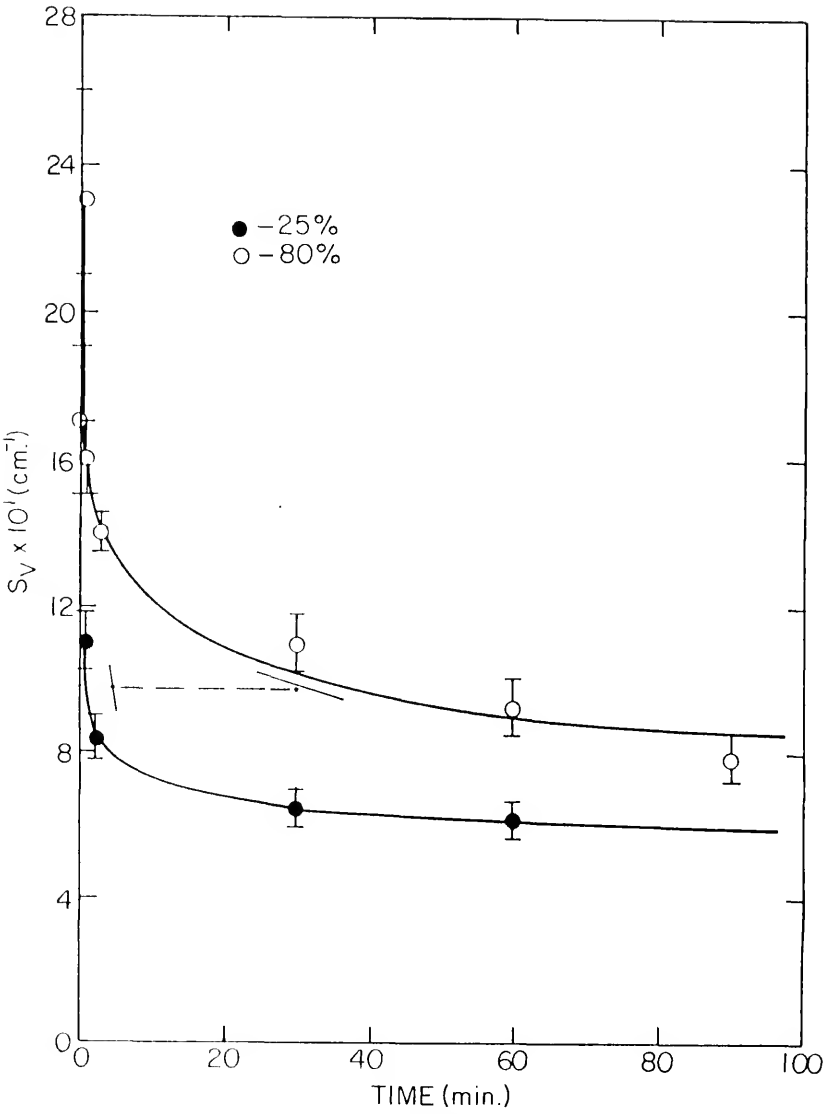

Figure (36). Grain boundary surface area per unit volume versus annealing time.

Figure (37). Grain edge length per unit volume versus annealing time.

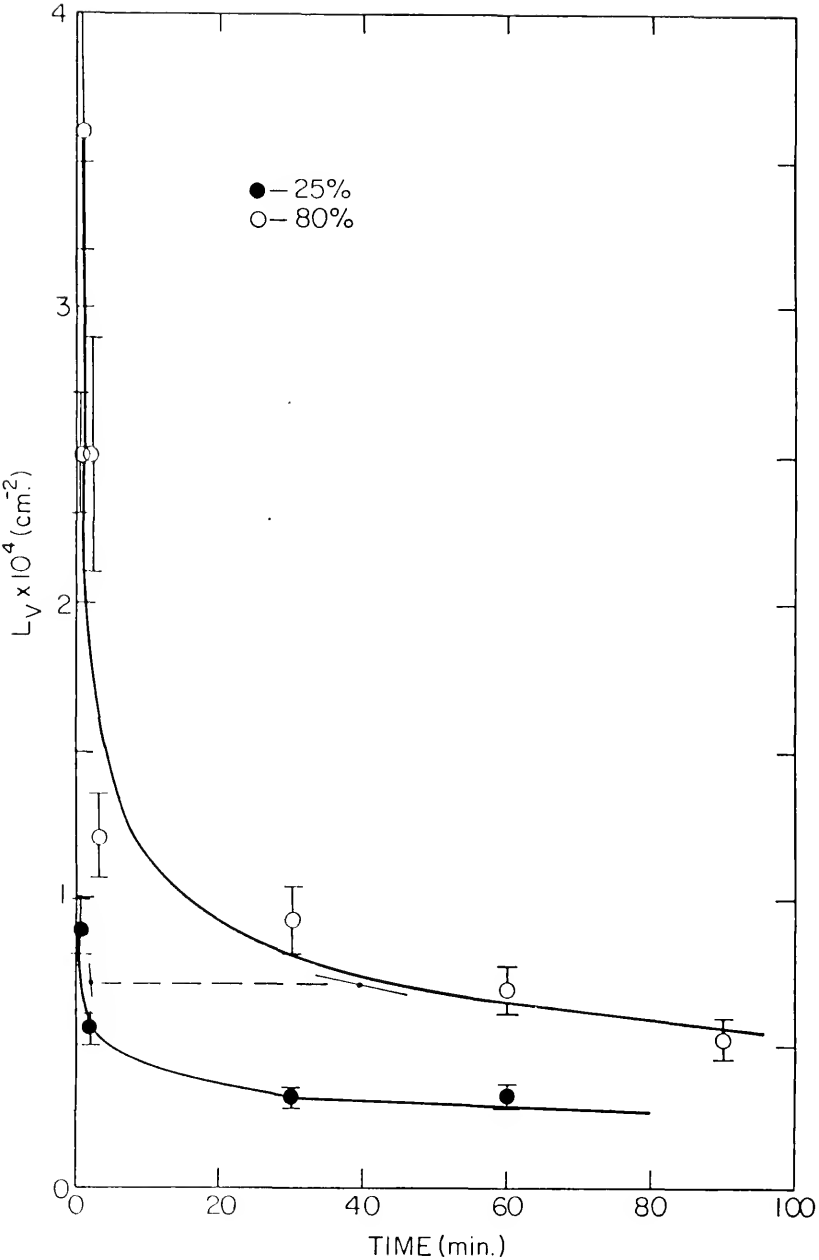
4
3
2
1
0
0
20
40
60
80
100
TIME (min.)
$L_V \times 10^4$ (cm.$^{-2}$)
● – 25%
○ – 80%

Figure (38). Total grain boundary curvature per unit volume versus annealing time.

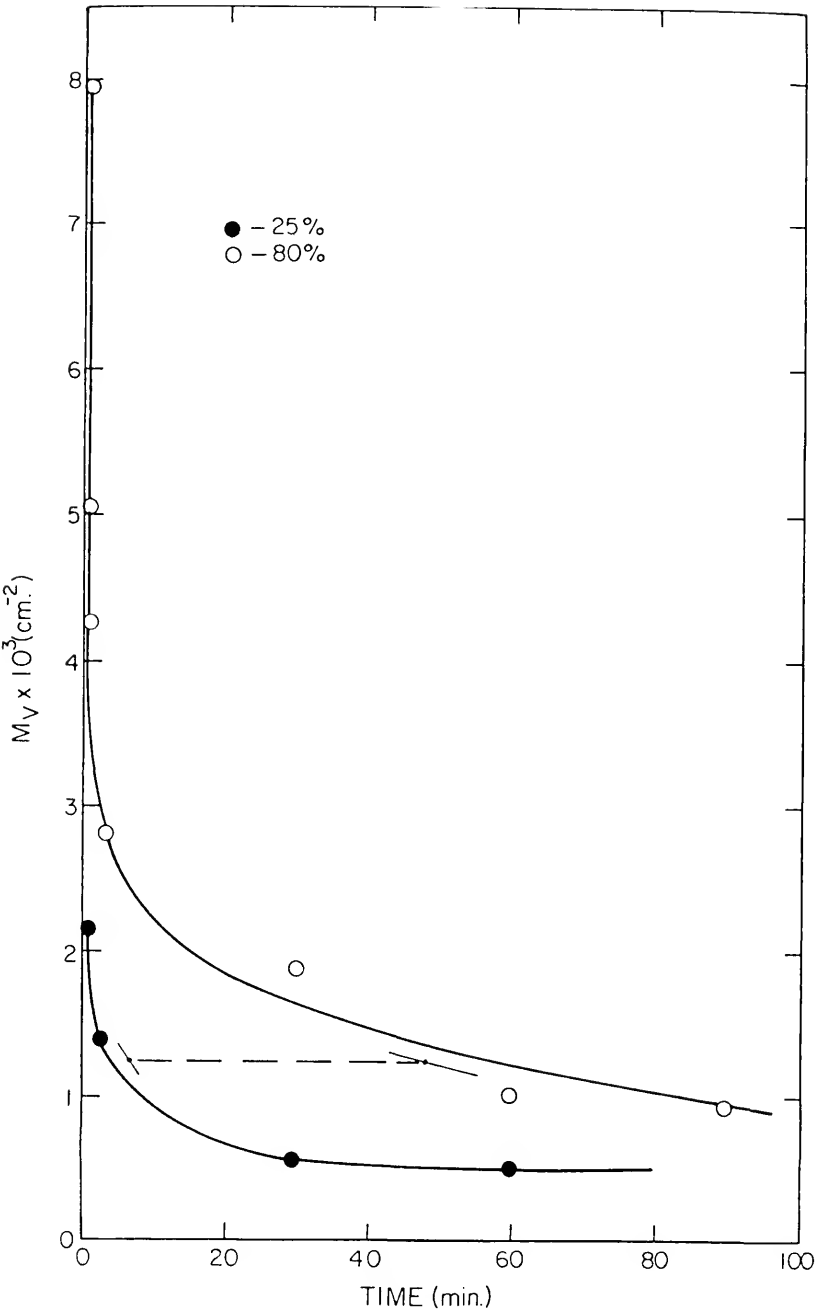
● – 25%
○ – 80%
$M_V \times 10^3 (cm.^{-2})$
TIME (min.)
0
1
2
3
4
5
6
7
8
0
20
40
60
80
100

grain growth, and continue to decrease at a progressively slower rate with time. The 80% deformed samples recrystallize to a smaller average grain size than the 25% group and after any given period of grain growth possess markedly larger values of the various properties.

The rate of change of a property at any given point along its path of decrease with time may be measured graphically by the slope of the line tangent to its curve at that point. In this manner dN_V/dt, dS_V/dt, dL_V/dt and dM_V/dt have been illustrated in Figs. (35)-(38) at equal values of N_V, S_V, L_V and M_V, for each of the two groups of samples. It can be seen that for each global property, the rate of decrease at constant value is always greater for the 25% deformation group than for the 80% group. At $N_V = 5 \times 10^4$ cm^{-3}, in Fig. (35), the rate of loss of grains from the system is 8000/min. for the 25% deformed material and 400/min. for that deformed 80%, a 20:1 difference. This previously unreported results tends to support the prior hypothesis, since the lesser deformed material has been shown to have the broader grain size distribution, and greater percentage of triangular faces.

Average Properties of Grains

The grain growth rate is perhaps more easily visualized as the rate of increase of an average grain

size than as the rate of decrease of the global properties. Figures (39)-(42) illustrate the increase of the average volume, average surface area, average edge length, and average total curvature per grain with time of grain growth. Also, Fig. (43) shows the decrease in average mean curvature of grain boundary with time, as the average mean radius of grain boundary curvature increases. The values of the above properties, calculated through Eqs. (9)-(13), are listed in Table 10.

It can be seen that the rate of increase of each property, related to average grain size, is greater for the series of samples deformed 25% than for the series deformed 80%. The comparison of the values of $d\bar{V}/dt$ at constant $\bar{V}$, shown by the tangent lines in Fig. (39), allows the most meaningful observation of the rates of grain growth of the two series of specimens. As emphasized by Rhines and Craig (9), the rate of increase of the average grain volume is the only pure measure of grain growth (with the exception of the related dN_V/dt), unbiased by changed in grain shape or anisotropy. As mentioned previously, the grain growth process is itself the successive loss of grains from the system—the only event which can increase $\bar{V}$. The tangents to the growth curves in Fig. (39) are at the same average grain volume

Figure (39). Average grain volume versus annealing time.

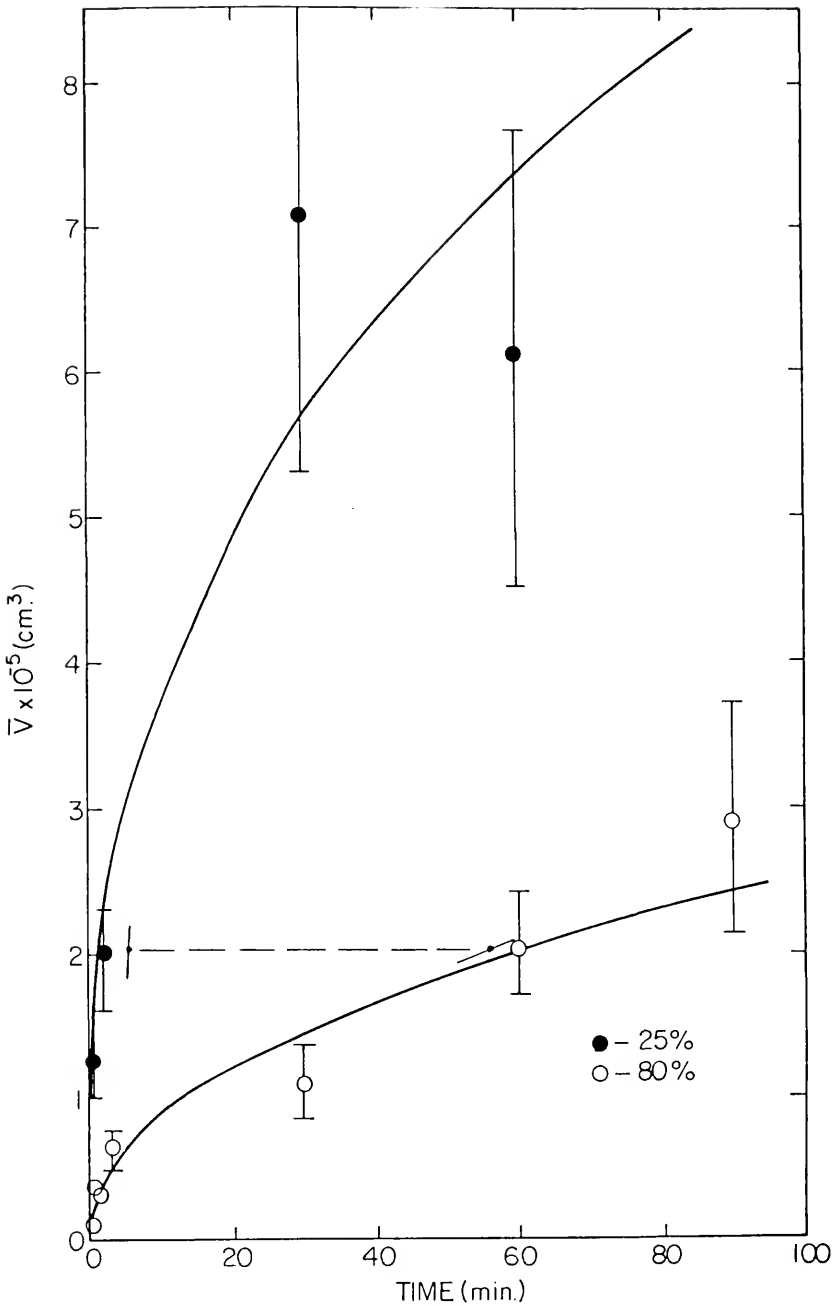
8
7
6
5
4
3
2
1
0
$\bar{V} \times 10^5$ (cm.^{3})
0
20
40
60
80
100
TIME (min.)
● – 25%
○ – 80%

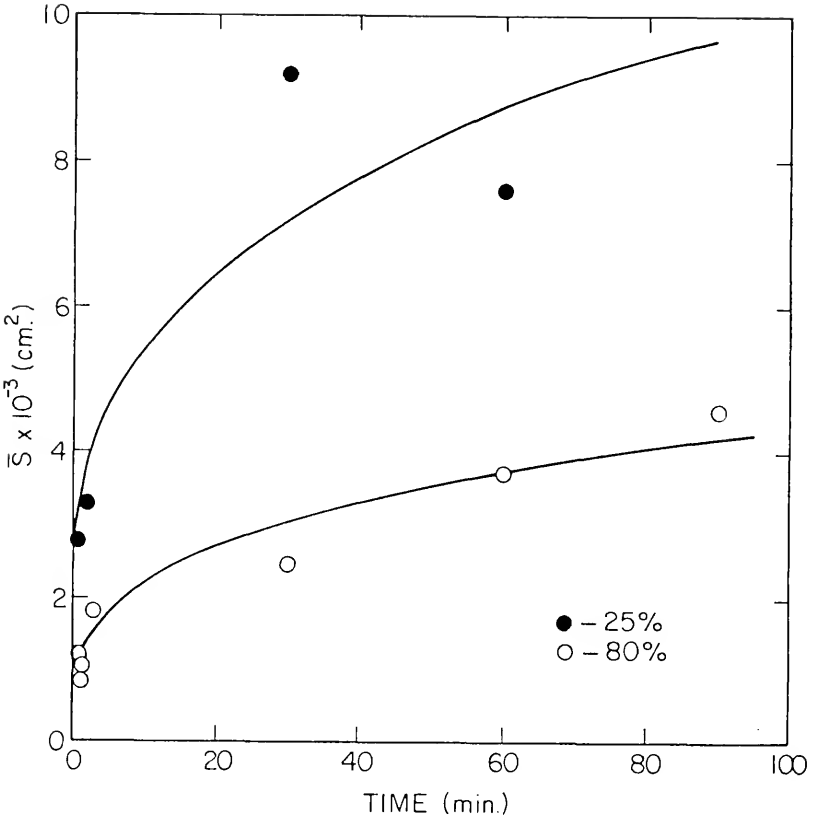

Figure (40). Average surface area per grain versus annealing time.

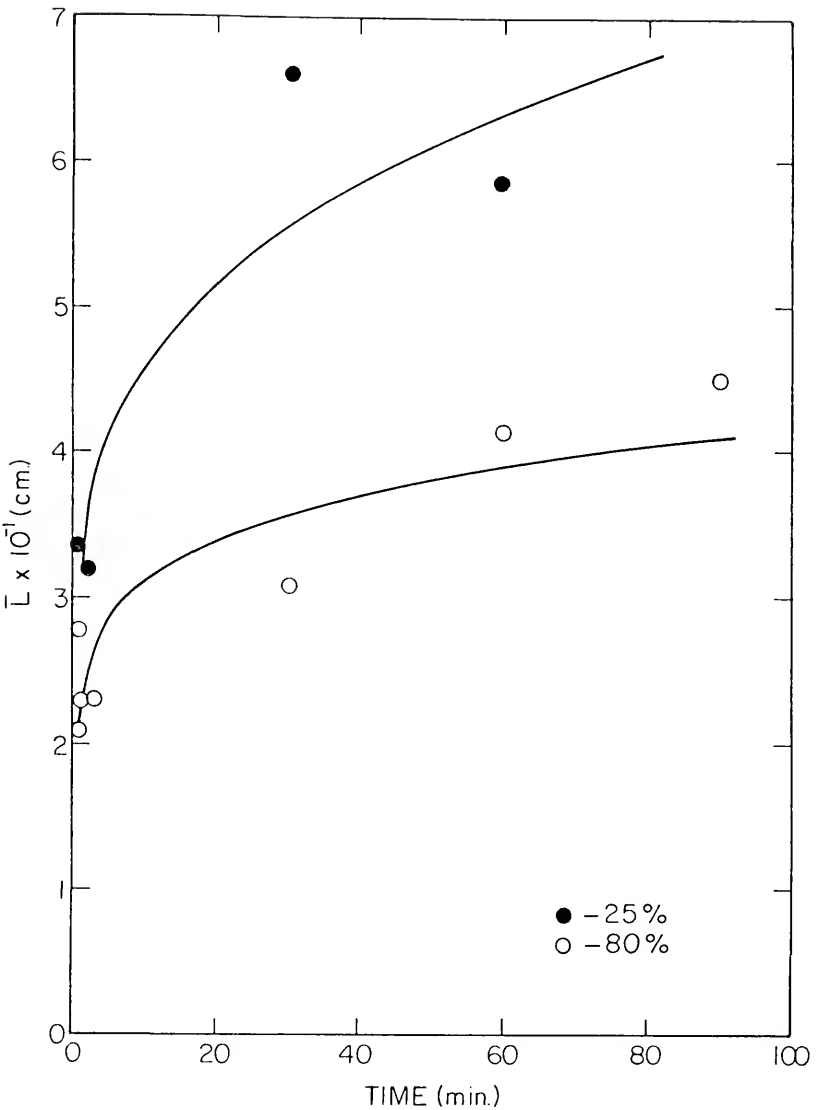

Figure (41). Average edge length per grain versus annealing time.

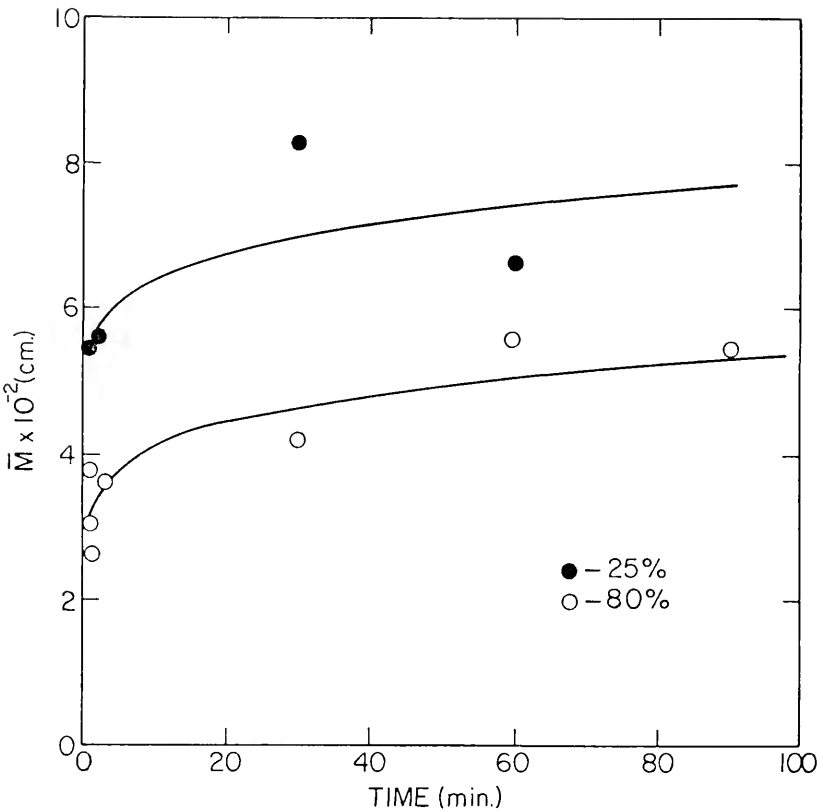

Figure (42). Average total curvature per grain versus annealing time.

Figure (43). Average mean curvature of grain boundary versus annealing time.

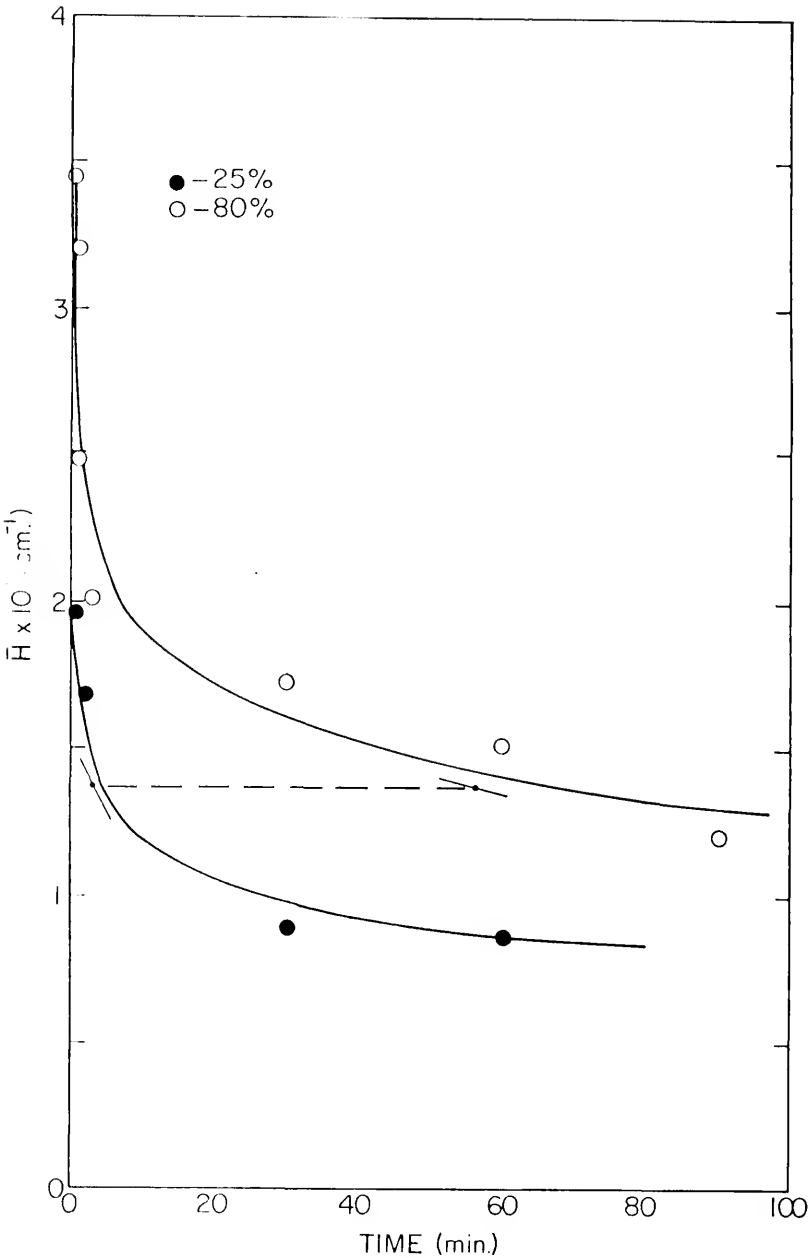
● – 25%
○ – 80%
$\bar{H}$ x 10 (cm.$^{-1}$)
TIME (min.)
0
1
2
3
4
0
20
40
60
80
100

of 2×10^{-5} ($cm.^3$), comparable to the values of N_V at which the tangent lines were drawn in Fig. (35). The values of $d\bar{V}/dt$ at this volume are 32×10^{-7} ($cm.^3/min.$) and 1.6×10^{-7} ($cm.^3/min.$) for the 25% and 80% deformed series, respectively. This 20-fold difference in growth rate is the same as was observed through N_V, at this average grain size.

Further insight into the process may be obtained through Figs. (44)-(47) in which N_V, S_V, L_V and M_V are graphed versus time of anneal on logarithmic axes. With the exception of minor random deviations among the samples, the above properties all plot linearly on such a graph. The correlation coefficients, r, of the calculated best fit lines shown in the figures are all greater than or equal to 0.97. For each series, the calculated slopes of the lines vary among the parameters in the proportion

$$S_V : M_V, L_V : N_V = n : 2n : 3n$$

This results directly from the relationship of Eqs. (15)-(21). Also, in most of these figures, the slope of line representing the 25% deformed group is slightly less than that of the 80% group. Intercomparison of the slopes yields the following approximate values of n:

Figure (44). Number of grains per unit volume versus annealing time (logarithmic axes).

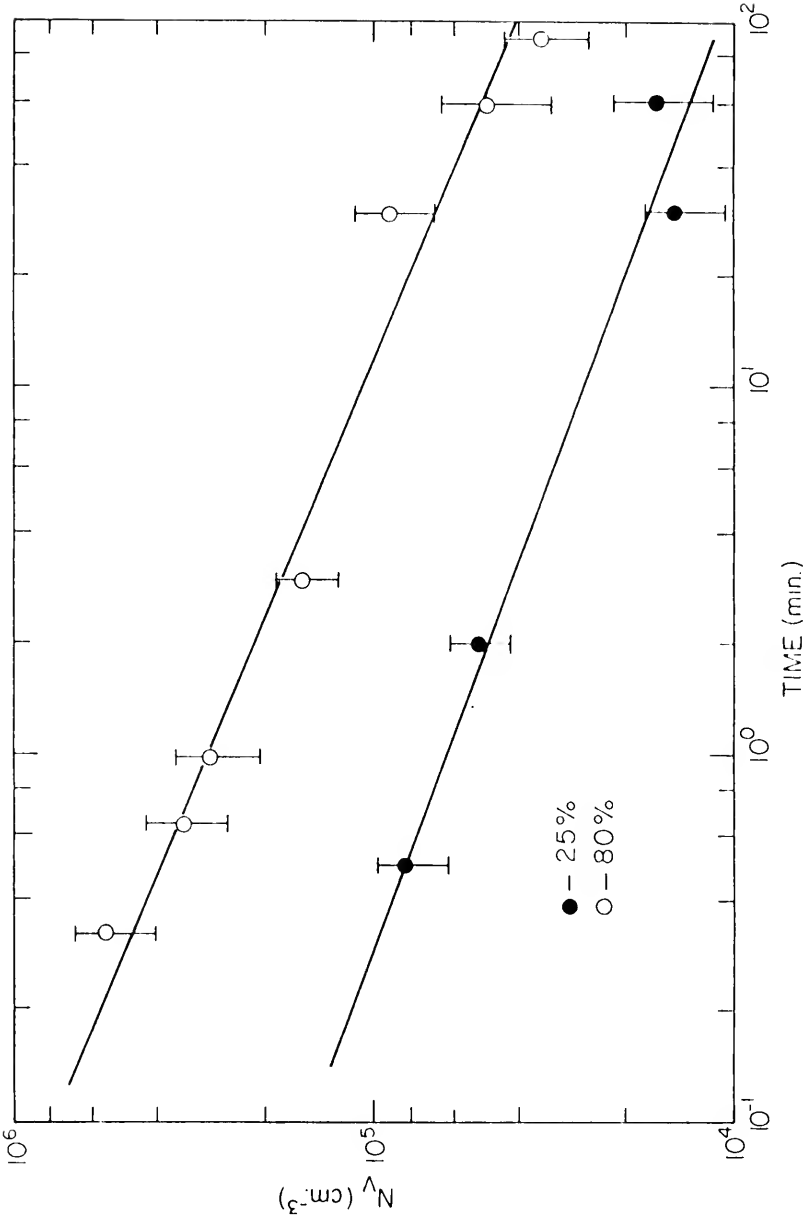
N_v (cm^{-3})
10^6
10^5
10^4
10^{-1}
10^0
10^1
10^2
TIME (min.)
● – 25%
○ – 80%

Figure (45). Grain boundary surface area per unit vilume versus annealing time (logarithmic axes).

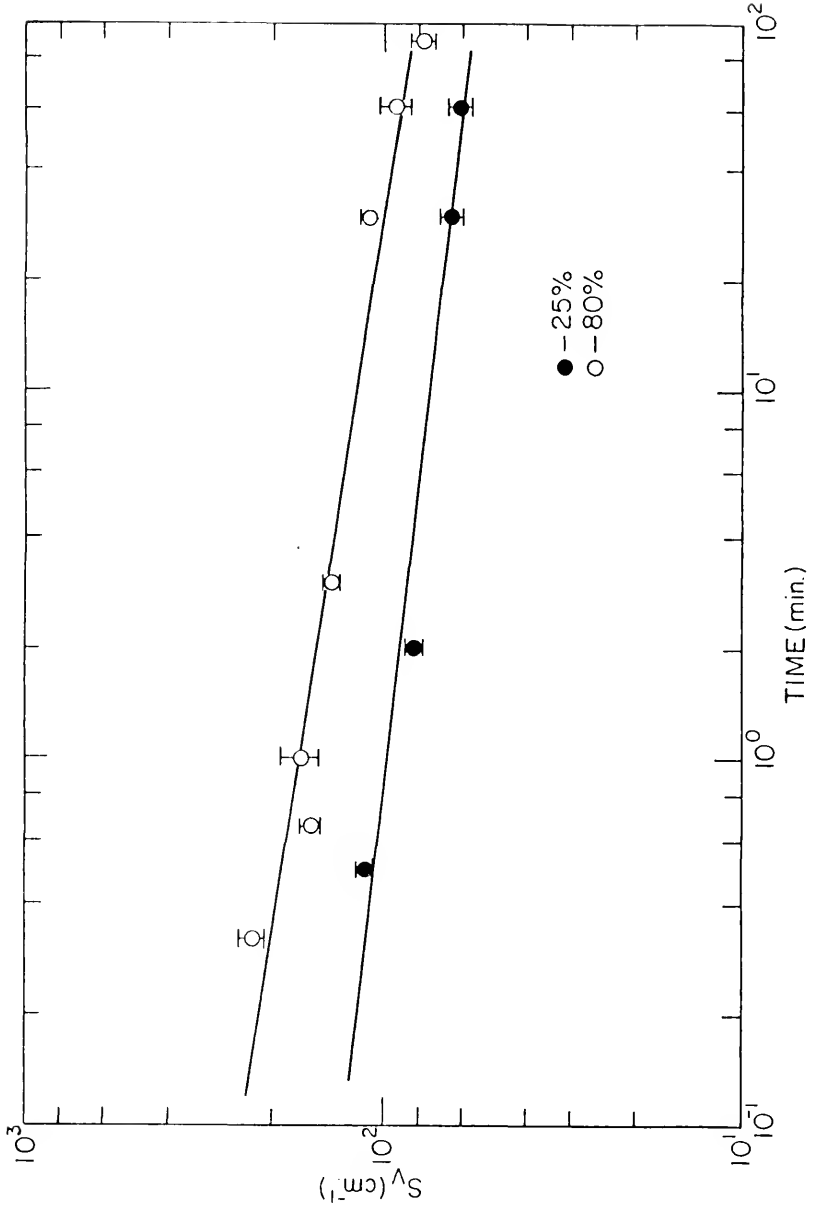
$S_V(cm^{-1})$
10^3
10^2
10^1
10^{-1}
10^0
10^1
10^2
TIME (min.)
● – 25%
○ – 80%

Figure (46). Grain edge length per unit volume versus annealing time (logarithmic axes).

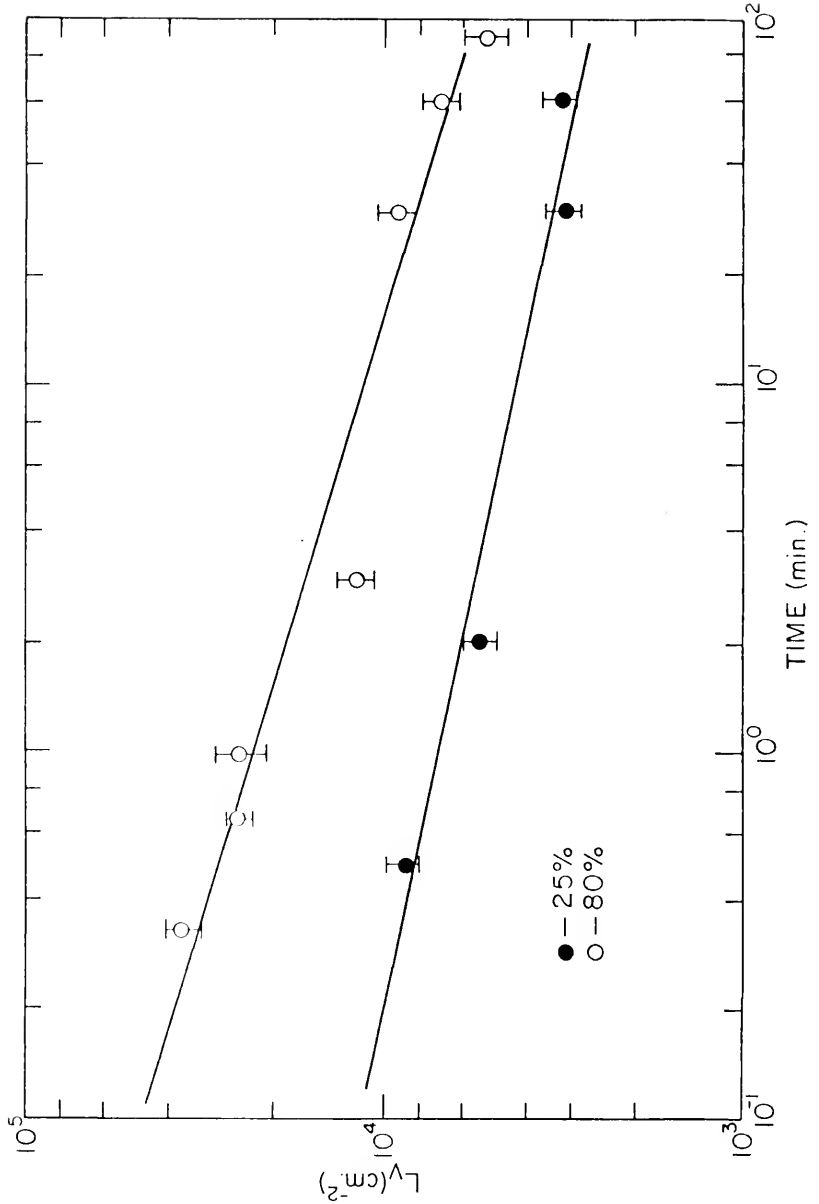
10^5
10^4
10^3
$L_V(cm.^{-2})$
10^{-1}
10^0
10^1
10^2
TIME (min.)
● — 25%
○ — 80%

Figure (47). Total grain boundary curvature per unit volume versus annealing time (logarithmic axes).

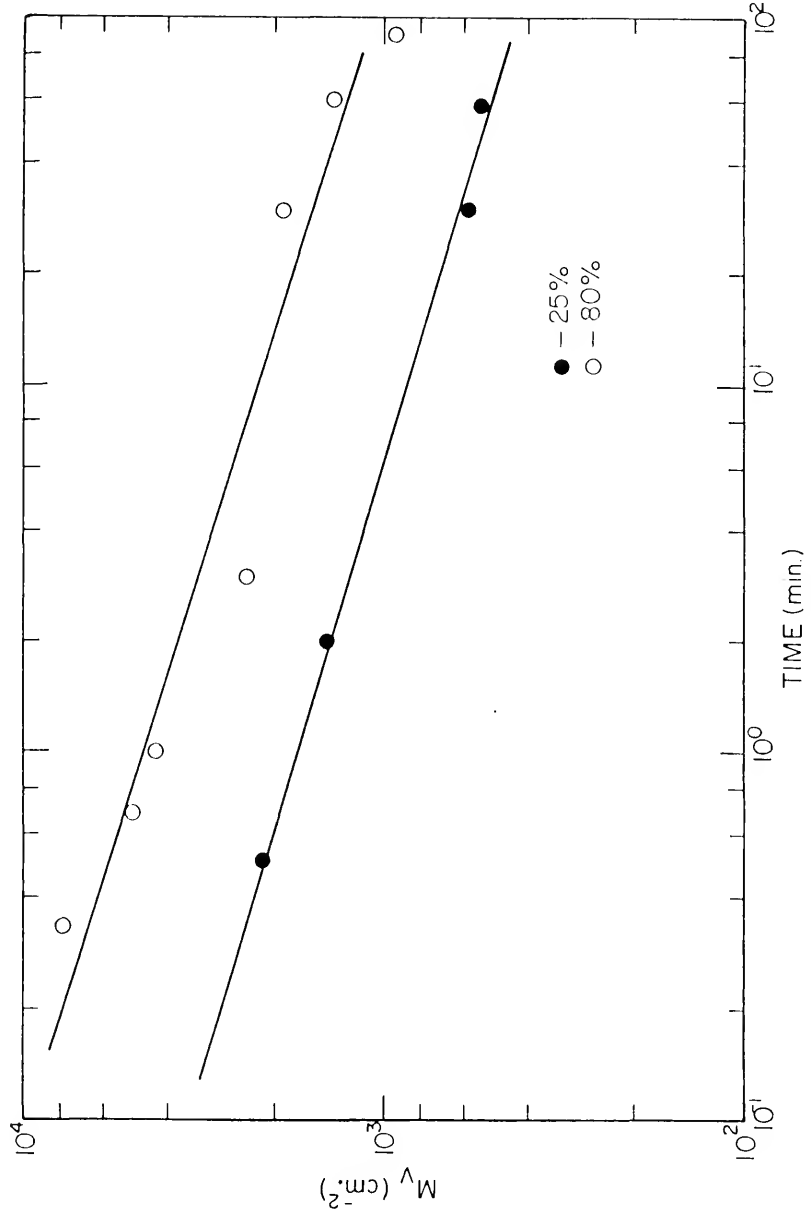
M_v (cm.$^{-2}$)
10^4
10^3
10^2
10^{-1}
10^0
10^1
10^2
TIME (min.)
● – 25%
○ – 80%

25% group : $n \simeq 0.11$

80% group : $n \simeq 0.15$

Figures (48)-(52) illustrate the related logarithmic plots of the average properties $\bar{V}$, $\bar{S}$, $\bar{L}$, $\bar{M}$, and $\bar{H}$. The correlation coefficients of the best-fit lines were again high, greater than or equal to 0.96, with the exception of the $\bar{M}$ and $\bar{L}$ plots in which r ranged from 0.81 to 0.92. From Eqs. (15)-(21), the slopes of these lines should, and do, vary in the proportion

$$\bar{L},\ \bar{M},\ \bar{H},\ \bar{\lambda} : \bar{S} : \bar{V} = n : 2n : 3n$$

The good fit of the data in this type of plot is indicative of a relationship of the form

$$\ell n\ Y = \ell n\ A + bn\ \ell n\ t \tag{38}$$

or

$$Y = A\ t^{bn} \tag{39}$$

where Y may be any of the above parameters; A is a constant, related to some initial value of Y; $b = \pm(1, 2,$ or 3), depending on the parameter represented by Y; n is the previously given value of slope for the respective deformations; and t is the time of grain growth. Thus the various properties experimentally obey the following time dependencies:

$$N_V = A_1\ N_{V_0}\ t^{-3n} \tag{40}$$

Figure (48). Average grain volume versus annealing time (logarithmic axes).

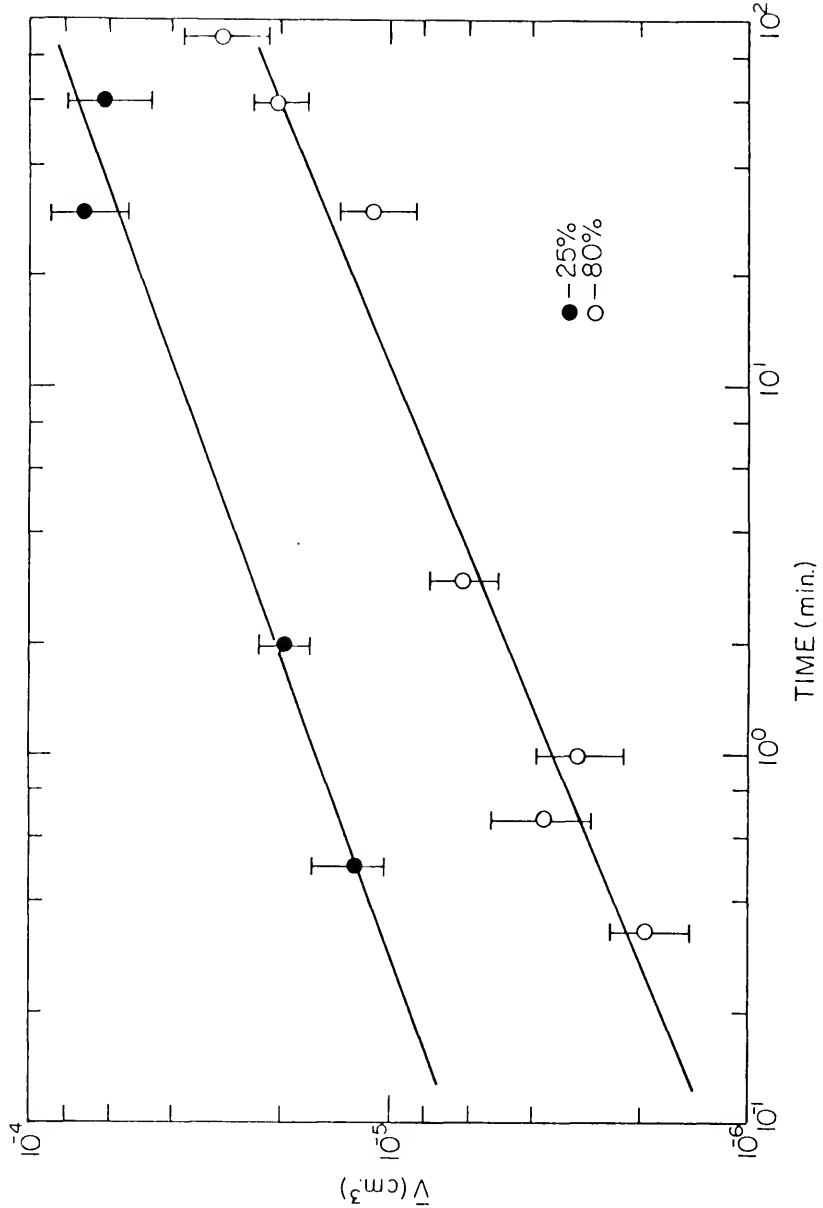
10^{-4}
10^{-5}
10^{-6}
$\bar{V}$ (cm.^{3})
10^{-1}
10^{0}
10^{1}
10^{2}
TIME (min.)
● – 25%
○ – 80%

Figure (49). Average surface area per grain versus annealing time (logarithmic axes).

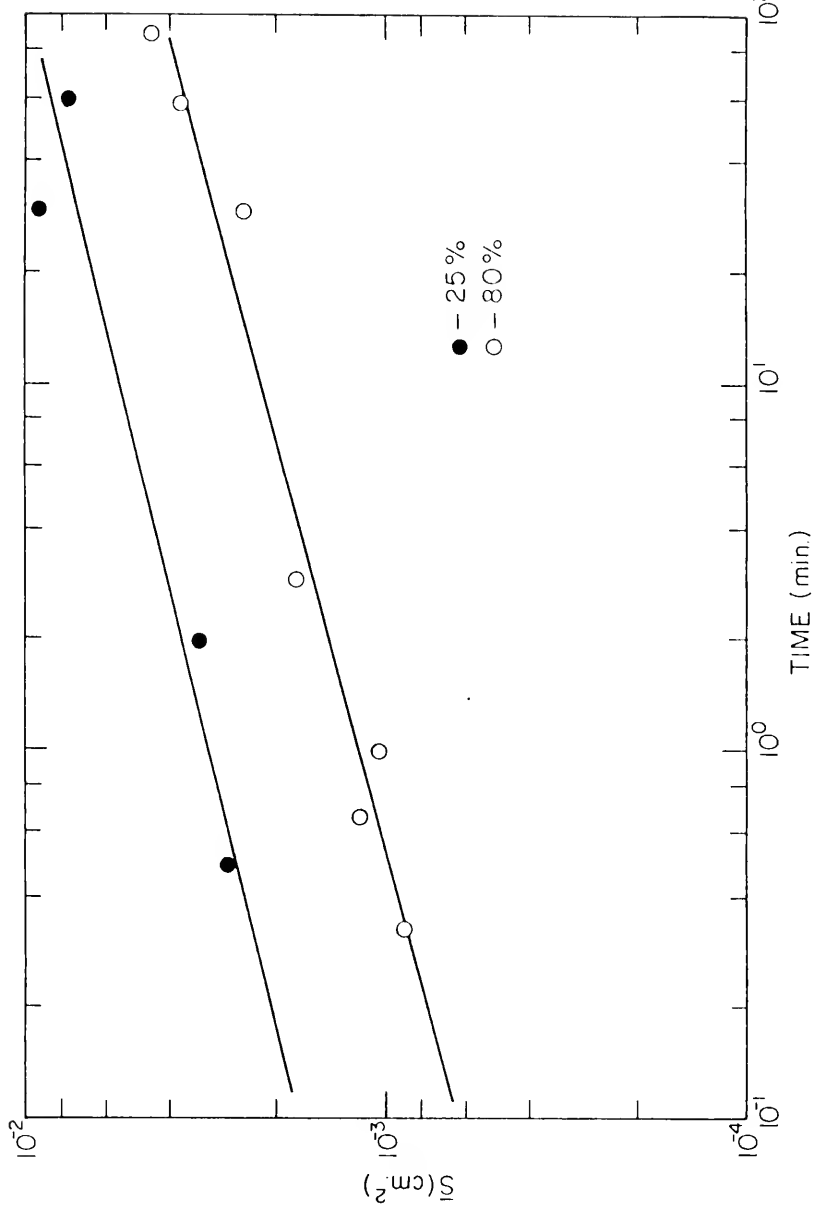
10^{-2}
10^{-3}
10^{-4}
10^{-1}
10^{0}
10^{1}
10^{2}
TIME (min.)
S(cm.$^{-2}$)
● – 25%
○ – 80%

Figure (50). Average edge length per grain versus annealing time (logarithmic axes).

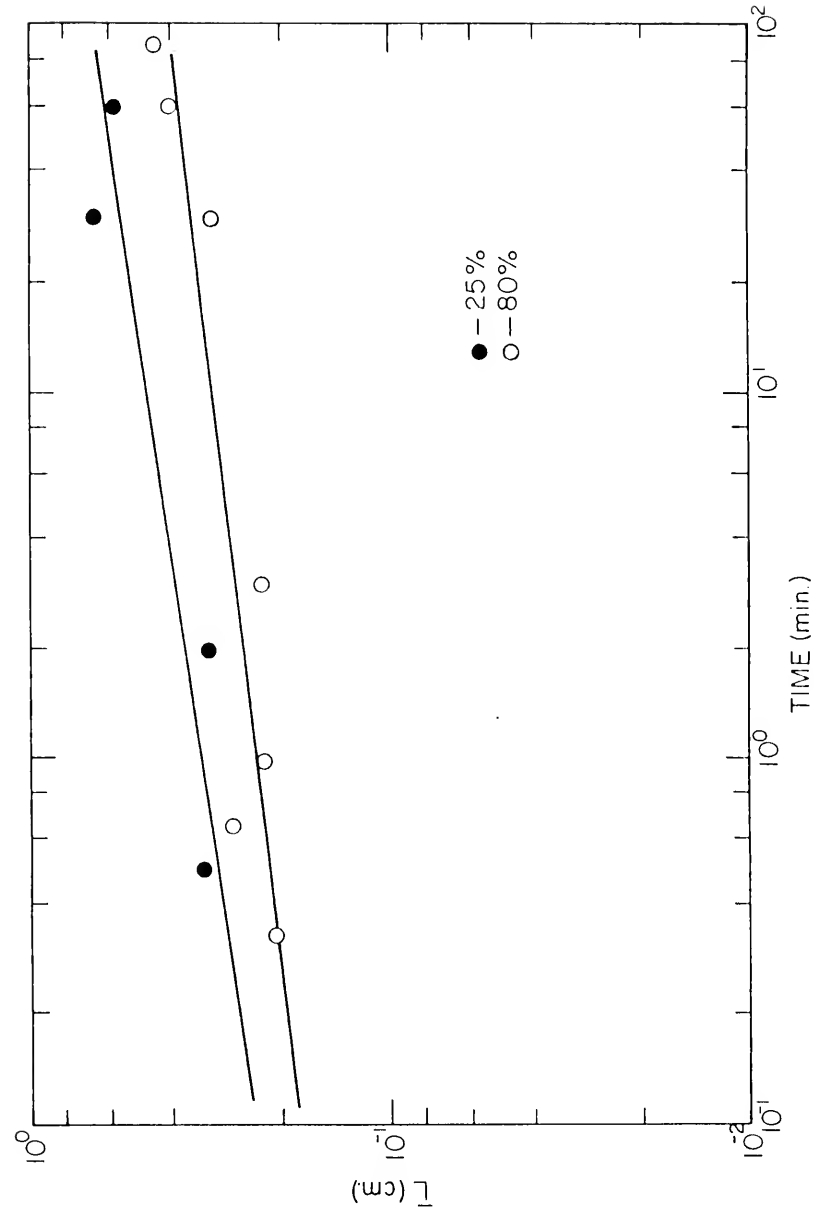
10^{0}
10^{-1}
10^{-2}
10^{-1}
10^{0}
10^{1}
10^{2}
$\bar{L}$ (cm)
TIME (min.)
● — 25%
○ — 80%

Figure (51). Average total curvature per grain versus annealing time (logarithmic axes).

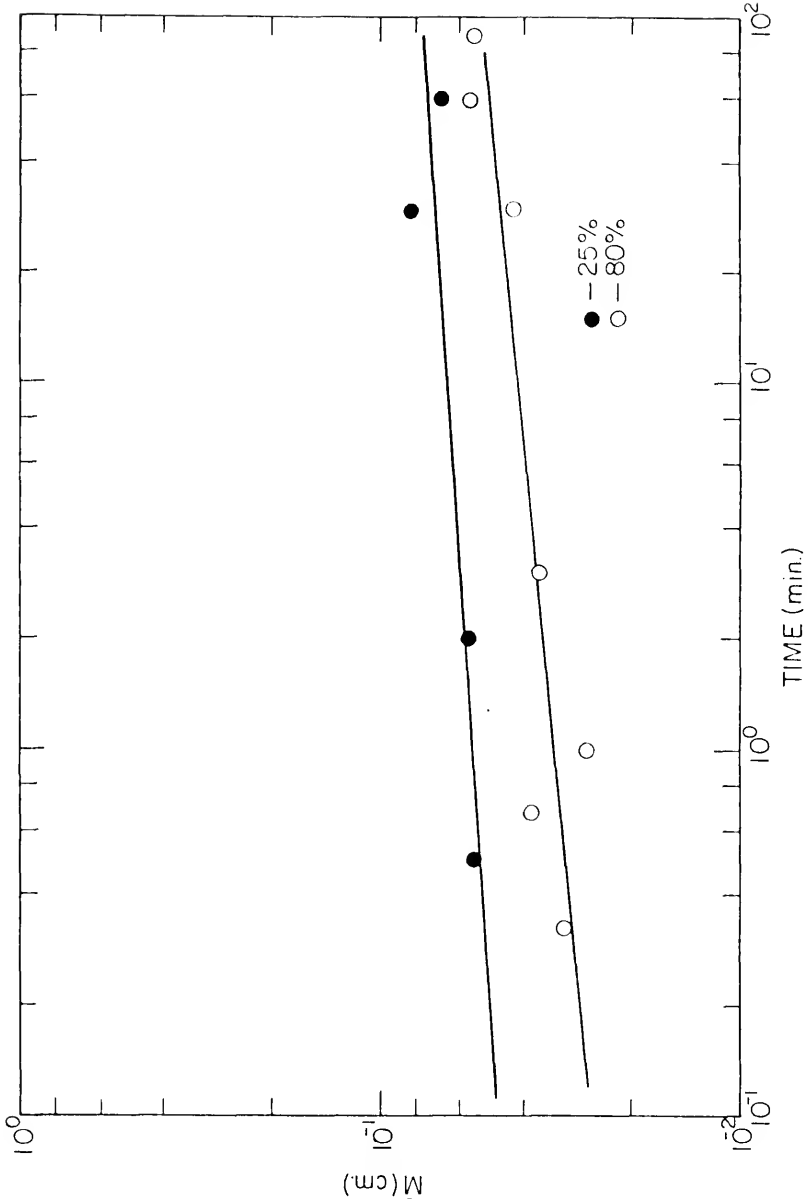
M (cm.)
TIME (min.)
25%
80%

Figure (52). Average mean curvature of grain boundary versus annealing time (logarithmic axes).

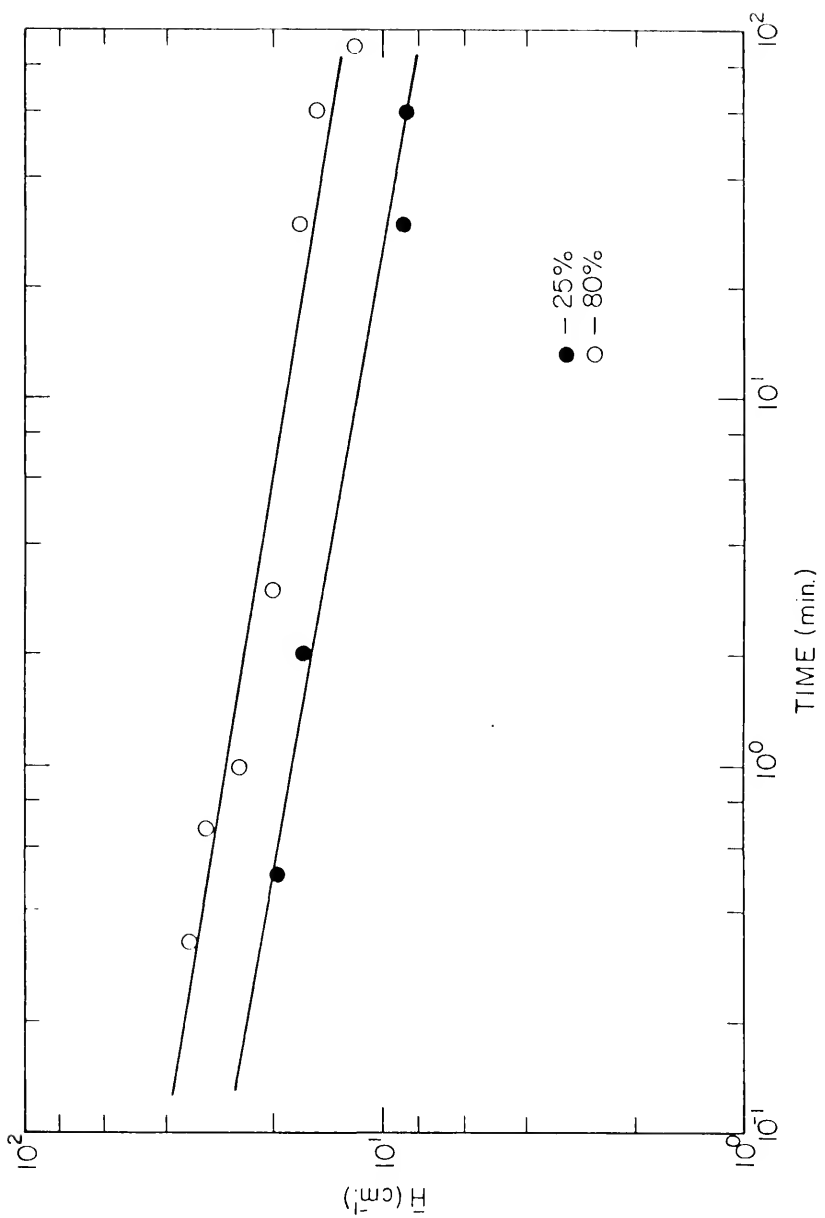
10^2
10^1
10^0
10^{-1}
$\bar{H}$ (cm^{-1})
10^0
10^1
10^2
TIME (min.)
● — 25%
○ — 80%

$$L_V = A_2 \, L_{V_0} \, t^{-2n} \tag{41}$$

$$M_V = A_3 \, M_{V_0} \, t^{-2n} \tag{42}$$

$$S_V = A_4 \, S_{V_0} \, t^{-n} \tag{43}$$

$$\bar{V} = (1/A_1 \, N_{V_0}) \, t^{3n} \tag{44}$$

$$\bar{S} = (2A_4 \, S_{V_0}/A_1 \, N_{V_0}) \, t^{2n} \tag{45}$$

$$\bar{L} = (3A_2 \, L_{V_0}/A_1 \, N_{V_0}) \, t^{n} \tag{46}$$

$$\bar{M} = (2A_3 \, M_{V_0}/A_1 \, N_{V_0}) \, t^{n} \tag{47}$$

$$\bar{H} = (A_3 \, M_{V_0}/A_4 \, S_{V_0}) \, t^{-n} \tag{48}$$

$$\bar{\lambda} = (2/A_4 \, S_{V_0}) \, t^{n} \tag{49}$$

The curved lines representing the trends of the data in Figs. (35)-(43) were obtained from the best fit lines of the logarithmic plots of Figs. (44)-(52).

Metric Shape Factors

Also of interest are the experimentally measured metric shape factors. As previously stated, these unitless combinations of two or more global properties may be employed to determine the presence or absence of a

constant microstructural state over the course of a kinetic process. Figures (53)-(59) illustrate the relationships of Eq. (15)-(21) using data from the present grain growth experiments. In each figure, the points representing the shortest annealing times are farthest from the origin of the growth. As grain growth progresses the values of the global properties decrease and the point moves toward the origin, generally in a straight path, the slope of which is the value of the steady-state shape factor. In these figures, there appears to be no discernible difference in the paths followed by the two groups of samples. The deviations of the data points, above and below the line, appear to be random and are probably due to inaccuracy of measurement.

The lines representing the path of microstructural change in these figures have been purposely drawn through the origin. The slopes of the lines have been chosen to provide a good fit in the individual graphs yet produce consistency among those figures which are interrelated. For example $(L_V/N_V^{2/3})/(S_V/N_V^{1/3})^2$ must equal L_V/S_V^2. The resulting relationships for these data are as follows:

$$S_V/N_V^{1/3} = 2.5$$

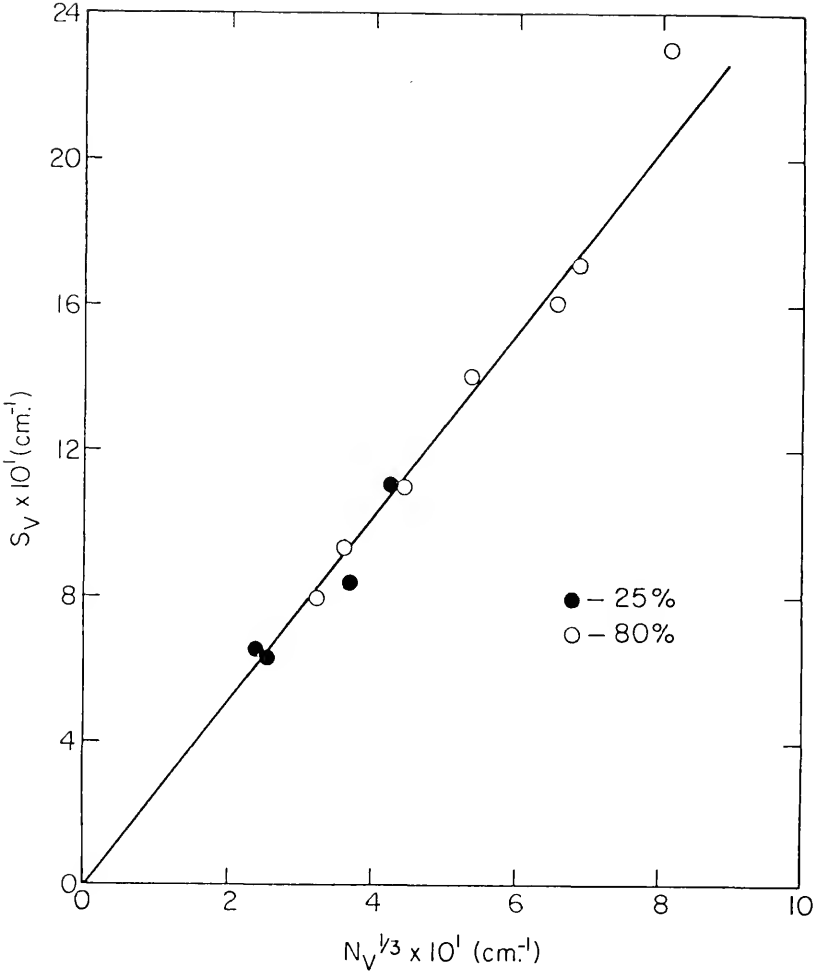

Figure (53). Surface area per unit volume versus (number of grains per unit volume)$^{1/3}$.

Figure (54). Edge length per unit volume versus (number of grains per unit volume)$^{2/3}$.

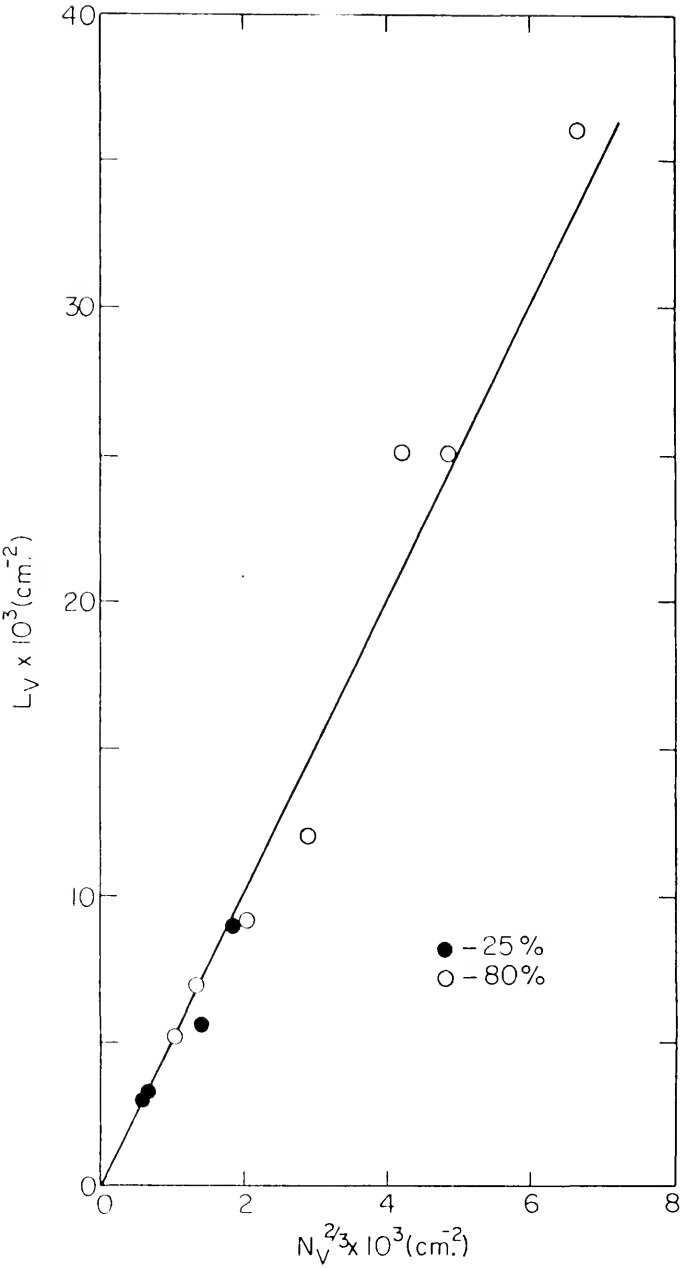
40
30
20
10
0
0
2
4
6
8
$L_V \times 10^3 (cm.^{-2})$
$N_V^{2/3} \times 10^3 (cm.^{-2})$
● – 25 %
○ – 80 %

Figure (55). Total curvature per unit volume versus (number of grains per unit volume)$^{2/3}$.

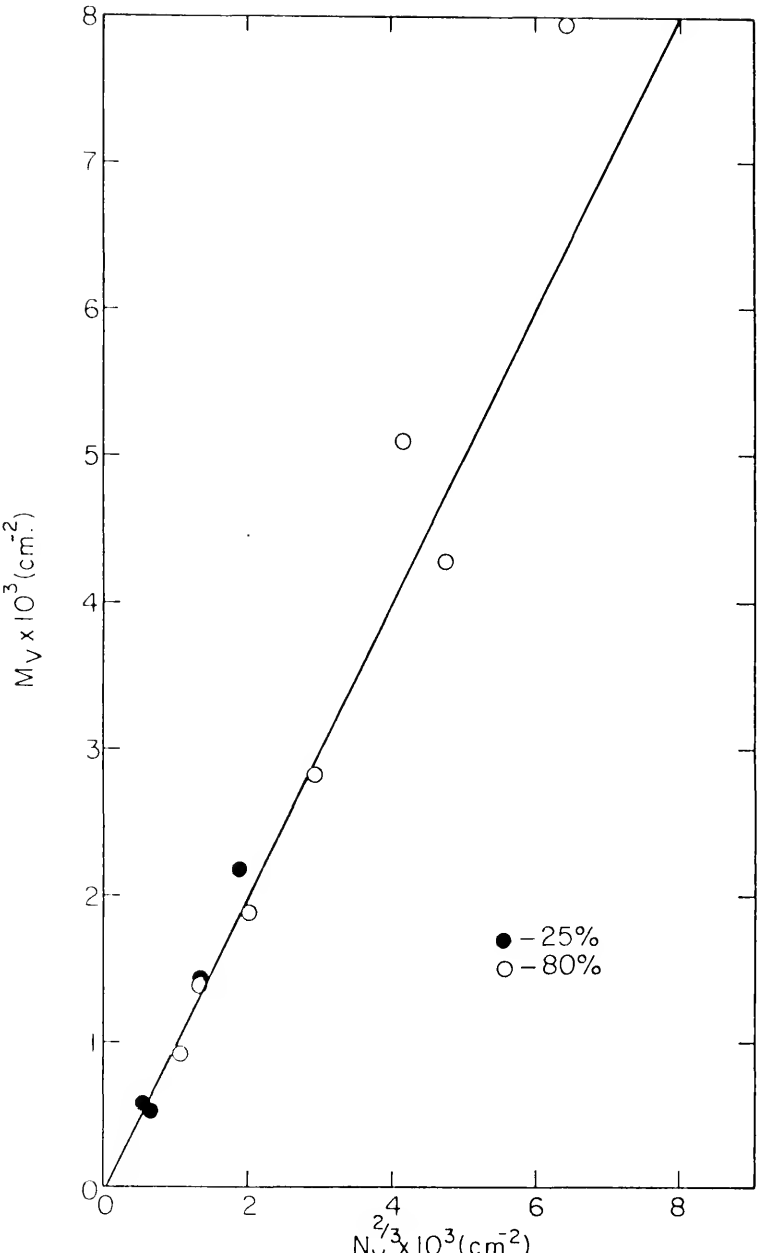
8
7
6
5
4
3
2
1
0
0
2
4
6
8
$M_V \times 10^3 (cm.^{-2})$
$N_V^{2/3} \times 10^3 (cm.^{-2})$
● – 25%
○ – 80%

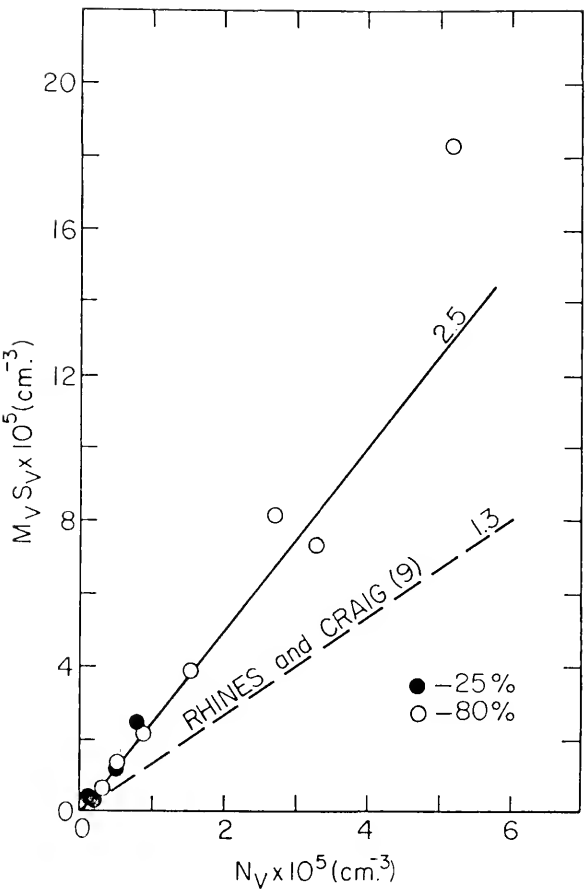

Figure (56). Product of total curvature per unit volume and surface area per unit volume versus number of grains per unit volume. Present data and results of Rhines and Craig (9).

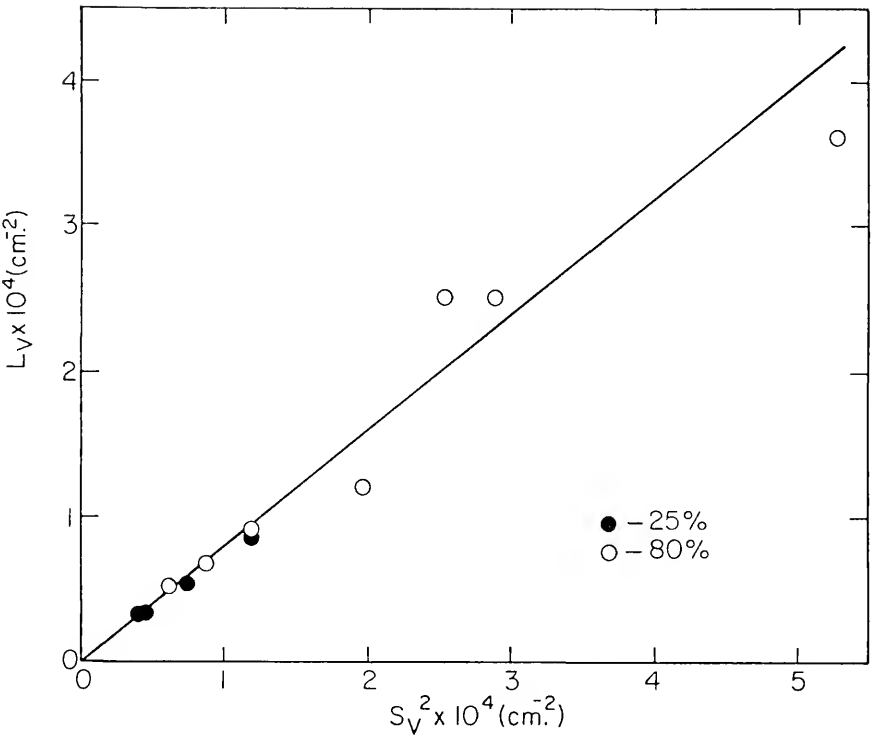

Figure (57). Edge length per unit volume versus (surface area per unit volume)^2.

Figure (58). Total curvature per unit volume versus edge length per unit volume.

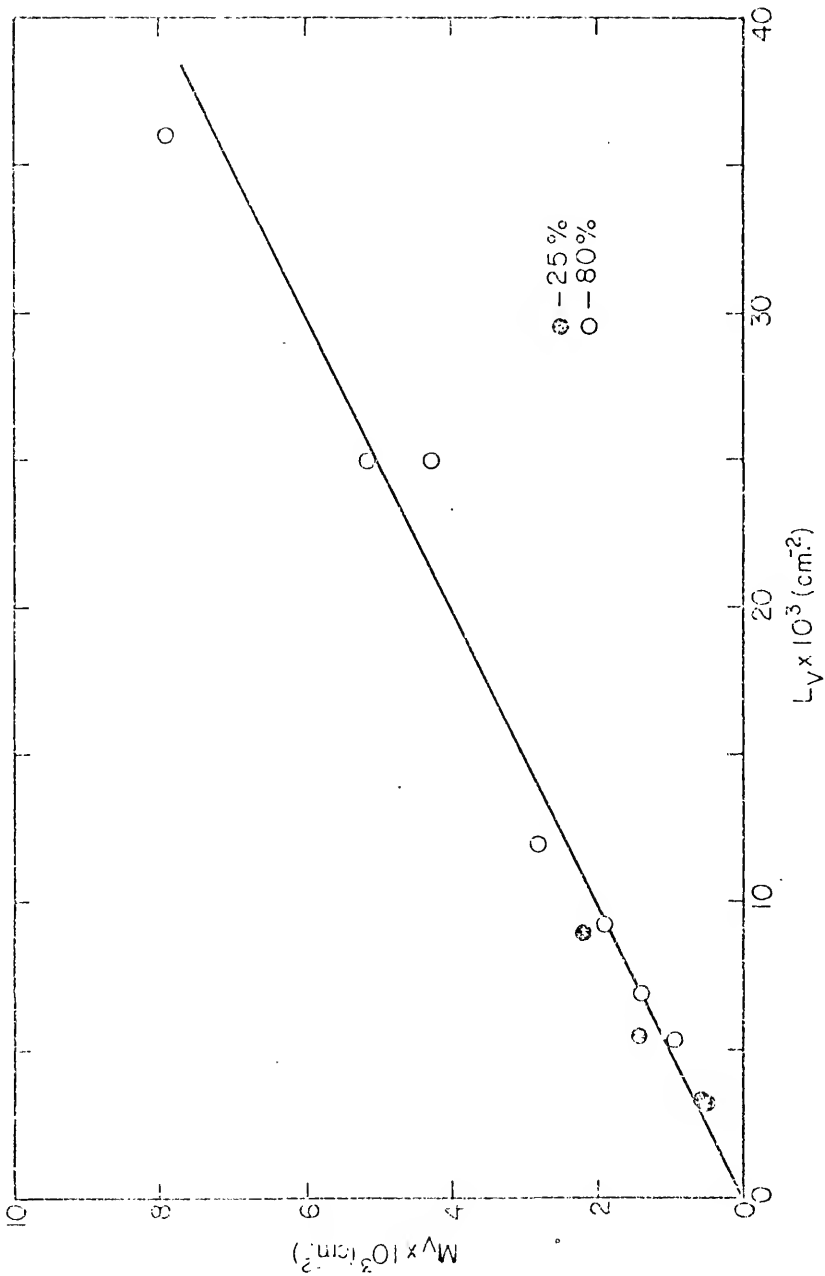
● - 25%
○ - 80%
$M_V \times 10^3 (cm.^2)$
$L_V \times 10^3 (cm.^{-2})$
0
2
4
6
8
10
0
10
20
30
40

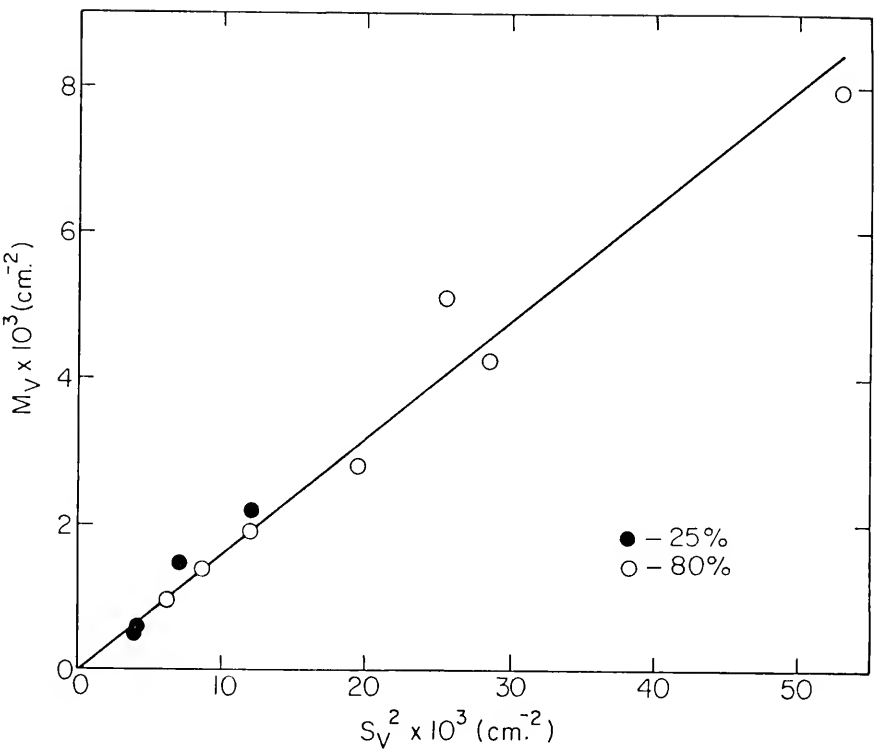

Figure (59). Total curvature per unit volume versus (surface area per unit volume)^2.

$$L_V/N_V^{2/3} = 5$$

$$M_V/N_V^{2/3} = 1$$

The remainder are dependent upon the above ratios:

$$M_V/L_V = 0.2$$

$$L_V/S_V^2 = 0.8$$

$$M_V/S_V^2 = 0.16$$

$$M_V\ S_V/N_V = 2.5$$

Rhines and Craig (9) also found $M_V\ S_V/N_V$ to remain constant throughout grain growth. The different slopes exhibited by their data and that of the present study [Fig. (56)], for similar material, is undoubtedly due to differences in the methods of measurement of M_V and S_V.

Anisotropy

Tables 6, 8, and 9 list information concerning the microstructural anisotropy of the specimens. Included are the values of the directed N_L, P_A, and T_A measurements, the amounts of planar and isotropic grain surface area and edge length, and the relative fractions of anisotropic surface and edge present in the samples. Most of the values of the oriented fractions are consistent within each series. The occasional deviations are most likely

due to measurement of an unrepresentative area of the sample, containing a coarser or finer than normal grain size.

Within each sample group, there appears to be no consistent trend of change in the degree of edge or surface anisotropy over the period of grain growth. This result is consistent with the previous observation of the metric shape factors remaining constant throughout the process. It can also be seen that, overall, the group deformed 80% possesses slightly greater anisotropy than the 25% group. This difference is unnoticeable in Figs. (53)-(59). In Figs. (53) and (55), sample 80-1 appears to have relatively larger values of S_V and M_V in proportion to N_V than the other samples. These deviations are magnified further in the plot of M_V S_V versus N_V [Fig. (56)]. However the degrees of anisotropy for this sample, given in Tables 6 and 9, appear to be normal, indicating that the deviations more likely represent an unrepresentative location of measurement, instead of deviation from the constant path of microstructural change.

Discussion

The findings of this chapter demonstrate that the rate of grain growth may vary among similar types of

materials of the same average grain size, annealed at similar temperatures. This phenomenon has gone unnoticed over a number of years of grain growth research. Undoubtedly, this has been due, at least in part, to the unobviousness of a reason why this behavior should occur. Beck (63), who was influenced by the results of experiments dealing with differences in prior annealing temperature, dismissed such a phenomenon in the early days of grain growth research. His brief observation of deformation effects (4) showed little variation.

Walker (64) had previously collected extensive grain growth data over a wide range of deformations and annealing temperatures. In analyzing Walker's data, however, neither Burke (51) nor Beck (63,65) observed the marked difference in growth rate among specimens of equal average grain size, which had previously been deformed by different amounts. Illustrated in Fig. (60), this facet of Walker's data has gone unnoticed until the present investigation. This behavior, in 70-30 brass, compares well with observations of the present studies, using aluminum [Fig. (61)].

The plot of $\bar{V}$ versus time on a logarithmic plot [Fig. (48)] does not, at first consideration, make apparent the 20-fold difference in $d\bar{V}/dt$ which was

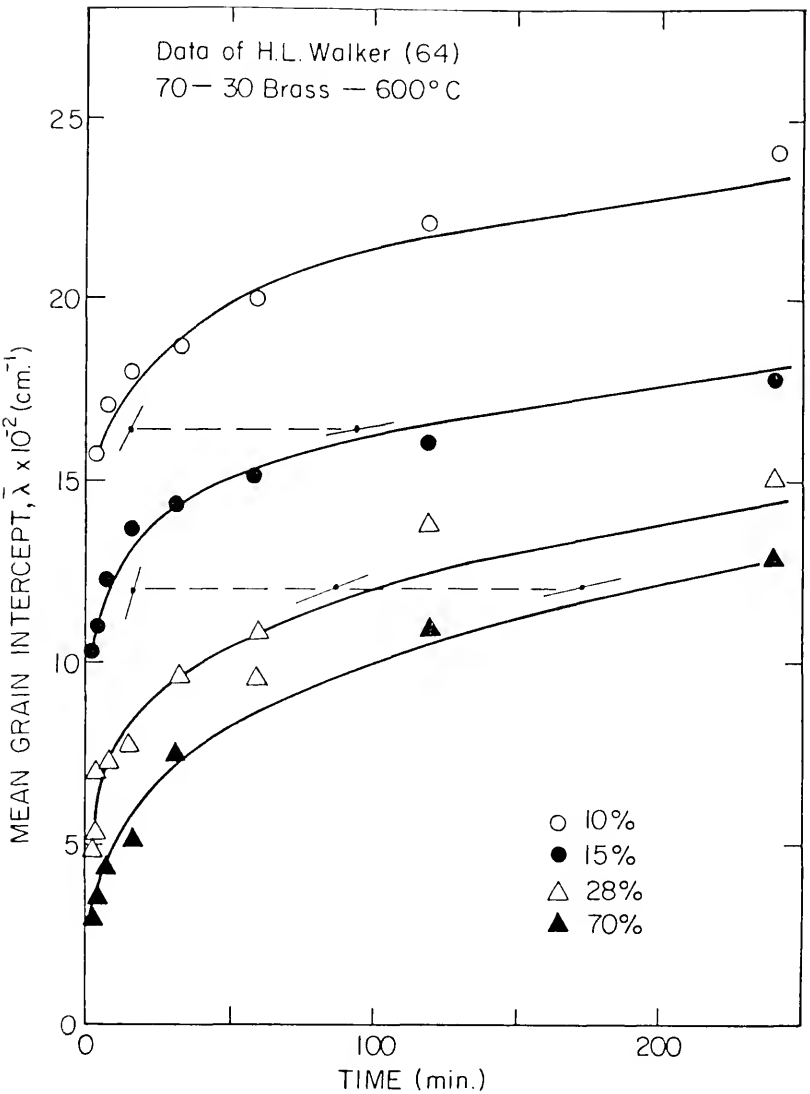

Figure (60). Mean grain intercept versus time of grain growth for 70-30 brass specimens deformed by different amounts and annealed at 600°C. Tangent lines indicate rates of grain growth at comparable grain sizes. Data of Walker (64).

Figure (61). Mean grain intercept versus time of anneal for specimens of the present study, which were deformed 25% and 80% prior to annealing at 635°C. Tangent lines indicate rates of grain growth at comparable average grain sizes.

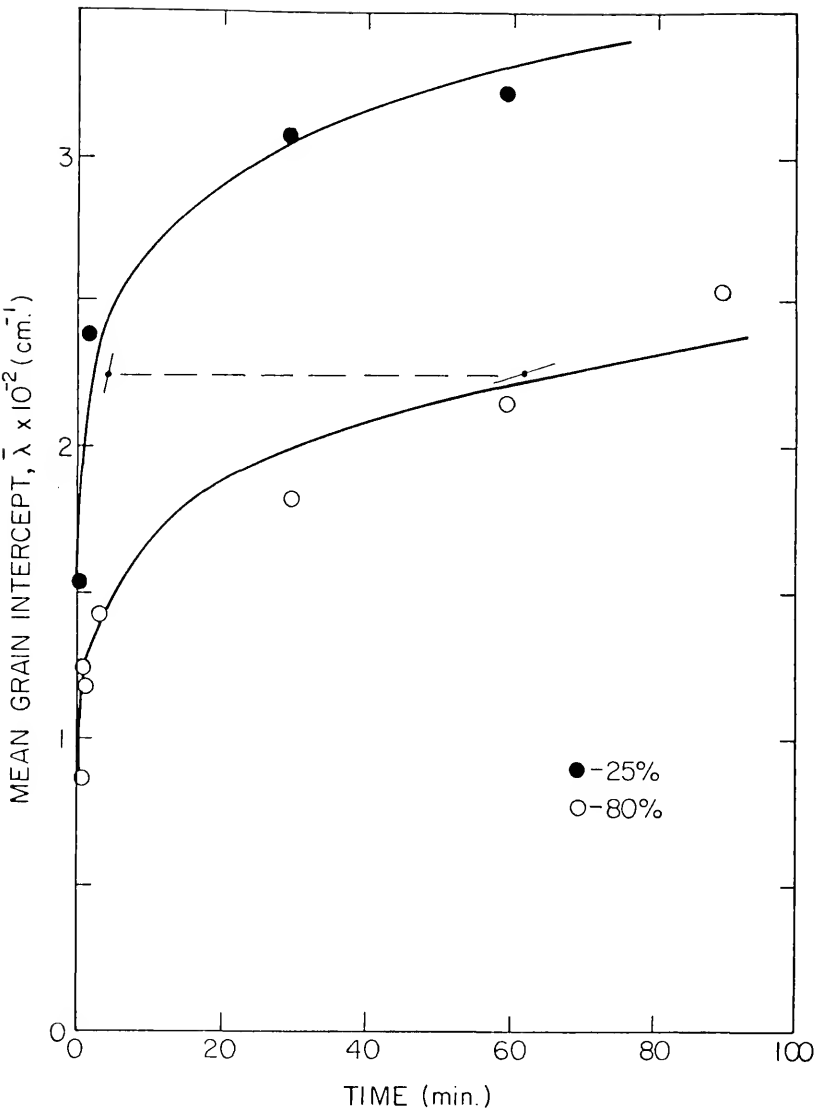
MEAN GRAIN INTERCEPT, $\bar{\lambda} \times 10^{-2}$ (cm.$^{-1}$)
TIME (min.)
0
1
2
3
0
20
40
60
80
100
●-25%
○-80%

measured from the tangent lines of Fig. (39). This difference becomes more visible when, as shown in Fig. (62), specimen 25-1 is shifted along the time axis to the growth curve for the 80% deformed specimens. If growth rate were dependent only on instantaneous grain size, the other 25% specimens should follow the growth path of the 80% group, when their annealing times are transposed along the time axis by the same amount as 25-1. As shown in Fig. (62), the 25% specimens exhibit a much faster growth rate than the 80% group when this is done, and their path becomes non-linear, contrary to Beck's supposition.

The degree of difference between the growth rates of the two series of specimens may be analyzed through the logarithmic plot of Fig. (48), to determine whether it remains constant throughout the growth process or whether it is variable. As mentioned in the experimental results, the growth laws of the two groups may be represented by

$$\overline{V_1} = K_1 \, t^{3n_1} \tag{50a}$$

and

$$\overline{V_2} = K_2 \, t^{3n_2} \tag{50b}$$

where K and n are constants and the subscripts, 1 and 2,

Figure (62). Average grain volume versus time of anneal (logarithmic axes), as in Fig. (48). The annealing times of the 25% deformed specimens have been increased by 20 min. to place specimen 25-1 in coincidence with the growth path of the 80% series.

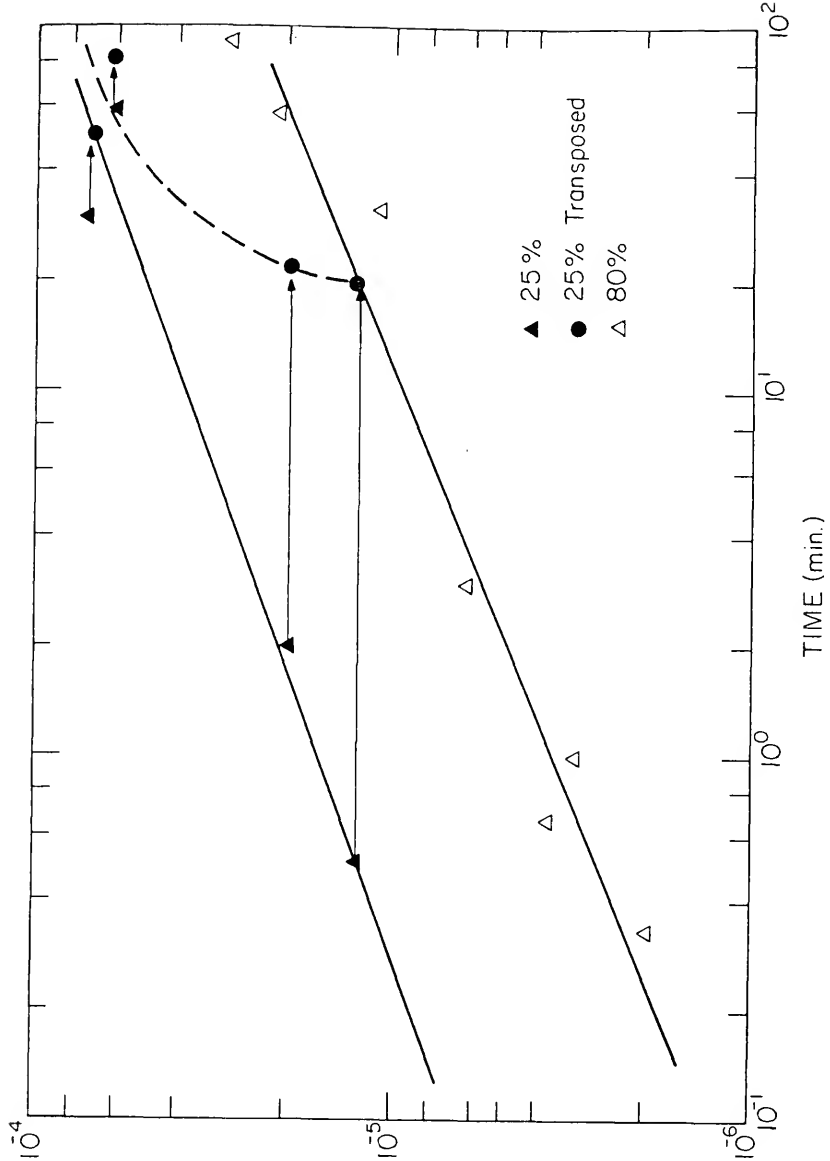
10^{-4}
10^{-5}
10^{-6}
$\bar{V}$ (cm^3)
10^{-1}
10^{0}
10^{1}
10^{2}
TIME (min.)
▲ 25 %
● 25% Transposed
△ 80%

refer to the respective series of deformed specimens. Differentiating, to obtain $d\bar{V}/dt$ with respect to grain volume, and equating the expressions for each series yields

$$\frac{d\bar{V}_1}{dt} = \frac{n_1}{n_2} \frac{K_1^{1/3}}{K_2^{1/3}} \frac{d\bar{V}_2}{dt} \tag{51}$$

Since the values of n and K are all constants, in the respective empirical growth laws given above, the rates of growth of the two series must differ by a fixed amount, at equal values of $\bar{V}$, throughout grain growth.

On consideration of the observed variation of $\ell n\ \sigma_V$ with deformation, the difference in growth rate would appear to be due to the variation of some influence of the grain size distribution. Theoretically, this influence could be through the resulting degree of face curvature, the frequency of dynamic, 3-edged faces, or through both. The lack of measurable difference between the metric shape factors of the two deformation series [Figs. (53)-(59)] tends to rule out the first, and more traditional, of the above explanations. Reconsideration of the E_F data, however, lends strong support to the notion of a topological mechanism controlling the process.

In Fig. (63), the frequencies of triangular faces have been replotted versus true strain. The percentages of these faces at the projected equivalents of 25% and 80% engineering strain are seen to be $\sim$4% and $<<$1% respectively. Although the exact frequency of faces could not be measured for the 80% deformed specimens, due to the fineness of their grain sizes, the trend shown in Fig. (63) indicates that the difference in frequencies between the two series could be as great as 20, the observed difference in the rate of grain growth. Furthermore, the constancy of the degree of difference between the rates of grain growth of the two series, throughout the process, is consistent with the apparent invariant nature of the topological state.

It thus appears that although grain boundary curvature is undoubtedly the driving force for grain growth, the rate at which the process occurs is governed by the availability of the necessary topological features. For a given amount of grain growth to occur in a specimen, with the maintenance of a fixed relative grain size distribution, a finite number of triangular faces must be generated and lost. The greater the steady-state frequency of triangular faces present, due to the form of the grain size distribution, the proportionately faster

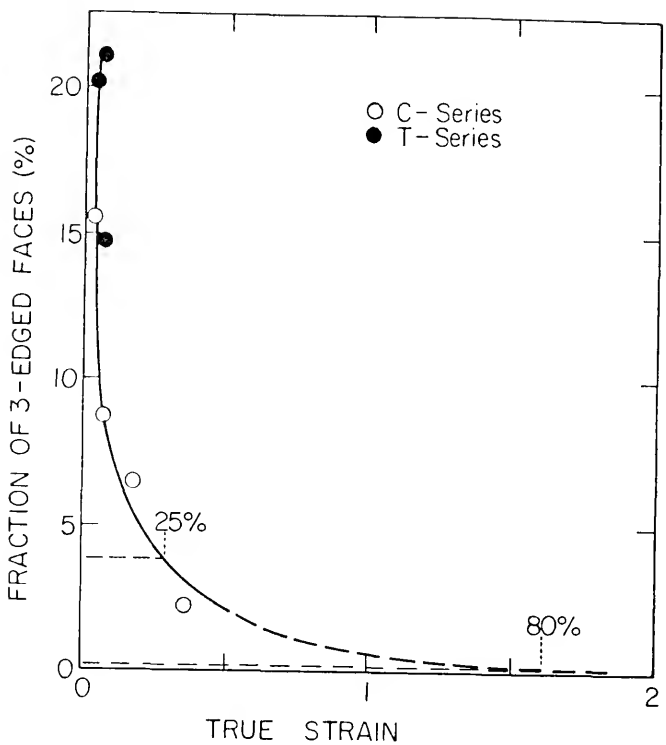

Figure (63). Percentage of faces with 3 or fewer edges versus true strain prior to recrystallization and grain growth.

can the necessary events occur. The rate of grain growth may thus be thought of as at least approximately proportional to the percentage of triangular faces within a material. This result supports, and to an extent, adds to the topological models of grain growth which have previously been put forth (8-10).

CONCLUSIONS

The above studies of the distribution of grain sizes in annealed and cast metals have shown that this distribution is not merely an end product of evolutionary microstructural processes, but is a viable property in itself, which in turn controls other microstructural properties and processes. Several of the effects and relationships which have been found in this investigation, with regard to the grain size distribution are given below.

1. The grain size distributions of recrystallized, grain grown, and cast metals are consistently log-normal in form. The relative width or degree of dispersion of the distribution may be intentionally adjusted over a considerable range of values. Increased solidification rates and increased amounts of deformation prior to recrystallization decrease the width of the grain size distribution, as measured through $\ell n\ \sigma_V$, the standard deviation of the logarithms of grain sizes.

2. The distributions of the numbers of faces per grain (F_G) and edges per grain face (E_F) are log-normal in form. The widths of these distributions, $\ell n\ \sigma_F$ and $\ell n\ \sigma_E$, are directly proportional to $\ell n\ \sigma_V$, the width of

the grain size distribution. The distributions of these topological features may also be controlled through deformation and, presumably, solidification rate.

3. The frequencies of 3-edged faces and 4-faced grains are directly proportional to $\ell n\ \sigma_E$ and $\ell n\ \sigma_F$, and therefore are similarly proportional to $\ell n\ \sigma_V$ as well. The prevalence of these features may thus be controlled through deformation and annealing or solidification processing.

4. Grain growth may occur at rates which differ greatly among similar specimens of equal average grain size, annealed at the same temperature, depending on the amount of deformation they have received prior to the recrystallization. The lack of measurable difference in the amount of boundary curvature in such specimens tends to exclude variation in driving force as the cause of this phenomenon. The multifold decrease in the frequencies of 3-edged faces with increased deformation, similar in magnitude to the decrease in the rate of grain growth, suggests that for a given driving force, the rate of grain growth is controlled by the rate of occurrence of the topological events required for growth. Once the grain size distribution has evolved through recrystallization, its form remains unaffected by later grain growth.

APPENDIX A
GRAIN WEIGHT DATA

Specimen C-1*

Weight $X10^{-4}$ (gm.)	Number of grains
≤1	15
2- 10	36
11- 20	24
21- 30	22
31- 50	17
51- 75	23
76-125	18
126-300	20
301-600	2

Specimen C-2*

Weight $X10^{-4}$ (gm.)	Number of grains
≤1	15
2- 5	23
6- 10	17
11- 15	16
16- 20	16
21- 25	10
26- 30	11
31- 35	11
36- 50	10
51- 80	15
81-300	5

Specimen C-3*

Weight $X10^{-4}$ (gm.)	Number of grains
≤1	12
2	8
3	8
4- 5	14
6- 10	14
11- 15	7
16- 20	9
21- 30	7
31- 60	5

Specimen C-4*

Weight $X10^{-4}$ (gm.)	Number of grains
≤1	53
2	42
3	32
4	27
5- 6	53
7- 8	32
9- 10	25
11- 15	39
16- 25	36
26- 50	27
51-100	6

Specimen T-3*

Weight $X10^{-4}$ (gm.)	Number of grains
≤1	6
2- 10	1
11- 25	7
26- 50	9
51- 150	14
151- 250	13
251- 500	12
501-1000	12
1001-2000	7
2001-2500	1

Specimen T-6-1*

Weight $X10^{-4}$ (gm.)	Number of grains
≤0.1	22
0.2- 0.5	30
0.6- 1	32
2 - 5	59
6 - 10	31
11 - 15	17
16 - 30	19
31 -100	19
101 -200	5
201 -250	1

Specimen T-6-2*

Weight $X10^{-4}$ (gm.)	Number of grains
≤0.1	7
0.2- 0.5	30
0.6- 1	39
2 - 5	74
6 - 10	39
11 - 15	23
16 - 25	33
26 - 40	31
41 - 60	31
61 -200	36
201 -300	6

Specimen S-1*

Weight $X10^{-4}$ (gm.)	Number of grains
≤1	23
2	13
3	10
4	13
5	17
6-10	10
11-20	6
21-30	4
31-35	1

Specimen S-2*

Weight $X10^{-4}$ (gm.)	Number of grains
≤1	117
2- 5	79
6- 10	48
11- 15	55
16- 20	32
21- 25	33
26- 35	41
36- 60	41
61-100	53
101-300	24
301-400	2

Specimen S-3*

Weight $X10^{-4}$ (gm.)	Number of grains
≤1	51
2- 10	36
11- 20	29
21- 40	25
41- 100	20
101- 300	26
301- 600	21
601-1200	19
1201-3000	23
3001-7500	2

Specimen 80-1*

Vol. $X10^{-8}$ ($cm.^3$)**	Number of grains
3.43- 6.86	405
6.87- 13.7	634
13.8 - 27.5	1072
27.6 - 54.9	1295
55.0 -110	1012
111 -220	444
221 -439	64
440 -878	4

*Specimen designations are explained on pages 19, 21, 22 and 116.

**Due to the Coulter counter analysis being affected by the electrical conductivity of the aluminum grains, the true volume limits of the various size classes are all higher than those reported above, by equal proportions.

APPENDIX B
EDGES PER GRAIN FACE

N	Numbers of faces with N edges, for each specimen*						
	C-1	C-2	C-3	C-4	T-3	T-6-1	T-6-2
2	1	-	-	-	36	42	12
3	21	15	18	4	226	233	267
4	37	62	82	57	328	376	539
5	39	48	81	65	262	257	451
6	26	31	49	27	188	175	294
7	11	12	29	16	177	99	165
8	7	4	13	1	65	50	96
9	-	-	-	1	35	31	39
10	-	-	-	-	24	20	24
11	-	-	-	-	12	11	8
12	1	-	-	-	5	2	5
13	-	-	-	-	2	2	1
14	-	-	-	-	1	-	2
15	-	-	-	-	-	1	-
16	-	-	-	-	1	2	-
17	-	-	-	-	2	-	-
18	-	-	-	-	-	-	-
19	-	-	-	-	-	1	-
26	-	-	-	-	-	1	-

*Specimen designations are explained on pages 19 and 21.

APPENDIX C
FACES PER GRAIN

N	Numbers of grains with N faces, for each specimen* T-3	T-6-1	T-6-2
3	3	7	-
4	5	1	6
5	9	10	5
6	6	10	10
7	6	14	13
8	4	8	9
9	3	6	13
10	5	5	8
11	5	2	12
12	5	4	5
13	5	6	7
14	5	2	6
15	1	5	7
16	4	2	8
17	2	4	3
18	2	1	3
19	-	2	3
20	2	1	2
21	3	1	5
22	3	-	2
23	3	2	2
24	4	1	3
25	1	1	3
26	1	-	-
27	1	1	-

continued

Appendix C - continued.

N	Numbers of grains with N faces, for each specimen* T-3	T-6-1	T-6-2
28	-	-	-
29	-	4	2
30	1	1	-
31	-	-	1
32	-	-	1
33	-	1	1
35	-	1	-
37	1	-	1
38	1	-	-
39	-	-	1
41	-	-	1
42	1	-	-
48	-	-	1
56	1	-	-
58	-	1	-
59	-	1	-

*Specimen designations are explained on page 21.

APPENDIX D
MEASUREMENT OF THE LINEAL FEATURES OF ANISOTROPIC MICROSTRUCTURES

The Saltykov Model

The Saltykov model (1,11,58) assumes that the lineal features in anisotropic microstructures may be considered as infinitesimal segments, separable into several components, each with a fixed type of orientation: a) a linear component of line segments all parallel to some axis, b) a planar component of segments oriented isotropically within a plane, and c) a three-dimensionally isotropic component. Each of the four general microstructural classes [Figs. (64a)-(64d)]—isotropic, planar, linear, and planar-linear—is then the combination of a different set of the above components:

(a) isotropic microstructure; isotropic component only

(b) planar microstructure; isotropic and planar components

(c) linear microstructure; isotropic and linear components

(d) planar-linear microstructure; isotropic, planar and linear components

Figure (64). Characteristic microstructural orientations. Adapted from (11) and (58).

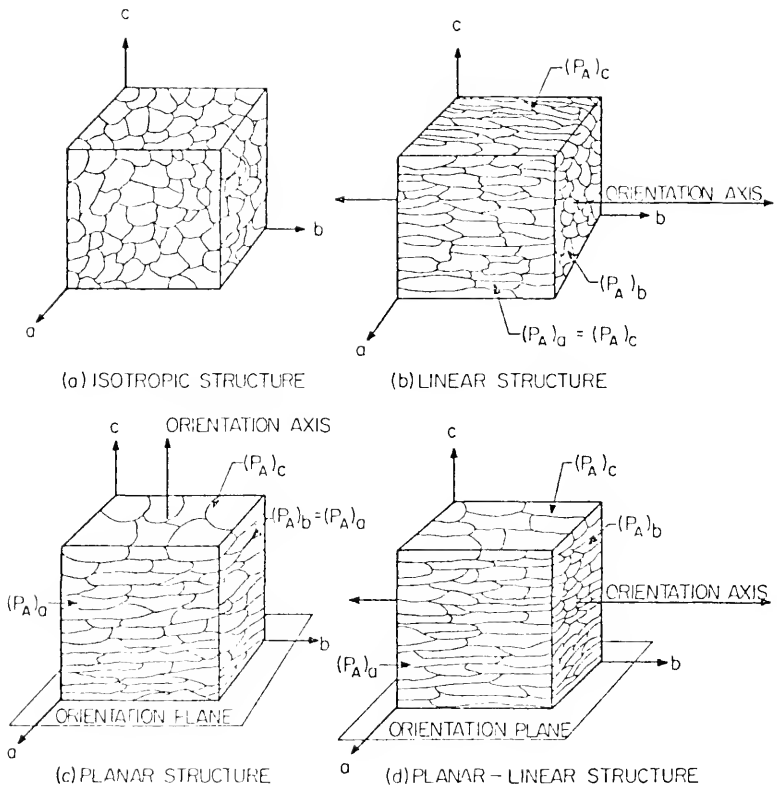
c
b
a
(a) ISOTROPIC STRUCTURE
c
$(P_A)_c$
ORIENTATION AXIS
b
$(P_A)_b$
$(P_A)_a = (P_A)_c$
a
(b) LINEAR STRUCTURE
c
ORIENTATION AXIS
$(P_A)_c$
$(P_A)_b = (P_A)_a$
$(P_A)_a$
b
ORIENTATION PLANE
a
(c) PLANAR STRUCTURE
c
$(P_A)_c$
$(P_A)_b$
ORIENTATION AXIS
$(P_A)_a$
b
ORIENTATION PLANE
a
(d) PLANAR – LINEAR STRUCTURE

For a given class of microstructure, L_V may be determined separately for each component, the total L_V for the structure being the sum of the components.

A relative degree of orientation may also be calculated by dividing L_V of any particular component by the total L_V, yielding the fraction of all lines having the orientation of that component.

Saltykov has previously developed equations for the analysis of lines in the linear class only. The corresponding equations for the planar and planar-linear classes are developed below.

Planar-Linear Structure

Saltykov's planar-linear class of anisotropy [Fig. (64d)] is typified by the microstructure of a rolled polycrystalline metal. The features* of such structures tend towards being both (a) elongated along an axis, termed the orientation axis, and (b) compressed into alignment with a plane parallel to this axis, the

*This analysis will consider only those microstructural features which are one-dimensional in space. Although the grain edges used as examples in the following derivations are not visible in Figs. (64a)-(64d), except for their points of emergence, their patterns of orientation will, of necessity, be related to those of the illustrated grains themselves.

orientation plane. The grain edge network of a planar-linear microstructure is thus composed of all three components of line-planar, linear, and isotropic-which may be calculated individually. Measurement of total L_V requires the evaluation of P_A on all three planes shown in Fig. (64d).

A test section parallel to the orientation plane intersects only isotropic component. The density of intersections with this plane,* $(P_A)_c$, yields the length per unit volume of isotropic edge, $(L_V)_{is}$:

$$(L_V)_{is} = 2(P_A)_c \qquad \text{(D-1)}$$

The calculation of the planar component, $(L_V)_{pl}$, requires the measurement of $(P_A)_a$ on a section perpendicular to the orientation plane and parallel with the orientation axis. Intersections from both planar and isotropic edges appear in this view. Since the density of intersections with isotropic component is again $(P_A)_c$, subtraction yields $(P_A)_{pl}$, the density of intersections on this plane from planar oriented lines alone:

$$(P_A)_{pl} = (P_A)_a - (P_A)_c \qquad \text{(D-2)}$$

*The terms $(P_A)_a$, $(P_A)_b$, and $(P_A)_c$ refer to P_A evaluated on the planes perpendicular to the similarly labeled axes in Figs. (64b)-(64d). As a convention, axes of elongation will always be parallel to the b-axis and axes of compression will parallel the c-axis.

This leads to the statistical problem of determining the relationship between the length per unit volume of line randomly oriented within a plane and the number of intersections it makes with a test plane perpendicular to the orientation plane. Consider a cubic volume [Figs. (65a) and (65b)] with edge length $\mathcal{L}$ and face area $\mathcal{L}^2$, which contains a number of infinitesimal line segments, $d\lambda$, oriented at random within a plane parallel to one side of the cube. If the cube is sectioned uniformly across its width with a test plane perpendicular to the orientation plane, P{int}, the probability of the plane intersecting an individual $d\lambda$, of orientation θ, is proportional to $dz(\theta)$, the <u>projected</u> length of $d\lambda$ in the direction perpendicular to the test plane:

$$dz(\theta) = d\lambda|\cos\ \theta| \qquad \text{(D-3)}$$

The ratio of the projected length of $d\lambda$ along the sectioning axis to $\mathcal{L}$, the total length sectioned over yields P{int}:

$$P\{\text{int}\} = \frac{dz(\theta)}{\mathcal{L}} = \frac{d\lambda|\cos\ \theta|}{\mathcal{L}} \qquad \text{(D-4)}$$

If the cube is sectioned N times by a plane of area $\mathcal{L}^2$, there will be $\frac{Nd\lambda|\cos\ \theta|}{\mathcal{L}}$ intersections with $d\lambda$ and a total area $N\mathcal{L}^2$ sectioned. Letting $dP_A(\theta)$ equal the average number of intersections with a single segment

Figure (65). (a) Isolated grain from planar oriented microstructure. Heavy grain edge segments have planar orientation, others are arrayed isotropically. (b) Relation of dz (θ), the projected length of a planar oriented line segment to θ, the relative angle of orientation of the segment.

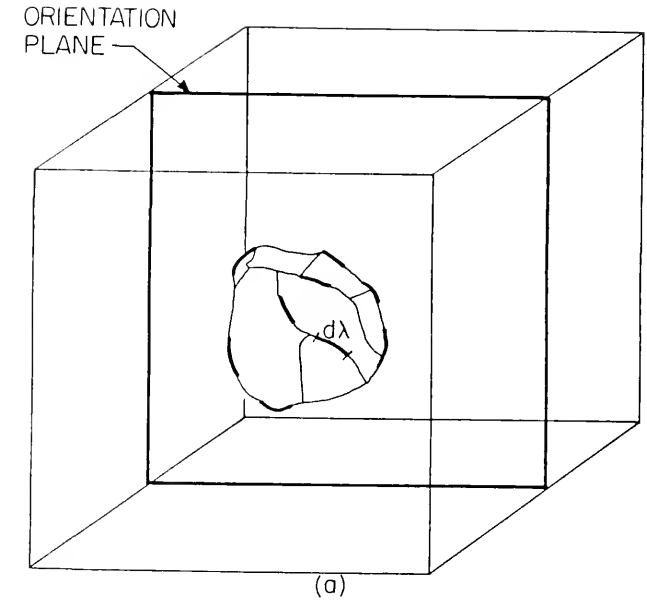
ORIENTATION
PLANE
dλ

(a)

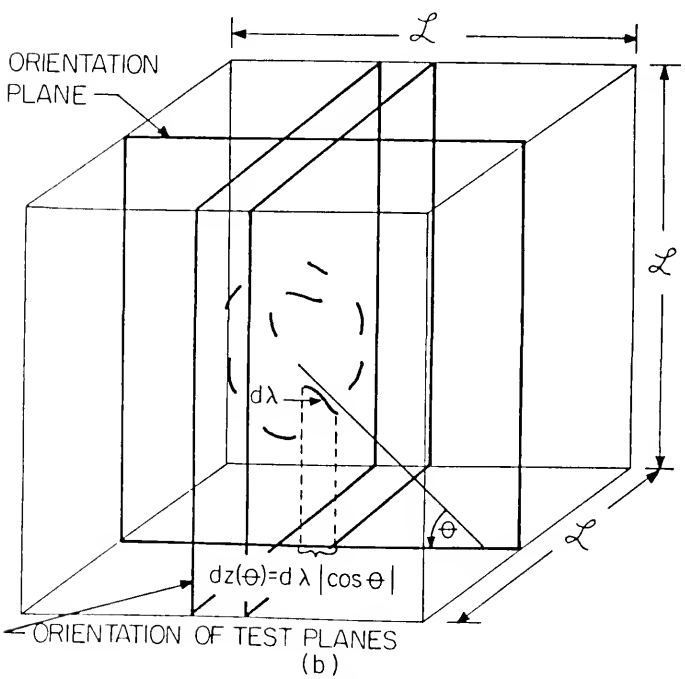
ℒ
ORIENTATION
PLANE
ℒ
dλ
θ
ℒ
dz(θ)=dλ|cosθ|
ORIENTATION OF TEST PLANES

(b)

oriented at some fixed θ, per unit area of test plane, yields

$$dP_A(\theta) = \frac{\text{total number of intersections}}{\text{total area sectioned}}$$

$$= \frac{Nd\lambda|\cos\ \theta|/}{N\mathcal{L}^2} = \frac{d\lambda|\cos\ \theta|}{\mathcal{L}^3} \qquad \text{(D-5)}$$

Since the planar segments to be measured are distributed at random within the orientation plane, $dP_A(\theta)$ must be averaged over all possible θ, by multiplying each incremental value of $dP_A(\theta)$ by the fraction of all possible orientations which lie within a narrow range $d\theta$. This fraction, $P(\theta)\ d(\theta)$, is given by

$$P(\theta)\ d(\theta) = \frac{d\theta}{\text{total possible range of orientations}}$$

$$= \frac{d\theta}{\pi} \qquad \text{(D-6)}$$

The segments are considered to only have an orientation range of π within the plane, since they have no sign of directionality.

Averaging $dP_A(\theta)$ over all θ yields

$$\overline{dP_A} = \int_{\theta=0}^{\pi} dP_A(\theta)\ P(\theta)\ d\theta = \int_{\theta=0}^{\pi/2} \frac{d\lambda|\cos\ \theta|}{\mathcal{L}^3} \quad \frac{d\theta}{\lambda}$$

$$= \frac{2d\lambda}{\mathcal{L}^3} \qquad \text{(D-7)}$$

where $\overline{dP_A}$ is the average number of intersections per unit area that parallel section planes would make with a

segment whose orientation within the plane was allowed to vary at random during the sectioning. Summing the number of intersections from the many $d\lambda$ within the orientation plane,

$$\overline{P_A} = \int_{\lambda} \frac{2d\lambda}{\pi \ell^3} = \frac{2(L)_{pl}}{\pi V} = \frac{2}{\pi} (L_V)_{pl} \qquad \text{(D-8)}$$

where $(L)_{pl}$ is the total length of planar oriented edge in the cube, ℓ^3 is equivalent to V, the volume of the cube, $(L_V)_{pl}$ is the resulting length of planar edge per unit volume and $\overline{P_A}$ is the average number of intersections from all planar oriented segments per unit area of test plane perpendicular to the orientation plane. Rearranging and noting that $\overline{P_A} = (P_A)_{pl}$,

$$(L_V)_{pl} = \frac{\pi}{2} \overline{P_A} = \frac{\pi}{2} (P_A)_{pl}^{*} \qquad \text{(D-9a)}$$

Combining with Eq. (D-2) yields

$$(L_V)_{pl} = \frac{\pi}{2} [(P_A)_a - (P_A)_c] \qquad \text{(D-9b)}$$

The density of intersections on a plane perpendicular to both the orientation axis and orientation plane $(P_A)_b$, includes points from all three components of edge.

*This result is the three-dimensional analog of the basic equation $L_A = \pi/2\ N_L$, relating the length per unit area (L_A) of random line on a plane to the number per unit length (N_L) of intersections of the line with a test line.

Subtraction yields $(P_A)_{lin}$, the density of intersections from linear component only:

$$(P_A)_{lin} = (P_A)_b - (P_A)_a \qquad \text{(D-10)}$$

The length per unit volume of parallel lines intersected by a perpendicular plane is exactly equal to the number of intersections per unit area on the plane. Using this relationship with Eq. (D-10) yields

$$(L_V)_{lin} = (P_A)_{lin} = (P_A)_b - (P_A)_a \qquad \text{(D-11)}$$

The total length of all edge per unit volume is given by the sum of the component lengths. Defining

$q_1 = \frac{(P_A)_b}{(P_A)_a}$ and $q_2 = \frac{(P_A)_c}{(P_A)_a}$,

$$(L_V)_{total} = (L_V)_{is} + (L_V)_{pl} + (L_V)_{lin}$$

$$= (P_A)_a \left[q_1+(2-\tfrac{\pi}{2})q_2+(\tfrac{\pi}{2}-1)\right] \qquad \text{(D-12)}$$

A planar-linear component, representing all non-isotropic edge, may also be computed:

$$(L_V)_{pl\text{-}lin} = (L_V)_{pl} + (L_V)_{lin}$$

$$= (P_A)_a \left[(q_1-1)+\tfrac{\pi}{2}(1-q_2)\right] \qquad \text{(D-13)}$$

Equations (D-14)-(D-16) yield the fractional amount of all line which is of the various component orientations. Degree of planar orientation:

$$(\Omega)^{L_V}_{pl} = \frac{(L_V)_{pl}}{(L_V)_{total}} = \frac{\frac{\pi}{2}(1-q_2)}{q_1+(2-\frac{\pi}{2})q_2+(\frac{\pi}{2}-1)} \qquad \text{(D-14)}$$

Degree of linear orientation:

$$(\Omega)^{L_V}_{lin} = \frac{(L_V)_{lin}}{(L_V)_{total}} = \frac{q_1 - 1}{q_1 + (2 - \frac{\pi}{2}) q_2 + (\frac{\pi}{2} - 1)} \qquad \text{(D-15)}$$

Degree of planar-linear orientation:

$$(\Omega)^{L_V}_{pl\text{-}lin} = \frac{(L_V)_{pl\text{-}lin}}{(L_V)_{total}} = \frac{(q_1 - 1) + \frac{\pi}{2}(1 - q_2)}{q_1 + (2 - \frac{\pi}{2}) q^2 + (\frac{\pi}{2} - 1)} \qquad \text{(D-16)}$$

It should be noted that Eqs. (D-14) and (D-15) result from Eq. (D-16) when $q_1 = 1$ and $q_2 = 1$, respectively.

Planar Structure

The grain boundary network of a uniaxially compressed polycrystal is an example of Saltykov's "planar" class of anisotropic microstructure [Fig. (64c)]. The features of such structures tend towards being aligned within a plane, but are not simultaneously elongated as in the planar-linear structure. This structure, composed of only the planar and isotropic components is thus a subset of the more general planar-linear case. The values of $(L_V)_{is}$, $(L_V)_{pl}$, $(L_V)_{total}$ and $(\Omega)^{L_V}_{pl}$ are again obtained through Eqs. (D-1), (D-9b), (D-12) and (D-16), simplified by the condition $q_1 = 1$, defining a planar structure.

Linear Structure

The linear class of microstructure, for which Saltykov has derived equations, is again a subset of the

planar linear class. It is composed of only linear and isotropic components and is defined by the condition $q_2 = 1$. The values of $(L_V)_{is}$, $(L_V)_{lin}$, $(L_V)_{total}$ and $(\Omega)^{L_V}_{lin}$ may thus be obtained from the above general equations. Paradoxically, there is thus no need to rigidly classify a specimen before analysis, although it may be convenient for descriptive purposes.

Length of Projected Line

The value of $(L_V)^{hk\ell}_{proj}$, the total length of line per unit volume projected in any direction, <hkℓ>, relative to the orientation axes, may be measured directly on a specimen, from the relationship

$$(L_V)^{hk\ell}_{proj} = (P_A)^{hk\ell} \qquad \text{(D-17)}$$

where $(P_A)^{hk\ell}$ is the value of P_A measured on the section plane normal to <hkℓ>, i.e. the {hkℓ} section plane. The value of $(L_V)^{hk\ell}_{proj}$ may also be calculated from the Saltykov model, yielding additional information without requiring extra measurements.

Once $(P_A)_{is}$, $(P_A)_{pl}$, and $(P_A)_{lin}$ have been calculated in relation to the principal planes, they may be calculated for any other plane as well. The sum of the component values calculated for the {hkℓ} plane estimates $(L_V)^{hk\ell}_{proj}$ for the specimen. The isotropic component

contributes the same $(P_A)_{is}$ in all directions*:

$$(P_A)_{is}^{hk\ell} = (P_A)_{is} = (P_A)_c \qquad \text{(D-18)}$$

For the linear component,

$$(P_A)_{lin}^{hk\ell} = (P_A)_{lin} \, |\cos \alpha|$$

$$= [(P_A)_b - (P_A)_a][\frac{|K|}{\sqrt{h^2+k^2+\ell^2}}] \qquad \text{(D-19)}$$

where $|\cos \alpha|$ is effectively the cosine of the acute angle between the linear orientation axis (b-axis) and $\langle hk\ell \rangle$.

The planar component contributes

$$(P_A)_{pl}^{hk\ell} = (P_A)_{pl} \sin \beta$$

$$= [(P_A)_a - (P_A)_c][\sin \cos^{-1}(\frac{|\ell|}{\sqrt{h^2+k^2+\ell^2}})] \qquad \text{(D-20)}$$

where β is the acute angle between $\langle hk\ell \rangle$ and the orientation axis of the planar oriented segments (c-axis).

Summing the component values yields the theoretical total $(P_A)^{hk\ell}$:

$$(P_A)^{hk\ell} = (P_A)_a[q_2+(q_1-1)(\frac{|K|}{\sqrt{h^2+k^2+\ell^2}})+(1-q_2)$$

$$\sin \cos^{-1}(\frac{|\ell|}{\sqrt{h^2+k^2+\ell^2}})] \qquad \text{(D-21)}$$

*Using the previously mentioned axial convention, the following equations are applicable for all classes of anisotropy.

Note that this equation, like Eqs. (D-12) and (D-16), may be used for specimens with any type of anisotropy since $q_1 = 1$ and $q_2 = 1$, respectively, for planar and linear systems, cancelling the unnecessary P_A component.

The Tetrakaidecahedron Model

The tetrakaidecahedron (TKD) model, suggested by DeHoff (59), also allows the estimation of total L_V for an anisotropic body from P_A measured on two or three section planes. The model employs the edges of an anisotropic Kelvin tetrakaidecahedron (truncated octahedron) as an analog of the lineal features of a real microstructure. Using the same axial convention and notation as before, the calculated lengths of TKD edge projected in the three principal directions are compared to the projected lengths of real line determined from P_A measurements. The shape of the modeling TKD is then altered (flattened, elongated or both) such that it and the specimen have similar values of $(L_V)_{proj}$ in those three directions. The projected lengths of the TKD edges in various directions are assumed to be representative of those of the real specimen. $(L_V)_{total}$ of the specimen is then that of the TKD.

It should be emphasized that this model does not assume any relation of the TKD to average grain shape.

It is employed here simply as an orientable geometric array of lines, convenient for mathematical description.

The TKD has 36 edges, of equal length when equiaxed, and 14 faces: 8 hexagonal and 6 quadrilateral. The dimensions of the body, both equiaxed and anisotropic, enclosed by a parallelpiped with axial lengths a, b and c, are illustrated in Figs. (66a) and (67a). The six quadrilateral faces contact those of the parallelpiped such that the projected lengths of all TKD edges along the major axes [Figs. (66b) and (67b)], are directly proportional to the axial lengths, a, b, and c. Once $(L_V)_{proj} (=P_A)$ has been measured in the principal directions of a real specimen, the axial ratios of the model can be set such that $(L_V)_{proj}$ for the TKD and the specimen are proportional in corresponding directions. Employing for convenience the previously defined P_A ratios,

$$q_1 = \frac{(P_A)_b}{(P_A)_a} = \frac{b}{a} \qquad \text{(D-22)}$$

$$q_2 = \frac{(P_A)_c}{(P_A)_a} = \frac{c}{a} \qquad \text{(D-23)}$$

The relative lengths and orientations of the individual TKD edges vary with and may be calculated in terms of q_1 and q_2, i.e. the degree of anisotropy. The

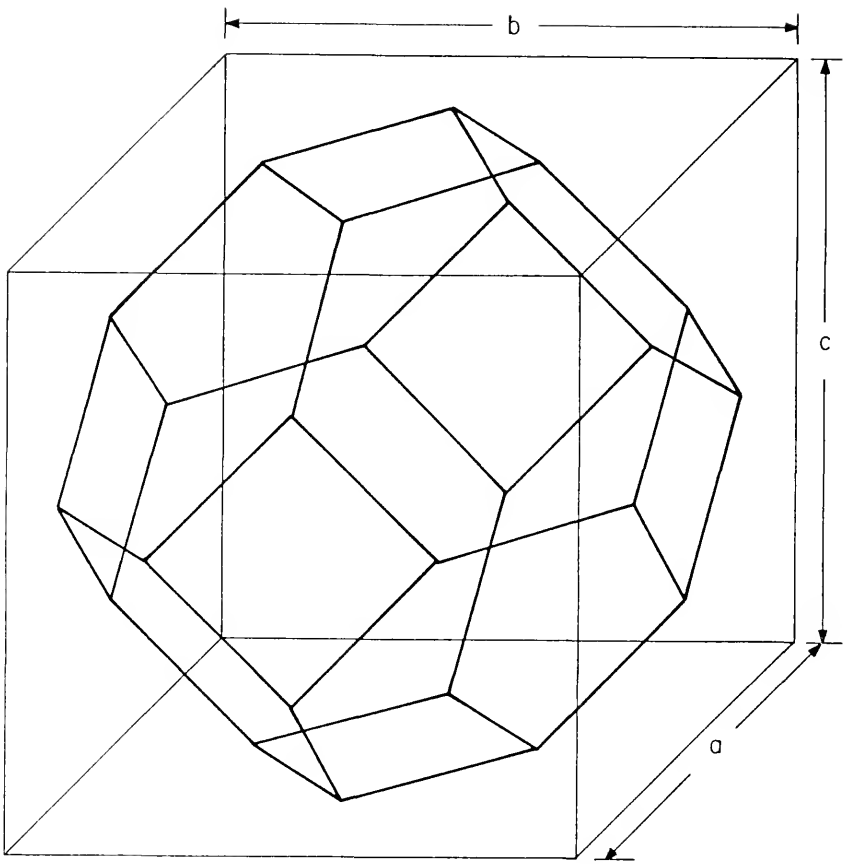

(a)

Figure (66). (a) Equiaxed tetrakaidecahedron: a = b = c; $q_1 = q_2$.

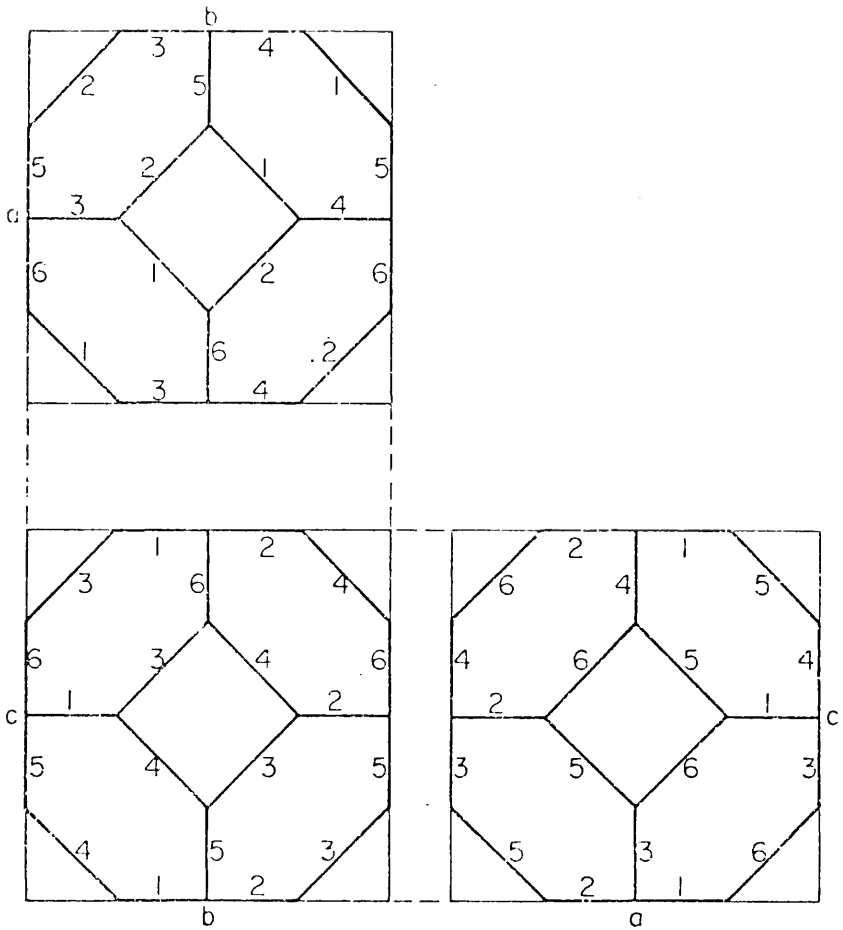

(b)

Figure (66). (b) Equiaxed tetrakaidecahedron, plan view. Edges of equal orientation and true length are numbered identically.

Figure (67). (a) Anisotropic tetrakaidecahedron: $a \neq b \neq c$; $q_1 = 1.75$, $q_2 = 0.625$.

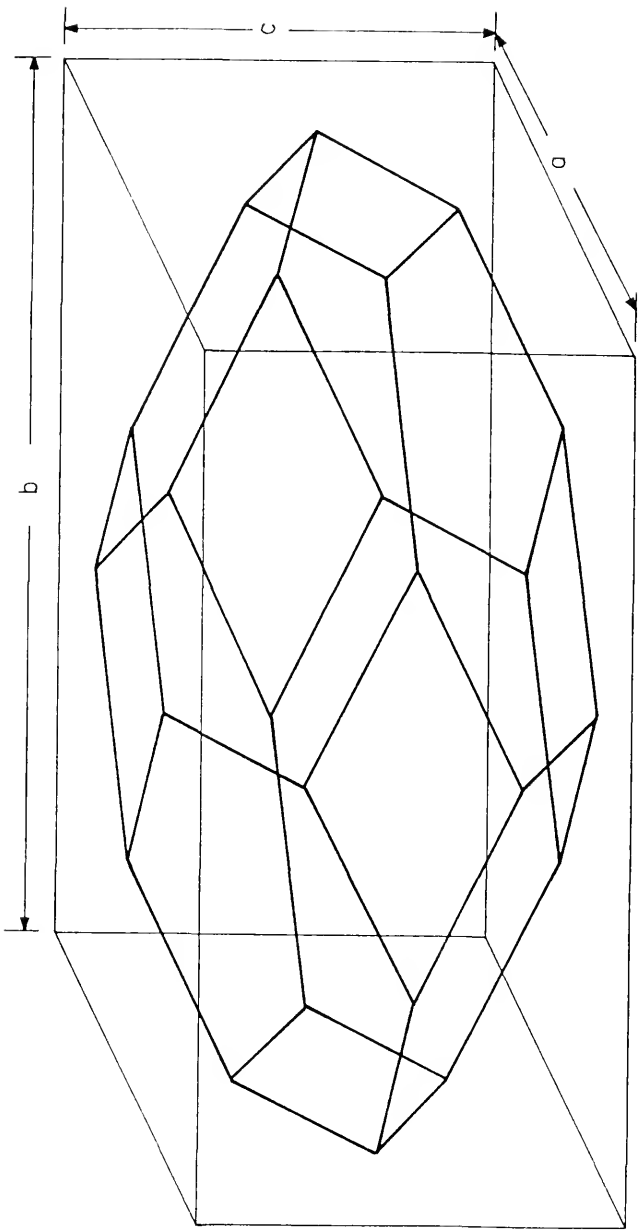

(a)

Figure (67). (b) Anisotropic tetrakaidecahedron, plan view. Edges of equal orientation and true length are numbered identically.

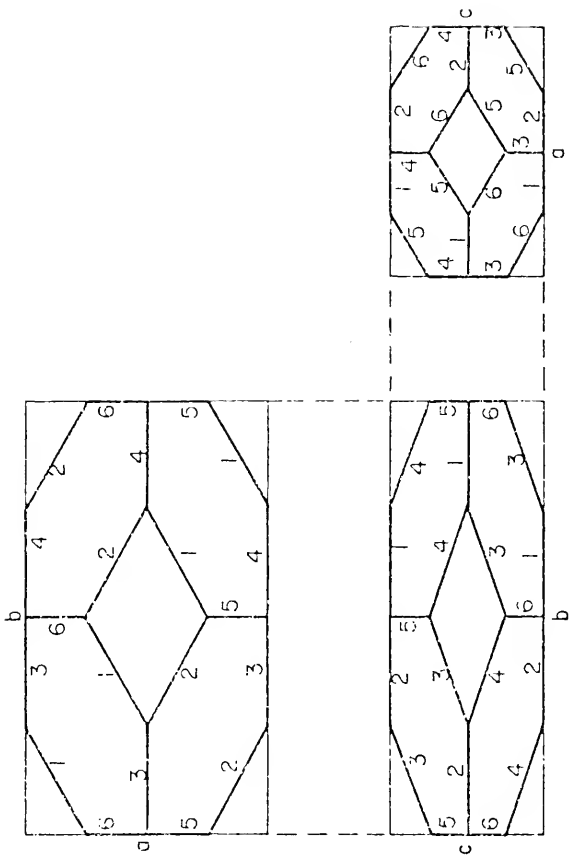

(b)

volume of the TKD remains one-half that of the parallelpiped regardless of its shape. Thus, the total L_V of the TKD, theoretically equal to that of the specimen, may easily be calculated once $(P_A)_a$, $(P_A)_b$, and $(P_A)_c$ have been measured and q_1 and q_2 are known. As with the Saltykov model (1,11,58), $(L_V)^{hk\ell}_{proj}$ may also be calculated for any direction, <hkℓ>.

The equations for the calculation of $(L_V)_{total}$ and $(L_V)^{hk\ell}_{proj}$ using the TKD model are derived below.

Total Line Length

The 36 edges of the TKD may be divided into 6 sets, each containing 6 lines of equal length and orientation. The lines belonging to sets i = 1,6, numbered identically in Figs. (66b) and (67b), may be expressed vectorially in terms of the axial lengths and ratios; e.g., for i = 1:

$$\vec{V}_1 = \frac{a}{4}\hat{X} + \frac{b}{4}\hat{Y} = \frac{a}{4}(\hat{X} + q_1\hat{Y}) \qquad \text{(D-24)}$$

The senses of the vectors are arbitrary and do not affect the following development. The values of η_i, the lengths of the individual lines in set i, are then given by $|\vec{V}_i|$, e.g.

$$\eta_1 = \frac{a}{4}\sqrt{1 + a_1^2} \qquad \text{(D-25)}$$

The value of $(L_V)_{total}$, the total length of edge per TKD

volume (taken as unity), is equal to the sum of the lengths of the 6 lines in all 6 sets:

$$(L_V)_{total} = \sum_{i=1,6} n_i = 3a[\sqrt{1+q_1^2} + \sqrt{q_1^2+q_2^2} + \sqrt{1+q_2^2}] \quad \text{(D-26a)}$$

For comparison with real microstructures, $(L_V)_{total}$ must be expressed in terms of P_A. This can be accomplished by inserting a scale factor into Eq. (D-26a), relating the lengths of specimen and TKD edges projected in a given direction. It can be seen in Figs. (66b) and (67b) that 24 of the 36 edges project a length of $\frac{a}{4}$ along the a-axis, yielding a total projected length in this direction of 6a, per TKD volume. Equating this with $(P_A)_a$, the projected length of real line along the a-axis of the specimen yields the scale factor:

$$a = \frac{(P_A)_a}{6} \quad \text{(D-27)}$$

Inserting this into Eq. (D-26a) yields $(L_V)_{total}$ for the specimen.

$$(L_V)_{total} = \frac{(P_A)_a}{2}[\sqrt{1+q_1^2} + \sqrt{q_1^2+q_2^2} + \sqrt{1+q_2^2}] \quad \text{(D-26b)}$$

For specimens with symmetry similar to Saltykov's planar and linear cases, Eq. (D-26b) is simplified, since $q_1 = 1$ and $q_2 = 1$, respectively. Thus, as was shown with the

Saltykov model, a specimen need not be classified by type of anisotropy prior to analysis, although knowledge of such symmetry simplifies the procedure.

Length of Projected Line

The value of $(L_V)^{hk\ell}_{proj}$, the length per unit volume of TKD line projected in some direction <hkℓ> relative to the orientation axes, is given by the sum of the projected lengths of the 6 lines in each of the 6 sets. The projected length of a line in set i in the <hkℓ> direction is given by $\eta_i|\cos\gamma_i|$, where $|\cos\gamma_i|$ is effectively the cosine of the acute angle between $\vec{V}_i$ and <hkℓ>. Therefore

$$(L_V)^{hk\ell}_{proj} = \sum_{i=1,6}^{6} \eta_i|\cos\gamma_i| \qquad \text{(D-28)}$$

The values of $|\cos\gamma_i|$ must be calculated individually for each line set, e.g. for i = 1:

$$|\cos\gamma_1| = \frac{(\frac{a}{4}\ \frac{b}{4}\ 0)}{\sqrt{(\frac{a}{4})+(\frac{b}{4})^2}} \cdot \frac{(h\ k\ \ell)}{\sqrt{h^2+k^2+\ell^2}}$$

$$= \frac{|h+q_1k|}{\sqrt{(1+q_1^2)(h^2+k^2+\ell^2)}} \qquad \text{(D-29)}$$

Entering the expressions for η_i and $|\cos\gamma_i|$, i = 1,6, in Eq. (D-28), and applying the scale factor yields

$$(L_V)^{hk\ell}_{proj} = \left[\frac{(P_A)_a}{4\sqrt{h^2+k^2+\ell^2}}\right]\left[|h+q_1k|+|h-q_1k|+|q_1k+q_2\ell|\right.$$

$$\left. + |q_1k-q_2\ell|+|h+q_2\ell|+|h-q_2\ell|\right] \qquad \text{(D-30a)}$$

Due to symmetry, the positive octant of possible <hkℓ> orientations is representative of the rest of a specimen and Eq. (D-30a) is further simplified. Noting this and Eq. (D-17),

$$(L_V)^{hk\ell}_{proj} = (P_A)^{hk\ell} = \left[\frac{(P_A)_a}{4\sqrt{h^2+k^2+\ell^2}}\right]$$

$$\left[2(h+q_1k+q_2\ell|+|h-q_1k|\right.$$

$$\left. + |q_1k-q_2\ell|+|h-q_2\ell|\right] \qquad \text{(D-30b)}$$

For specimens approximating the planar system ($q_1 = 1$) or linear system ($q_2 = 1$), Eqs. (D-30a) and (D-30b) are further reduced. Thus, for a specimen on which $(P_A)_a$, $(P_A)_b$ and $(P_A)_c$ have been measured, $(P_A)^{hk\ell}$ may be calculated for any other section plane.

The general equations for $(L_V)_{total}$ and $(L_V)^{hk\ell}_{proj}$ for both the Saltykov and TKD models are summarized in Table 11.

Test and Comparison of Methods

As a test, the two models have been used to characterize the grain edge network of a high purity aluminum

Table 11
General Equations for the Analysis of Lines in Space by the Saltykov and Tetrakaidecahedron Models

Saltykov Model	Tetrakaidecahedron Model
$(L_V)_{total} = (P_a)_a[q_1+(2-\frac{\pi}{2})q_2+(\frac{\pi}{2}-1)]$	$(L_V)_{total} = \frac{(P_A)_a}{2}[\sqrt{1+q_1^2}+\sqrt{q_1^2+q_2^2}+\sqrt{1+q_2^2}]$
$(L_V)_{is} = 2(P_A)_a\, q_2$	$L_{V_{proj}}^{hk\ell} = [\frac{(P_A)_a}{4\sqrt{h^4+k^2+\ell^2}}][2(h+q_1k+q_2\ell)+\lvert h-q_1k\rvert + \lvert q_1k-q_2\ell\rvert+\lvert h-q_2\ell\rvert]$*
$(L_V)_{pl} = (P_A)_a \frac{\pi}{2}(1-q_2)$	
$(L_V)_{proj}^{hk\ell} = (P_A)_a[q_2+\frac{(q_1-1)k}{\sqrt{h^2+k^2+\ell^2}} + (1-q_2)\sin\cos^{-1}(\frac{\lvert\ell\rvert}{\sqrt{h^2+k^2+\ell^2}})]$	
$(\Omega)^{L_V} = \frac{(q_1-1)+\frac{\pi}{2}(1-q_2)}{q_1+(2-\frac{\pi}{2})q_2+(\frac{\pi}{2}-1)}$	

*For h, k, and ℓ positive, otherwise use Eq. (D-30).

specimen rolled to 20% reduction in thickness. The 95% confidence intervals for the directed P_A measurements are

$$(P_A)_a = 3850 \pm 390 \ (cm^{-2})$$

$$(P_A)_b = 4430 \pm 430 \ (cm^{-2})$$

$$(P_A)_c = 2080 \pm 170 \ (cm^{-2})$$

yielding

$$q_1 = \frac{(P_A)_b}{(P_A)_a} = \frac{4430}{3850} = 1.15$$

$$q_2 = \frac{(P_A)_c}{(P_A)_a} = \frac{2080}{3850} = 5.40 \times 10^{-1}$$

The fact that neither q_1 nor q_2 is equal to unity, combined with the knowledge of the method of deformation and the microstructural appearance indicates that the grain edge configuration is planar-linear. Using Eqs. (D-12) and (D-26b),

Saltykov: $(L_V)_{total} = 7520 \ (cm^{-2})$

TKD: $(L_V)_{total} = 7570 \ (cm^{-2})$

Employing the Saltykov equations for the degree of anisotropy [Eqs. (D-14)-(D-16)], the fraction of all grain edge belonging to the planar and linear components may also be calculated:

$(\Omega)^{L_V}_{pl}$ = 0.37 (37% of all line is of planar orientation)

$(\Omega)^{L_V}_{lin}$ = 0.08 (8% of all line is of linear orientation)

$(\Omega)^{L_V}_{pl\text{-}lin}$ = 0.45 (a total of 45% of all line is oriented anisotropically)

The estimated value of $(L_V)_{total}$ varies by less than 1% between the two models. In fact, the difference calculated over a wide range of possible q_1 and q_2 values is generally less than 5%. Determining how well these models represent the true $(L_V)_{total}$ of the specimen requires a further test.

Values of $(L_V)^{hk\ell}_{proj}$ estimated by either model may be directly compared to those measured on the specimen. Similar measured and estimated values of $(L_V)^{hk\ell}_{proj}$, in a wide range of directions, would support the model and the validity of its estimation of $(L_V)_{total}$. Significant deviation between the two would tend to reject the model.

The differences between the values of $(L_V)^{hk\ell}_{proj}$ predicted by the two models themselves were first calculated over extreme ranges of q_1, q_2 and $\langle hk\ell \rangle$. They were generally less than 5% and almost always less than 15%,

with neither model producing consistently larger values than the other. The one condition which did produce estimations which differed significantly between the models was that of <hkℓ> being perpendicular to a hexagonal face of the TKD. In this circumstance, in which many of the TKD edges project no length in the <hkℓ> direction, TKD model predicted values of $(P_A)^{hk\ell}_{proj}$ consistently 20-30% less than the Saltykov model. This was considered to be the most discerning condition for comparing the values of $(P_A)^{hk\ell}$ measured on the specimen to those calculated by the models.

For the previously given values of q_1 and q_2 for the specimen, the hexagonal face of the resulting TKD was equivalent to a section plane of {112} orientation relative to the axes. The predicted and measured values are given below.

Measured: $(P_A)^{112} = 3120 \pm 310$ (cm^{-2})

Calculated (Saltykov): $(P_A)^{112} = 3340$ (cm^{-2})

Calculated (TKD): $(P_A)^{112} = 2660$ (cm^{-2})

The Saltykov prediction was only 7% greater than the measured value, within the range of experimental variation. The TKD value, however, was significantly less (15%) than the measured $(P_A)^{112}$.

A similar comparison was also performed on a section plane with a {111} type orientation relative to the orientation axes:

Measured: $(P_A)^{111} = 3960 \pm 370$ (cm^{-2})

Calculated (Saltykov): $(P_A)^{111} = 3860$ (cm^{-2})

Calculated (TKD): $(P_A)^{111} = 3670$ (cm^{-2})

In this case the Saltykov and TKD predictions were both acceptable, being 3% and 7% less than the measured value, respectively.

Conclusions

From these results, the Saltykov model appears to provide a viable means of analysis for spatial lines possessing the common patterns of anisotropy. The good agreement between calculated and measured values of $(L_V)_{proj}$, even on planes misoriented far from the principal ones, strongly supports the validity of the model and its estimation of $(L_V)_{total}$. Further, the ability of the model to estimate the fractions of line possessing various orientations yields useful information about the nature of oriented microstructures and the processes creating them.

The TKD model predicts values of $(L_V)_{total}$ and $(L_V)_{proj}$ similar to those of the Saltykov model over extreme degrees of anisotropy and in all but one critical direction. It cannot estimate the quantities of line arranged in various orientations.

Although the TKD model appears to have general validity, its limitations suggest that it should be rejected in deference to the more universally applicable Saltykov model.

APPENDIX E
SERIAL SECTION DATA

Sample 25-1*

Section	Number of new grains	Section thickness $X10^{-3}$ (in.)	Section volume $X10^{-4}$ ($cm.^3$)
1	6	0.35	0.93
2	10	0.20	0.53
3	11	0.37	0.99
4	2	0.23	0.61
5	13	0.80	2.1
6	13	0.50	1.3
7	10	0.67	1.8
8	19	0.73	2.0
9	9	0.50	1.3

Sample 25-2*

Section	Number of new grains	Section thickness $X10^{-3}$ (in.)	Section volume $X10^{-4}$ ($cm.^3$)
1	5	0.50	1.3
2	1	0.28	0.75
3	6	0.60	1.6
4	13	0.82	2.2
5	19	1.35	3.6
6	8	0.94	2.5
7	21	1.31	3.5
8	15	0.78	2.1
9	12	0.77	2.1

Sample 25-3*

Section	Number of new grains	Section thickness $X10^{-3}$ (in.)	Section volume $X10^{-4}$ ($cm.^3$)
1	5	0.55	2.1
2	1	0.22	0.83
3	1	0.38	1.4
4	6	1.22	4.6
5	19	2.45	9.3
6	7	1.62	6.1
7	7	1.96	7.4
8	8	1.65	6.3
9	9	1.71	6.5

Sample 25-4*

Section	Number of new grains	Section thickness $X10^{-3}$ (in.)	Section volume $X10^{-4}$ (cm.3)
1	2	0.55	2.1
2	1	0.45	1.7
3	8	1.52	5.8
4	12	2.30	8.7
5	15	2.23	8.5
6	16	2.85	11.
7	19	1.60	6.1
8	8	1.54	5.9

Sample 80-1*

Section	Number of new grains	Section thickness $X10^{-3}$ (in.)	Section volume $X10^{-4}$ ($cm.^3$)
1	8	0.20	0.11
2	1	0.40	0.21
3	5	0.35	0.18
4	12	0.40	0.21
5	19	0.55	0.29
6	8	0.40	0.21

Sample 80-2*

Section	Number of new grains	Section thickness $X10^{-3}$ (in.)	Section volume $X10^{-4}$ ($cm.^3$)
1	10	0.39	0.27
2	5	0.23	0.16
3	8	0.48	0.33
4	17	0.70	0.49
5	9	0.72	0.50
6	9	0.55	0.38

Sample 80-3*

Section	Number of new grains	Section thickness $X10^{-3}$ (in.)	Section volume $X10^{-4}$ ($cm.^3$)
1	2	0.29	0.21
2	18	0.60	0.42
3	12	0.33	0.23
4	14	0.75	0.52
5	13	0.60	0.42
6	11	0.50	0.35

Sample 80-4*

Section	Number of new grains	Section thickness $X10^{-3}$ (in.)	Section volume $X10^{-4}$ ($cm.^3$)
1	25	0.90	1.1
2	12	0.60	0.77
3	5	0.35	0.45
4	8	0.30	0.38
5	3	0.35	0.45
6	8	0.45	0.58
7	10	0.52	0.66
8	6	0.50	0.64
9	15	0.43	0.55
10	12	0.73	0.93
11	20	1.00	1.3

Sample 80-5*

Section	Number of new grains	Section thickness $X10^{-3}$ (in.)	Section volume $X10^{-4}$ ($cm.^3$)
1	19	0.50	1.2
2	6	0.40	0.97
3	9	0.30	0.73
4	12	0.90	2.2
5	13	0.50	1.2
6	13	0.70	1.7
7	7	0.37	0.90
8	8	0.59	1.4
9	21	0.70	1.7
10	24	1.05	2.6

Sample 80-6*

Section	Number of new grains	Section thickness $X10^{-3}$ (in.)	Section volume $X10^{-4}$ ($cm.^3$)
1	11	0.73	1.7
2	6	0.72	1.7
3	10	0.92	2.2
4	10	0.78	1.8
5	14	1.10	2.6
6	9	0.90	2.1

Sample 80-7

Section	Number of new grains	Section thickness $X10^{-3}$ (in.)	Section volume $X10^{-4}$ ($cm.^3$)
1	7	0.70	3.4
2	26	0.95	4.6
3	9	0.25	1.2
4	4	0.15	0.73
5	11	0.70	3.4
6	11	1.00	4.9
7	5	0.52	2.5
8	9	0.55	2.7
9	16	0.91	4.4
10	16	1.02	5.0

*Specimen designations are explained on page 116.

REFERENCES

1. R. T. DeHoff and F. N. Rhines, Quantitative Microscopy, McGraw-Hill, New York (1968).

2. H. B. Aaron, R. D. Smith, and E. E. Underwood, Proc. First Int. Cong. for Stereology, Vienna (1963).

3. P. Feltham, Acta Met. 1, 97-105 (1957).

4. P. A. Beck, Adv. in Phys. 3, 245-324 (1954).

5. K. Okazaki and H. Conrad, Trans. Jap. Inst. of Metals 13, 198-204 (1972).

6. F. C. Hull, unpublished data from quantitative metallography symposium, University of Florida (1961).

7. W. M. Williams and C. S. Smith, Trans. AIME 194, 755-765 (1952).

8. C. S. Smith, in Metal Interfaces, ASM, Cleveland (1952).

9. F. N. Rhines and K. R. Craig, Met. Trans. 5, 413-425 (1974).

10. J. H. Steele, Jr., in Microstructural Science, Volume 1, Elsevier (1973).

11. E. E. Underwood, Quantitative Stereology, Addison-Wesley, Reading, Mass. (1970).

12. G. Herdan, Small Particle Statistics, Elsevier, New York (1953).

13. M. Otala, Prac. Metallog. 11, 83-88 (1974).

14. J. L. Meijering, Philips Res. Rep. 8, 270-290 (1953).

15. E. N. Gilbert, Ann. Math. Statistics 33, 958-972 (1962).

16. K. W. Mahin, K. Hanson, and J. W. Morris, Jr., in Proc. of the 1976 Int. Conf. on Computer Simulation for Materials Applications, 39-49 (1976).

17. M. Hillert, Acta Met. 13, 227-238 (1965).

18. K. R. Craig, Ph.D. Dissertation, University of Florida, Gainesville (1971).

19. C. Desch, J. Inst. Metals 22, 241-276 (1919).

20. D. L. Robinson, private communication.

21. W. M. Wojcik, R. M. Raybeck, and E. J. Paliwoda, J. Metals 19 (2), 36-40 (1967).

22. G. W. Snedecor and W. G. Cochran, Statistical Methods, 6th ed., The Iowa State University Press, Ames (1967).

23. J. C. Kapteyn, Skew Frequency Curves in Biology and Statistics, Noordhoff, Astronomical Laboratory, Groningen (1903).

24. J. Aitchison and J. A. C. Brown, The Log Normal Distribution, Cambridge University Press, New York (1957).

25. F. Kottler, J. Franklin Inst. 250, 339-356 (1950).

26. W. A. Anderson and R. F. Mehl, Trans. AIME 161, 140-172 (1945).

27. R. A. Vandermeer and P. Gordon, Trans. AIME 215, 577-588 (1959).

28. P. A. Beck, P. R. Sperry, and H. Hu, J. Appl. Phys. 21, 420-425 (1950).

29. R. D. Doherty, Metal Science 8, 132-142 (1974).

30. S. P. Bellier and R. D. Doherty, Acta Met. 25, 521-538 (1977).

31. S. Weissmann, T. Imura, and N. Hosokawa, in Recovery and Recrystallization of Metals, Gordon and Breach, New York (1963).

32. F. N. Rhines, private communication.

33. W. A. Johnson and R. F. Mehl, Trans. AIME 135, 416-458 (1939).

34. A. Goldman, H. D. Lewis, and R. H. Moore, Los Alamos Scientific Lab., LA-3262 (1965).

35. J. Plateau, Annual Report of the Smithsonian Institution (1866).

36. Sir William Thomson (later Lord Kelvin), Phil. Mag. 24, 503-514 (1887).

37. F. T. Lewis, Proc. Am. Acad. of Arts and Sciences 58, 537-552 (1923).

38. J. W. Marvin, Am. J. Botany 26, 280-288 (1939).

39. E. B. Matzke, Am. J. Botany 33, 58-80 (1964).

40. R. L. Hulbary, Am. J. Botany 31, 561-580 (1944).

41. R. E. Williams, Science 161, 276-277 (1968).

42. L. Euler (1752) in A. L. Loeb, Space Structures, Addison-Wesley, Reading, Mass. (1976).

43. H. S. M. Coxeter, Ill. J. Math. 2, 746-758 (1960).

44. J. H. Steele, Ph.D. Dissertation, University of Florida, Gainesville (1967).

45. J. H. Steele, Jr., and B. Summers, private communication.

46. D. A. Rousse, M.S. Thesis, University of Florida, Gainesville (1973).

47. J. H. Steele, Jr., in Stereology and Quantitative Metallography, STP 504, ASTM, Easton, Pa. (1972).

48. A. L. Loeb, Space Structures, Addison-Wesley, Reading, Mass. (1976).

49. Z. Jeffries and R. S. Archer, The Science of Metals, McGraw-Hill, New York (1924).

50. J. E. Burke, Trans. AIME 180, 73-91 (1949).

51. J. E. Burke, J. Appl. Phys. 18, 1028 (1947).

52. P. A. Beck, M. L. Holzworth, and H. Hu, Phys. Rev. 73, 526-527 (1948).

53. P. A. Beck, J. C. Kremer, L. J. Demer, and M. L. Holzworth, Trans. AIME 175, 372-400 (1948).

54. J. P. Nielsen, in Recrystallization, Grain Growth, and Textures, ASM, Metals Park (1966).

55. C. S. Smith and L. Guttman, Trans. AIME 197, 81-87 (1953).

56. R. T. DeHoff, Trans. AIME 230, 764-769 (1964).

57. K. Okazaki and H. Conrad, Met. Trans. 3, 2411-2421 (1972).

58. S. A. Saltykov, Stereometric Metallography, 2nd ed., Metallurgizidat, Moscow (1958), English translation by Technical Documents Liaison Office, MCLTD, WP-AFB, Ohio.

59. R. T. DeHoff, private communication.

60. F. N. Rhines, R. T. DeHoff, and R. A. Rummel, AEC Contract No. AT-(40-1)-2851, Ann. Rept. (1962).

61. K. R. Craig, M.S. Thesis, University of Florida, Gainesville (1965).

62. F. N. Rhines, K. R. Craig, and D. A. Rousse, Met. Trans. 7A, 1729-1734 (1976).

63. P. A. Beck, J. Towers, and W. D. Manly, Trans. AIME 175, 162-177 (1948).

64. H. L. Walker, Univ. of Ill. Eng. Exp. Sta. Bull. No. 359, Univ. of Illinois (1945).

65. P. A. Beck, J. Appl. Phys. 18, 1028-1029 (1947).

BIOGRAPHICAL SKETCH

Burton Roe Patterson was born December 26, 1949, in Birmingham, Alabama. He attended Ensley High School, from which he graduated in June 1967. In May 1971, he graduated from Vanderbilt University with a Bachelor of Engineering degree in Materials Science and Engineering. He was employed for two years by Union Carbide Corporation as a metallurgist at the Y-12 Plant in Oak Ridge, Tennessee. In September 1973, Mr. Patterson enrolled as a graduate student in the Department of Materials Science and Metallurgical Engineering at the University of Florida. He received the Master of Science degree in December 1975, and since that time has pursued work toward the degree of Doctor of Philosophy. Mr. Patterson is a member of the American Society for Metals, the Metallurgical Society of the American Institute of Mining, Metallurgical and Petroleum Engineers, and Phi Kappa Phi, Tau Beta Pi, and Alpha Sigma Mu honor societies.

I certify that I have read this study and that in my opinion it conforms to acceptable standards of scholarly presentation and is fully adequate, in scope and quality, as a dissertation for the degree of Doctor of Philosophy.

Frederick N. Rhines, Chairman
Distintuished Service
Professor of Materials
Science and Engineering

I certify that I have read this study and that in my opinion it conforms to acceptable standards of scholarly presentation and is fully adequate, in scope and quality, as a dissertation for the degree of Doctor of Philosophy.

Robert E. Reed-Hill
Professor of Materials
Science and Engineering

I certify that I have read this study and that in my opinion it conforms to acceptable standards of scholarly presentation and is fully adequate, in scope and quality, as a dissertation for the degree of Doctor of Philosophy.

Robert T. DeHoff
Professor of Materials
Science and Engineering

I certify that I have read this study and that in my opinion it conforms to acceptable standards of scholarly presentation and is fully adequate, in scope and quality, as a dissertation for the degree of Doctor of Philosophy.

Richard L. Scheaffer
Professor of Statistics

This dissertation was submitted to the Graduate Faculty of the College of Engineering and to the Graduate Council, and was accepted as partial fulfillment of the requirements for the degree of Doctor of Philosophy.

June 1978

Hubert A. Bevis
Dean, College of Engineering

Dean, Graduate School

UNIVERSITY OF FLORIDA
3 1262 08553 2793